ACTA UNIVERSITATIS SZEGEDIENSIS



# ACTA PHYSICA ET CHEMICA

NOVA SERIES

TOMUS XXX

FASCICULI 1—2

AUSHAF 30 (1—2) (1—116) (1984)

HU ISSN 0324—6523 Acta Univ. Szeged
HU ISSN 0001—6721 Acta Phys. et Chem.

SZEGED, HUNGARIA
1984

ACTA UNIVERSITATIS SZEGEDIENSIS

# ACTA PHYSICA ET CHEMICA

NOVA SERIES

TOMUS XXX FASCICULI 1—2

AUSHAF 30 (1—2) (1984)

HU ISSN 0324—6523 Acta Univ. Szeged
HU ISSN 0001—6721 Acta Phys. et. Chem.

SZEGED, HUNGARIA
1984

Kiadja
a József Attila Tudományegyetem Természettudományi Kara
(Szeged, Aradi vértanúk tere 1.)



Kiadványunk rövidítése:
Acta Phys. et. Chem. Szeged

# DAMPING EFFECTS IN LETHARGIC GAIN

By

M. G. BENEDICT

Institute of Theoretical Physics, Attila József University
Szeged, Hungary

and

E. D. TRIFONOV

Herzen Pedagogical Institute, Leningrad, U.S.S.R.

*(Received October 15, 1983)*

The coherent amplification of a weak pulse by an inverted two-level medium is considered in the linear approximation. Analytic expressions are presented for the case of homogeneous and inhomogeneous broadening.

Considering the propagation of a coherent pulse, passing through a two level medium, one obtains relatively simple expressions for the transmitted amplitude, if one regards only the initial linear part of the process [1]. This means that one neglects the changes in the inversion — it is taken as a constant — during the interaction. This problem arises for instance at the so called induced superfluorescence [2, 3], where the initial polarization of the system is induced by a weak coherent pulse of small area. If damping processes are small, the signal, having passed a distance $x$ in an inverted medium, will be amplified coherently as $e^{\sqrt{x}}$ instead of the usual $e^x$ law. This effect is termed as lethargic gain [4], and has been observed in recent experiments [5]. In this paper we consider the effects of homogeneous and Lorentzian inhomogeneous broadening on this process.

The Maxwell—Bloch equations describing the interaction of an extended two-level system with a plane monochromatic wave are [6, 7]:

$$\frac{\partial A}{\partial x}+\frac{\partial A}{\partial t}=\int R(x,t,v)g(v)\,dv \tag{1a}$$

$$\frac{\partial R}{\partial t}=\left(-\frac{1}{T_2}+iv\right)R+2AZ \tag{1b}$$

$$\frac{\partial Z}{\partial t}=-(AR^*+A^*R) \tag{1c}$$

A system of units has been chosen where time is measured in units of $\Omega^{-1}=\frac{\hbar}{\mu}/\sqrt{2\pi N\hbar\omega_0}$, length in $c\Omega^{-1}$. $A$ is proportional to the slowly varying amplitude

of the electric field: $A=-iE/\sqrt{2\pi N\hbar\omega_0}$, $R$ is the polarization, $Z$ is half of the population difference between the upper and lower levels, $N$ is the density of the active atoms, $\omega_0$ is the carrier frequency of the field, $\mu$ is the dipole moment of the transition and $g(v)$ is the inhomogeneous line shape.

Assuming $Z=1/2$ during the whole process, we have two linear equations:

$$\frac{\partial A}{\partial x}+\frac{\partial A}{\partial t}=\int R(x,t,v)g(v)dv \tag{2a}$$

$$\frac{\partial R}{\partial t}=\left(-\frac{1}{T_2}+iv\right)R+A \tag{2b}$$

This approximation is valid for the initial part of the process until the inversion does not change considerably. A similar assumption has been used for investigating the delay time statistics of superfluorescence [8]. We shall see that this approximation remains valid for the whole process if homogeneous and inhomogeneous broadening are large enough to keep the pulse area small.

Eqs. (2) can be solved analytically for the case if $g$ had the following Lorentzian form:

$$g(v)=\frac{T^*}{\pi\left(1+(T^*v)^2\right)} \tag{3}$$

Let the incoming amplitude at $x=0$ have the time dependence $A_0(t)$ with $A_0(0)=0$. The solution of Eqs. (2) can be obtained by a Laplace transformation technique:

$$A(x,t)=\int_t^x\left(\frac{dA_0(t-\tau)}{dt}+\frac{1}{T}A_0(t-\tau)\right)I_0\left(\sqrt{2x(\tau-x)}\right)e^{-(\tau-x)/T}d\tau \tag{4}$$

Here $I_0$ is the modified Bessel function [9] and:

$$\frac{1}{T}=\frac{1}{T_2}+\frac{1}{T^*} \tag{5}$$

Thus Lorentzian inhomogeneous broadening has the same effect as $T_2$, they equally reduce the amplification. The polarization is given by

$$R(x,t,v)=\int_0^t A(x,\tau)e^{\left(-\frac{1}{T_2}+iv\right)(t-\tau)}dt \tag{6}$$

The amplification of a Gaussian input pulse of width $\sigma=0.2\ \Omega^{-1}$ is showing in Fig. 1. at the distance $x=1$. We see that for small $T$ the pulse area is not growing unlimitedly, which means that $Z=0.5$ is approximately valid through the whole process if the initial area is small. For larger $T$-s the rising amplitude at the right end is the radiation of the induced dipole moment. This nonlinear part can be treated only numerically [3].

We shall in some extent investigate the special case, when the incoming pulse is a step function, switched on at $t=0$: $A_0(t)=A_0\Theta(t)$. For $T=\infty$ (unbroadened case)

$$A(x,t)=A_0I_0\left(2\sqrt{x(t-x)}\right)\Theta(t-x) \tag{7}$$

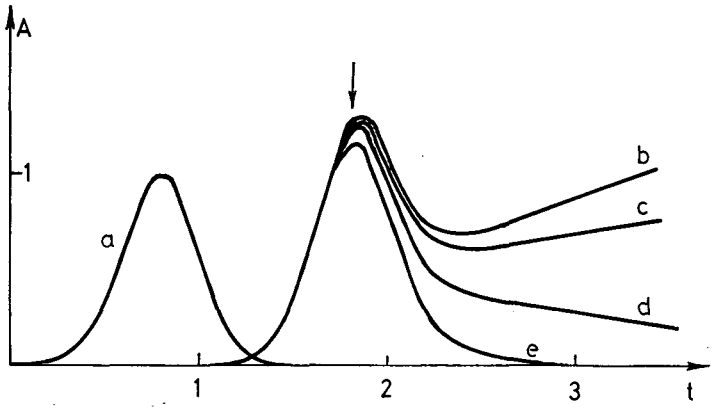


*Fig. 1.* The amplification of a Gaussian input pulse of width $\sigma=0.2\,\Omega^{-1}$ (amplitude) at a distance $x=1(c\Omega^{-1})$: a. input amplitude; b. amplified amplitude for $T=\infty$; c. $T=5$; d. $T=1$; e. $T=0.238$ The arrow shows the point where the peak would be translated by light speed

For a given $t-x$ and $x\gg 1$, $A(x)=A_0e^{\sqrt{x}}$ which is the case of lethargic gain [4]. If we have a finite $T$, the step-like incoming pulse will be transformed as

$$A(x,t) = A_0 I_0\left(2\sqrt{x(t-x)}\right)e^{-(t-x)/T}\Theta(t-x)+\frac{A_0}{T}\int_x^t I_0\left(2\sqrt{x(\tau-x)}\right)e^{-(t-x)/T}d\tau \quad (8)$$

For $t$ large enough, the first term goes to zero, the second to a constant. To determine this constant we choose the upper limit of the integral $t=\infty$ and obtain [9]:

$$A(x, t=\infty) = A_0 e^{Tx}$$

This is the usual Beer law for incoherent amp]ification. Eq. (8) shows the time dependence of achieving this limiting stationary case at a given $x$.

## References

[1] *Crisp, M. D..;* Phys. Rev. 1A 1604 (1970).
[2] *Vrehen, Q. H. F., M. F. H. Schuurmans:* Phys. Rev. Lett. **42** 224 (1979).
[3] *Malikov, R. F., E. D. Trifonov:* to be published
[4] *Hopf, F., P. Meystre, D. W. McLaughlin:* Phys. Rev. **A13** 777 (1976).
[5] *Chung, H. K., J. B. Lee, T. A. DeTemple:* Opt. Comm. **39** 105 (1981).
[6] *Allen, L., J. Eberly:* Optical Resonance and Two Level Atoms, Wiley, New York, (1975).
[7] *Маликов Р. Ф., В. А. Малышев, Е. Д. Трифонов:* в сб. Теория кооперативных когерентных эффектов в излучении, Ленинград (1980)
[8] *Haake F., J. W. Haus, H. King, G. Schröder, R. Glauber:* Phys. Rev. **23**, 1322 (1981).
[9] *Abramovitz, M. D., I. Stegun:* Handbook of Math. Functions Dover, New York, (1970).

## ЭФФЕКТЫ ЗАТУХАНИЯ ПРИ ЛЕТАРГИЧЕСКОМ УСИЛЕНИИ

*М. Г. Бенедикт и Е. Д. Трифонов*

Рассматривается когерентное усиление слабого импульса в двухуровневой системе в линейном приближении. Получены аналитические выражения для случая однородного и неоднородного уширения.

# FLUORESCENCE AND THE KINETICS OF EXCITED SINGLET STATES

by

M. HAUSER

Institut für Physikalische Chemie der Universität Stuttgart

This lecture is dedicated to Professor A. Weller on the occasion of his 60th birthday

*(Received September 2, 1983)*

Four basic rules for treating the kinetics of processes in the first excited singlet state are given. General formulae for investigating the responses of stationary, phase fluorometric, $\delta$-flash and general time dependent excitation are derived for systems with one and two excited species.

The breakdown of usual kinetic concepts in cases of time dependent rate factors, especially Förster—Galanin type energy transfer and nonstationary diffusion, is briefly demonstrated and a novel kinetic procedure, called convolution kinetics is given in three rules. — Dynamic tests and examples for calculations of the new kinetics (excimer as donor, multistep and two step energy transfer) are reported.

## 0. Introductory considerations

The spectroscopic significance of molecular fluorescence may be poor enough to justify its usual treatment as an appendix to general optical spectroscopy, as it has to do essentially with the longest wavelength singlet-singlett transition only. Most of the interesting phenomena in connexion with fluorescence refer to the time behaviour of molecular ensembles. It is the aim of this lecture to show that fluorescence phenomena can be treated in terms of chemical kinetics.

### *0.1 Generation and deactivation of exited molecules*

In accordance with Vavilov's law each absorbed light quantum transfers one molecule in its *f*irst *e*xcited *s*inglet state, which happens within a negligibly short time, of, say, $10^{-23}$ s; the very few exceptions need not be mentioned. Chemically speaking, a 'jump' from a minimum of the ground state hypersurface to a minimum of the FES (abbreviation for 'first excited singlet state') and from one thermally equilibrated state to the other, takes place. The detailed mechanism of the various ultrafast processes incorporated in that 'Vavilov-jump' $S_v \rightarrow S_1^*$ cannot yet quantitatively be elucidated in cases of practical importance, as subpicosecond kinetic spectroscopy is at its very beginning. In the following we deal with the FES of various species $A$, $B$, ...which we denote $A^*$, $B^*$, ... omitting the suffix.

After the Vavilov-jump of a species $A \rightarrow A^*$, say, the various processes appearing in Jablonski's term scheme can take place, namely spontaneous emission (SE),

intersystem crossing (ISC), and internal conversion (IC). From the 'Jablonski-processes' only the SE: $A^* \xrightarrow{n_e} A + h\nu$ is of fundamental necessity marking the upper limit to the lifetime $\tau$ of species in the FES: $\tau = 1/n_e \leqq 10^{-6}$ s*). The significance of IC with rate constant $n_1$ and ISC with rate constant $n_{ST}$ may vary from case to case depending on conditions. Besides the conditional IC and ISC there is a wealth of other conditional processes or types of physicochemical behaviour which may be classified by the keywords 'photochemistry' and 'energy transfer'. The range of rates of 'conditional' processes starting from the FES is between 'negligible' and 'widely outdoing' compared to the rate $n_e$ of 'necessary' SE.

### *0.2 Photochemical processes*

[1] Chemical reactions in the ground state correspond to movements along reaction pathways on the ground state hypersurface. The energy of cols between the minima corresponding to different chemical species has to do with the activation energy. Usually, species are in thermal equilibrium and need activation energy to undergo chemical change. It is perhaps one of the important features of the FES that quite analogously to the ground state there is a FES-hypersurface with almost the same conditions for chemical processes as in the ground state. But in many cases the FES-reactivities are higher because of higher electronic energy content from which lower activation energies $E_a^*$ may result. But the complexity of chemical behaviour is drastically reduced in the FES compared to the chemistry in the ground state or even in the (longer lived) excited triplet state. We only need consider

0.21 Monomolecular processes, for instance

dissociation $A^* \xrightarrow{n_d} P^* + Q$
isomerization $A^* \rightarrow B^*$

0.22 Bimolecular processes such as

association $A^* + B \xrightarrow{k_a} (AB)^*$
quenching $A^* + Q \rightarrow A + Q$
collisional energy transfer

$$A^* + B \rightarrow A + B^*$$

(Förster type transfer needs particular kinetic treatment.) All these processes except quenching can be thought of as movements on the same FES-hypersurface being called adiabatic as energy changes smoothly and moderately, excitation being essentially conserved. The Jablonski-processes, however, though being monomolecular, too, are connected with discontinuous transitions between different hypersurfaces as is quenching (probably); this behaviour is called diabatic.

---

* If no measuring value $n_e$ is available, a crude estimate is given by Ladenburg's formula $n_e \approx 1{,}5 n \bar{\nu}^2 \cdot f$
($n$ refractive index, $\bar{\nu}$ center of gravity wave number of fluorescence spectrum, $f$ oscillator strength of longest wavelength absorption transition).

## 1. The four rules of FES-kinetics

There are 4 rules necessary to deal quantitatively with FES-kinetics and to investigate it with the aid of fluorescence. The first rule was introduced already in the context of the Vavilov-jump and will only be repeated here. A second rule follows from that all bimolecular processes in FES are practically exactly pseudo first order. This is because all concentrations of excited species $A^*$, $B^*$, ... are so small that the concentrations of unexcited partners must be very much larger and thus can be taken together with the bimolecular rate constant $k_a$ to get a brutto first order rate constant $k_a \cdot [P]$ comparable to $n_e$ (of SE). All monomolecular processes are of the first order per se, ergo ... (see below).

A third rule follows from the fact that light intensities from conventional sources are small (it is not valid with high power laser excitation).

*1st rule:* Each absorbed light quantum transfers a molecule to its first excited singlet state;

*2nd rule*: All processes starting from the first excited singlet state are of the first order;

*3rd rule:* All concentrations of unexcited species are taken to be constant in kinetics of first excited singlet state.

These three rules usually suffice to write down the kinetic (simultaneous first order) differential equations of a FES-reaction scheme, which either must be given or is constructed for trial. The fourth rule is necessary for the understanding of fluorescence. It may be derived as follows:

Suppose a complex reaction mechanism be given (not necessarily in the FES). Looking at some part of it we may see educts, intermediates, products and forward and backward reaction steps

$$\begin{array}{c} \ldots U \rightleftharpoons V+W \rightleftharpoons X+\ldots \\ \Big\downarrow k_y \\ Y+Z \end{array}$$

From a certain species $V$, say, may start a first order process with rate constant $k_y$ one of the products of which, $Y$, is not produced otherwise. Then if it is possible to measure the rate of production of $Y$

$$\frac{d[Y]}{dt} = k_y[V]\left(= -\frac{\delta_y[V]}{dt}\right),$$

we see that we thus can know $[V]$ at any instant of time! This is valid irrespective of all other processes which may influence $[V]$ (the process with $k_y$ is only one of which and thus is denoted by $\delta_y$). In FES kinetics all processes are of the first order. Thus, instead of considering the concentrations $[U]$, $[V]$, $[Y]$, ... we may write in the same equations the amounts (=numbers of species or moles in the reaction vessel) denoted by $\langle U\rangle$, $\langle V\rangle$, $\langle Y\rangle$, ... In case of the 'reaction SE': $A^* \xrightarrow{n_e} A + h\nu$, we may identify $A^*$ with $V$ and $h\nu$ with $Y$ (the fluorescence quanta of $A^*$ will not be produced otherwise). While it would be difficult to measure the rate of photochemically produced $A$, it is easy to measure the number of light quanta escaping from the vessel ... It is the total

quantum flux which in principle we get by measuring the fluorescence intensity on all elements of a closed surface surrounding the cuvette.

*4th rule*: The fluorescence flux (=integral intensity over a closed surface surrounding the fluorescence cuvette) of a species is at any time *equal* to the number of corresponding excited species (in FES) times its spontaneous emission rate constant.

If only a spectral or spatial fraction of fluorescence is measured, rule 4 is valid with 'proportional' instead of 'equal'. In general it is a serious mistake (made even by well-known scientists) to say that fluorescence intensity be proportional to the "concentration" of excited species: This statement is as wrong as the claim that radioactivity be given by the "concentration" of active matter. Really in both cases it is the amount or number of species considered**). Really we ought to be sure that our fluorescence spectrometer measures the integral of excited species' concentration distribution over the sample space and not its concentration, which is a complicated function of exitation geometry etc. in most cases (!) This function must be known if reabsorption cannot be neglected.

### *1.1 Simple applications of rules 1—4.*

If only one excited species is present (namely in the absence of adiabatic photoreactions) we get according to rules 1—3

$$\frac{d\langle A^*\rangle}{dt} = -n\langle A^*\rangle + I_a(t) \tag{1}$$

where $$n = \sum n_i = n_e + n_{ST} + \ldots + n_a[P] + \ldots \tag{2}$$

The solution function $\langle A^*\rangle(t)$ depends strongly on $I_a(t)$, the time dependence of excitation. The most simple case to realize is:

#### *1.1.1. The photostationary state*

If $I_a = I_{as}$ = constant and $t \to \infty$ we get from Eq. (1)

$$\langle A^*\rangle_s = \frac{I_{as}}{n} \tag{3}$$

from which follows the stationary fluorescence flux $F_s$ when applying the 4th rule

$$F_s = n_e\langle A^*\rangle_s = \frac{n_e}{n} I_{as}. \tag{3a}$$

---

** Perhaps we can understand the 4th rule better from $\operatorname{div} \vec{f}_A = -\frac{\delta_e[A^*]}{dt}$ where $\vec{f}_A$ is the fluorescence intensity (=flux density) vector, and the right hand side represents the time change of concentration $[A^*]$ by emission. Applying Gauss' theorem we see that the flux $F_A$ (=surface integral of $\vec{f}_A$) is found by integration of concentration over the space giving $\frac{\delta_e}{dt}\int [A^*]\, dv = -\frac{\delta_e\langle A^*\rangle}{dt}$ which is $= n_e\langle A\rangle^*$ according to our above reasoning. Our 'divergence principle of fluorescence' may also not be very familiar to spectroscopists, but is in accordance with general principles.

In the stationary state, the fluorescence quantum yield $\Phi = \frac{n_e}{n} = \frac{F_s}{I_{as}}$ can be determined from the fluxes (intensities) $F_s$ and $I_{as}$. Inserting Eq. (2) in Eq. (3) and marking entities referring to concentration of partner or quencher $[P]=0$ by index 0, we get the Stern—Volmer—Eq.

$$\frac{\langle A^* \rangle_{so}}{\langle A^* \rangle_s} = \frac{F_{so}}{F_s} = 1 + \frac{n_a}{n_o}[P]. \tag{4}$$

While the absolute measurement of quantum yield $\Phi$ needs 'integrating photometry' with respect to direction and wavelength, a Stern—Volmer plot needs only a spatial and/or spectral fraction of $F_s$, or an instrumental signal, provided the over all proportionality factors do not vary with concentration $[P]$. In the case of several quenchers all the concentrations except one must be constant.

### *1.1.2. The δ-excitation*

The solution of Eq. (1) in the case that $I_\delta = \delta(t-O)$ is called the $\delta$-response $\langle A^* \rangle_\delta$.

$$\delta(t-o) = o \text{ if } t \neq o \text{ but } \int_{o+\varepsilon}^{o+\varepsilon} \delta(t-o)\,dt = 1$$

$\varepsilon$ is an arbitrarily small number. For many reasons we make use of Laplace transform. If we denote $\mathbf{L}\langle A^* \rangle_\delta = y_0$, $\mathbf{L}t = x$, with $\mathbf{L}\delta(t-O) = 1$, the transformed Eq. (1) reads

$$y_o x = -n y_o + 1; \; y_o = (x+n)^{-1}.$$

The backward transform yields $\mathbf{L}^{-1} y_\delta = \langle A^* \rangle_\delta = e^{-nt}$ for $t > O$ and $\langle A^* \rangle_\delta = O$ for $t < O$.
The $\delta$-response according to Eq. (6) is typical for a directly excited species without population by other processes, while a linear Stern—Volmer plot is not, as it may result from more complicated mechanisms, too.

### *1.1.3. Arbitrary time dependence of excitation*

Analogously to $\delta$-excitation we get by Laplace transform if $\mathbf{L}\langle A^* \rangle = y$ and $\mathbf{L}I_a = J$: $y = (1+n)^{-1} \cdot J$. The transform of the $\delta$-response is multiplied with the transform of $I_a$. Applying the rule for backward transform of a product we get

$$\langle A^* \rangle = \langle A^* \rangle_\delta * I_a = I_a * \langle A^* \rangle_\delta = \int_{\vartheta=o}^{t} I_a(t-\vartheta)\langle A^* \rangle_\delta(\vartheta)\,d\vartheta. \tag{7}$$

The response on arbitrary excitation is given by the convolution 'product' of $\delta$-response and excitation function. As this can be performed for any $I(t)$, obviously all kinetic information is contained in $\langle A^* \rangle_\delta$. No other choice of $I_a$ can give additional knowledge.

*1.1.4. The phase fluorimeter response (= Fourier transform of δ-response)*

In this case

$$I_a = I_{as}(1+q\cos\omega t), \text{ resp. } I_{as}(1+qe^{i\omega t}), \tag{8}$$

where $o \leqq q \leqq 1$. Again one looks at the behaviour for $t \to \infty$.

By inserting Eq. (8) in Eq. (7) we can convince ourselves that the corresponding $\langle A^* \rangle_P$ is the Fourier transform of $\langle A^* \rangle_\delta$. This is important because excitation of the form Eq. (8) can be realized with much better approach to ideality than δ-excitation and the strain of the system by light intensity may be kept much smaller.

The mathematical procedure of $\langle A^* \rangle_P$ calculation is extremely simple, namely almost the same as in the photostationary state. Allowing for the time-dependent term in Eq. (8), $n$ merely has to be replaced with $(n+i\omega)$ where the factor $e^{i\omega t}$ appears. The result may be written in the form

$$\langle A^* \rangle_P = \frac{I_{as}}{n}(1+m\cos(\omega t-\varphi)), \text{ resp. } \frac{I_{as}}{n}(1+me^{i(\omega t-\varphi)}), \tag{9}$$

where $m = q \cdot \cos\varphi$ and $n = \omega \cot\varphi$.

## *1.2. Systems with 2 excited species*

There are two types of such systems. Either the photochemical primary process (starting from the directly excited species) is bimolecular and its inverse process is monomolecular or vice versa. Examples of the former are excimer and exciplex systems, while FES protolytic reactions belong to the latter.

Exciplex/excimer system

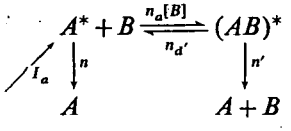


FES Protolytic reaction

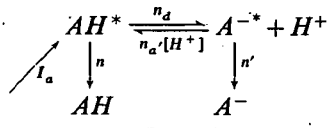


In both systems we suppose that only one of the two excited species is primarily optically populated (only with the protolytic reaction it is possible — in a narrow pH region — to generate $AH^*$ and $A^{-*}$ simultaneously by light absorption but without being faced with new aspects). In the left hand side system if $B = A$ we have an excimer system.

Applying rules 1—3 to both systems we find, after proper arrangement, simultaneous first order differential equations with constant coefficients; the meanings of $X$, $Y$, and the $n_{ik}$ are given in List 1.

$$\frac{dX}{dt} = n_{11}X + n_{12}Y + I_a \quad \frac{dY}{dt} = n_{21}X + {}_{22}Y. \tag{10}$$

*List 1*

| $X = \langle A^* \rangle \quad Y = \langle (AB)^* \rangle$ | | $X = \langle AH^* \rangle \quad Y = \langle A^{-*} \rangle$ |
|---|---|---|
| $-(n + n_a[B])$ | $n_{11}$ | $-(n + n_d)$ |
| $n'_d$ | $n_{12}$ | $n'_a[H^+]$ |
| $n_a[B]$ | $n_{21}$ | $n_d$ |
| $-(n' + n'_d)$ | $n_{22}$ | $-(n' + n'_a[H^+])$ |

The characteristic equation following from Eq. (10) we need not solve.

$$(\lambda + n_{11})(\lambda + n_{22}) - n_{12}n_{21} = 0 \tag{10a}$$

Instead of its roots $\lambda_1$ and $\lambda_2$ we consider Vieta's identities

$$\lambda_1 + \lambda_2 = -(n_{11} + n_{22}) \quad \lambda_1\lambda_2 = n_{11}n_{22} - n_{12}n_{21} \tag{11}$$

With the meaning of the $n_{ik}$ from *List 1* we see that all four kinetic constants of the above reaction schemes can be determined by plotting the experimentally determined left hand sides of Eqs. (12) versus concentration of the unexcited reaction partner. The equations of the stratight lines are given below ,continuing *List 1*

| | | |
|---|---|---|
| $n + n' + n'_d + n_a[B]$ | $\lambda_1 + \lambda_2$ | $n + n' + n_d + n'_a[H^+]$ |
| $n(n' + n'_d) + n'n_a[B]$ | $\lambda_1\lambda_2$ | $n(n' + n'_a[H^+]) + n'n_d$ |

(12)

*1.2.1. The δ-responses*

By the Laplace procedure (or another one) we find from Eqs. (10)

$$X_\delta = -\frac{\lambda_1 + n_{22}}{\lambda_2 - \lambda_1} e^{-\lambda 1 t} + \frac{\lambda_2 - n_{22}}{\lambda_2 - \lambda_1} e^{-\lambda 2 t}$$

$$Y_\delta = \frac{n_{21}}{\lambda_2 - \lambda_1} (e^{-\lambda 1 t} - e^{-\lambda 2 t}) \tag{13}$$

(With respect to Eqs. (11) various equivalent preexponential factors can be written). If at least one of the biexponential functions can be measured there are various procedures to determine $\lambda_1$ and $\lambda_2$, from which, as we have seen, the kinetic constants can be ascertained. Practically, this '$\lambda$-procedure' will function only if $\lambda_1$ and $\lambda_2$ are sufficiently different, factor ...23 at least, and if the participating processes are not too fast. In many cases of partical importance $\lambda_2 \simeq 300$ ps needing 20...30 ps time resolving power, which no commercially available decay time measuring apparatus really affords with biexponential problems. Usually only the slower time constant $\lambda_1$ can be measured which is of less significance.

*Fig. 1* shows the result of a discussion of Eqs. (10a) for an excimer system. We see that $n < \lambda_1 < n'$. As $n'_d$ may be $10^8 \ldots 10^9\,s^{-1}$, $n_a[B]$ must then be of the same order of magnitude to give reasonable excimer formation and thus one needs a time resolution

in the ps region. Fortunately, the time dependent measurements can be combined with stationary results; otherwise FES kinetic analysis would be restricted to 'show' systems such as pyrene excimers [3].

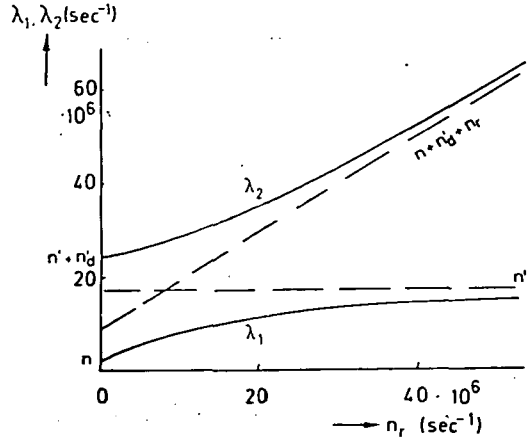


*Fig. 1.*

*1.2.2. The photostationary state*

The procedure of solving Eqs. (10) with $I_a = I_{as} = \text{const.}$ is not simpler than applying Eq. (7) to Eqs. (13), which can be done without specifying for the *l.h.s.* or *r.h.s.* scheme. We get

$$X_s = -I_{as}\frac{n_{22}}{\lambda_1\lambda_2} \quad Y_s = I_{as}\frac{n_{21}}{\lambda_1\lambda_2} \tag{14}$$

Inserting the *l.h.s.* constants of *List 1* we get the Stern—Volmer-relation and a complementary one

$$\frac{F_{Aso}}{F_{As}} = 1 + [B]/[B]_{1/2} \quad \frac{F_{ABs\infty}}{F_{AB}} = 1 + [B]_{1/2}/[B]. \tag{15}$$

With the common 'half value concentration'

$$[B]_{1/2} = \frac{n(n' + n'_d)}{n' n_a} \tag{16}$$

In Eqs. (15) the index *'Aso'* means 'of species $A$ in the stationary state at concentration $O$'. Index '$ABS\infty$' means 'species $AB$, stationary at concentration versus $\infty$'. In both formulae, '$o$' and '$\infty$' are sometimes replaced with 'max'. Moreover, in accordance with reasons given in the context of Eq. (4), the quotients of total fluxes Eqs. (15) may be replaced with the quotients of

i) relative fluxes ('intensities')
ii) quantum yields $\varphi_{I_{max}}/\varphi_I$
iii) amounts of excited species $\langle I^*\rangle_{max}/\langle I^*\rangle$, where $I^*$ means $A^*$ or $(AB)^*$.

Finally, introducing the quantum yield quotients in Eqs. (15) we find what sometimes

is called the 'adiabaticity relation'

$$\frac{\Phi_A}{\Phi_{A\max}} + \frac{\Phi_{AB}}{\Phi_{AB\max}} = 1 \tag{17}$$

Eqs. like (17) will hold for all systems, where processes deactivating excited species (to the ground state) are in competition with the adiabatic processes (producing excited species) exclusively and no additional deactivation taking place 'in between' excited educt and product. Eqs. (15)—(17) were derived for the exciplex/excimer systems *l.h.s.* For the FES protolytic reactions and possibly for other systems obeying the *r.h.s.* scheme, no such symmetrical Stern—Volmer type equations as (15) are valid. If $[H^+]=0$ we get $\varphi_{A^-max}=\frac{n_d}{n+n_d}\cdot\frac{n'_e}{n'}$ and simultaneously $\varphi_{AH\,min}=\frac{n_e}{n+n_d}$ whereas $\varphi_{AH\,max}=\frac{n_e}{n}$ with. $[H^+]\to\infty$ as can be derived from Eqs. (14) inserting the constants of *List 1*, *r.h.s.*, and rule 4. Instead of Eqs. (15) we have

$$\left(\frac{F_{AHs\infty}}{F_{AHs}}-1\right)^{-1} = \frac{n}{n_d}\left(1+\frac{n'_a[H^+]}{n'}\right) \quad \frac{F_{A^-so}}{F_{A^-s}} = 1+\frac{n'_a[H^+]}{(n+n_d)n'} \tag{18}$$

Remarks i)—iii) (behind Eq. (16)) and a relation corresponding to Eq. (17) are valid, too. The more complicated behaviour Eqs. (18) allows the kinetic analysis to be performed almost completely in the stationary state, as was done by Weller as long ago as the 50ies! Another relation, which is valid for both reaction schemes again, follows immediately from the second Eq. (10)

$$\frac{Y_s}{X_s} = -\frac{n_{21}}{n_{22}} \tag{19}$$

Refering to List 1 and making use of remarks i)—iii) various useful formulae may be derived from Eq. (19). It is true, a Stern—Volmer procedure does not need the spectral characteristics of the instrument to be known as is the case with Eq. (19) and relations derived from it. The most commercially available fluorescence spectrometers measure wrong if the penetration depth of excitation changes or if cuvettes with optical disadvantages (such as tubes) are used. The quotient of two fluorescence components, however, is measured correctly in such cases even with turbid samples. Instrument manufacturers have solved the problem of allowing for different spectral characteristics much better than that of changing sample geometry. Fluorescence probing in biological systems for investigation of surface phenomena *etc.* is preferably based on Eq. (19).

### *1.2.3. Phase fluorimeter responses (two excited species)*[4]

With the Eq. (7) procedure we find from Eqs. (8) and (13)

$$X_p = I_{as}\left(-\frac{n_{22}}{\lambda_1\lambda_2}+pe^{i\omega t}\,\frac{(i\omega-n_{22})[\lambda_1\lambda_2-\omega^2-i\omega(\lambda_1+\lambda_2)]}{(\lambda_1\lambda_2-\omega^2)^2+\omega^2(\lambda_1+\lambda_2)^2}\right. \tag{20a}$$

$$Y_P = I_{ah}\left(\frac{n_{21}}{\lambda_1\lambda_2}+pe^{i\omega t}n_{21}\,\frac{\lambda_1\lambda_2-\omega^2-i\omega(\lambda_1+\lambda_2)}{(\lambda_1\lambda_2-\omega^2)^2+\omega^2(\lambda_1+\lambda_2)^2}\right). \tag{20b}$$

Both Eqs. (20) and (20b) may be brought to the form of Eq. (9)

$$X_P = -I_{as}\frac{n_{22}}{\lambda_1\lambda_2}(1+pe^{i(\omega t-\Psi)}) \tag{21a}$$

$$Y_P = I_{as}\frac{n_{21}}{\lambda_1\lambda_2}(1+re^{i(\omega t-x)}) \tag{21b}$$

The expression for the phase angle $\Psi$ of the primarily excited species

$$\omega\cot\Psi = \frac{(\omega^2-\lambda_1\lambda_2)n_{22}+\omega^2(\lambda_1+\lambda_2)}{\lambda_1\lambda_2-\omega^2+(\lambda_2+\lambda_2)^2} = \frac{n_{12}n_{21}n_{22}-n_{11}(\omega^2+n_{22}{}^2)}{n_{12}n_{21}+n_{22}{}^2+\omega^2} \tag{22a}$$

is not simple and needs curve fitting for evaluation. The expressions for the 'modulation degrees' $p$ and $r$ following from Eq. (20) may be omitted as these parameters are difficult to measure with reasonable accuracy. The phase angle $\chi$ of the secondarily excited species, however, is very convenient for evaluation

$$\omega\cot X = \frac{\lambda_1\lambda_2-\omega^2}{\lambda_1+\lambda_2} \tag{22b}$$

By plotting the *l.h.s.* of Eq. (22b) versus $\omega^2$ one gets $\lambda_1\cdot\lambda_2$ and $\lambda_1+\lambda_2$ from straight line parameters. Having performed these measurements for various concentrations of the unexcited reaction partner, Eqs. (12) are applied to find the kinetic constants. One can see that phase fluorometry at a set of different frequencies is essentially equivalent to measuring $\delta$-responses.

Finally we get a simple relation between measurable parameters and kinetic constants by first forming the ratio of periodic and constant term in Eqs. (20a) and (20b), respectively, and then the quotient of these ratios. With the notations of Eqs. (21) we get formally similar to Eqs. (9)

$$\frac{r}{p} = n_{22}(\omega^2+{}^2_{22})^{-1/2} = \cos(\chi+\psi); \quad -n_{22} = \omega\cot(\chi-\psi) \tag{23}$$

As only one parameter, $n_{22}$, is determined experimentally, the modulations degrees' quotient ma be a reasonable magnitude, too. The *r.h.s.* Eq. (23) which also may be derived from Eqs. (22a, b) is very useful in the *r.h.s.* cases of List 1.

## 2. FES kinetics with time dependent rate factors

It is a common feature of Förster—Galanin type energy transfer [5] ET and of diffusion controlled molecular encounter according to Smoluchowski's theory that the rate factors $k_{A\to B}$ and $k_{diff}$ of both these bimolecular processes explicitly depend on time. In Smoluchowski's expression

$$k_{\text{diff}} = k_{SE}\left(1+\frac{b}{t^{1/2}}\right) \tag{25}$$

the constant $b=10^{-4}...10^{-5}\ s^{1/2}$ allowing for non-stationary diffusion is small enough to be neglected in many cases, but the similar time dependence of ET is essential

$$\bar{k}_{A\to B} = [B]_o^{-1} \cdot \left(\frac{n}{t}\right)^{1|2} \tag{26}$$

$[B]_0$ denotes the critical concentration of unexcited acceptor $B$ and $n$ the reciprocal lifetime of the excited donor $A^*$ in the absence of $B$. While Eq. (65) is given in usual form, Eq. (26) is perhaps not so well known. ET kinetics is usually described by the decay function $F(t)/F(o)$ which means the relative fluorescence flux ('intensity') after $\delta$-excitation and is identical with

$$\langle A^*\rangle_\delta = \exp -\left(nt + 2\frac{[B]}{[B]_o}(nt)^{1/2}\right) \tag{27}$$

In the total rate of decay

$$\frac{d\langle A^*\rangle_\delta}{dt} = -\left(n + \frac{[B]}{[B]_0}\left(\frac{n}{t}\right)^{1/2}\right)\langle A^*\rangle_\delta \tag{27a}$$

we notice the rate factor $\bar{k}_{A\to B}$ given by Eq. (26) while $n$ describes the deactivation. The special type of ET kinetics [5] is a consequence of

*a)* the strong dependence of the fundamental transfer rate $n_{ET}$ on the distance $r$ of a donor-acceptor pair; $r_0$ denotes the critical distance $n_{ET}=n\left(\frac{r_0}{r}\right)^6$

*b)* the distribution of the (great number of) unexcited acceptors in the surrounding of any excited donor. The form of Eqs. (26) and (27) is characteristic of homogeneous random three dimensional distribution. Other dimensionalities and/or spatial limitations of distribution will give rise to functions different from Eqs. (26) and (27) and thus may be recognized [6]. It was shown some time ago [7] that processes with time dependent rate factors such as Eqs. (25) and (26) must not be contained in kinetic differential equations as results turn out to be more or less nonsensical. This can shortly be seen for instance from Eq. (16) by replacing $n_a$ with $\bar{k}_{A\to B}$ from Eq. (26). In the stationary state $t\to\infty$ we get $[B]_{1/2}\to\infty$ which means no ET taking place at finite acceptor concentrations $[B]$ and no $B^*$ being formed. Really the whole concept of kinetic differential equations is valid only if all participating processes obey coefficients or rate factors which are independent of time!

Only the response on direct $\delta$-excitation is equally fundamental with and without time dependent rate factors. This so-called ideal decay function must be known from statistical calculations [5, 6] or ultimately by experiment then allowing all cases of kinetic schemes and types of excitation to be treated by the general mathematical procedure called 'convolution kinetics'. On direct excitation the ideal decay function $f_\delta$ is identical with the $\delta$-response, *e.g.* $\langle A^*\rangle_\delta = f_{A\delta}$ in the case of Eq. (27) but for the kinetically formed species $Y$ in section 1.2, $f_{Y\delta}=\exp(-n_{22}t)$ and is not given by $Y_\delta$ from Eq. (13).

In one of the simplest but non trivial cases of convolution kinetics direct excitation of $A$ by light with $I_a(t)$

$$\begin{array}{ccc} & A^* \xrightarrow{k(t)} & B^* \\ I_a \nearrow & \downarrow n & \downarrow n' \\ & A & B \end{array}$$

strangely enough Eq. (7) from section 1.13 should be applied to get

$$\langle A^* \rangle = I_a * f_{A\delta} \tag{7}$$

In the case of ET, $k(t)$ in the above scheme is given by Eq. (26) and $f_{A\delta} = \langle A^* \rangle_\delta$ is given by Eq. (27). In the important stationary case $I_a = I_{ao}$ const. we get from Eq. (7) by calculating the convolution integral

$$\langle A^* \rangle_s = \frac{I_{ao}}{n} (1 - \sqrt{\pi}\gamma \exp \gamma^2 \operatorname{erfc} \gamma) \tag{28}$$

$$\gamma = [B]/[B]_o$$

Eq. (28) is is accordance with Förster's result [5] which was derived in another way (but is misprinted in the original paper).

It should be noticed that with time dependent $k(t)$ Eq. (7) cannot be derived by the differential equations procedure nor by Laplace transform. Consequently Eq. (28) needs a reasonable foundation, too. In order to justify the use of Eq. (7) with $k(t)$ we could refer to Kubo's linear response theory[8]. The next question for the time dependence of $\langle B^* \rangle$ is not answered by this theory, much less how to treat more complicated reaction schemes. A new complete general procedure will be given below. Before this Eq. (28) deserves some more attention.

Without much reasoning, $\langle B^* \rangle_s$ for the stationary state is derived with the aid of the adiabaticity relation Eq. (17) knowing that $\langle A^* \rangle_{smax} = I_{ao/n}$ and $\langle B^* \rangle_{smax} = I_{ao/n'}$ (as for $\gamma \to \infty B^*$ behaves like it were directly excited). We get

$$\langle B^* \rangle_s = \frac{I_{ao}}{n'} \sqrt{\pi}\gamma \exp \gamma^2 \operatorname{erfc} \gamma \tag{28a}$$

Moreover, as there is no backward step in the reaction scheme, we can find the phase fluorimeter response $\langle A^* \rangle_p$ by the replacement procedure $n \to n + i\omega$, *cf.* section 1.14. But as $n$ is contained in $\gamma$, too, we additionally must replace $\gamma \to \gamma \cdot \left(\frac{n}{n+i\omega}\right)^{1/2}$ in Eq. (28). Using the tabulated values [9] of the complex erfc, $\langle A^* \rangle_p$ follows in closed form (needing no numerical approximation, but collecting the real and imaginary parts is laborious). Finally, as can be later clearly understood, $\langle B^* \rangle_p$ would follow consequently from Eq. (28a) with the $\gamma$ transform mentioned and $n' \to n' + i\omega$.

### *2.1. Introduction to the new concept of 'convolution kinetics'*

As we mentioned already, the ideal decay function $f_{X\delta}$ of excited species $X^*$ (on direct excitation being identical with $\langle X^* \rangle_\delta$) is considered as fundamental for the behaviour of $X^*$ in FES kinetics. In order to find $f_{X\delta}$ we may need to solve a master equation as with ET [5]. But for systems with time-independent rate factors only, $f_{X\delta}$ follows from ordinary FES kinetics presented in main section 1. In the final analysis questions concerning the ideal decay function must be decided by experiment.

Excitation with the intensity $I_a(t)$, (more correctly speaking $I_a(t)$ is a flux distribution), has the same effect as excitation with a continuous sequence of short pulses

similar to $\delta$-functions with area $I_a(\vartheta)d\vartheta$. Thus $I_a(t-\vartheta)d\vartheta$ produces at time $t-\vartheta$ an incremental amount of excited molecules $d\langle A^*\rangle$, decaying during the time interval $\vartheta$ according to $f_{A\delta}$ up to the remainder $I_a(t-\vartheta)\cdot f_{A\delta}(\vartheta)\cdot d\vartheta$. The total amount of $\langle A^*\rangle$ at time $t$ result from the sum (integral) of all such remainders generated by all foregoing incremental $\delta$-excitations. The procedure of summing up these remainders is nothing else but the convolution Eq. (7) in the form given in section 1.1.3. Thus the general significance of Eq. (7) is established.

We now understand why the rate of change of a population $\langle A^*\rangle$ or $\langle X^*\rangle$ is in general not given by its time derivative. This may be illustrated by many examples. In order to predict the development of the number of students at a university, one must know the time dependent probability of a student's stay there $\sim f_{St\delta}$, but the total number of students at any time $\sim\langle St\rangle$ is of little use. One must know how many students are in the first year, second year, and so on. This detailed information would not be needed if the probability of stay were described by a time independent rate factor *viz.* were given by a simple exponential $f_{St\delta}\infty e^{-nt}$. The latter is usually the case in chemical kinetics then justifying the well known concept of rate constants.

Allowing for the age structure of a population, or in other words its temporal inhomogeneity, by the convolution concept depends on the following prerequisits: The individuals neither interact nor interfere, (the latter means no square or higher terms in number or concentration), and there is a unique ideal decay function (= time dependenee of the probability of belonging to the population).

For completeness and for practical reasons we need a procedure for treating excitation of species $B^*$ on the expense of the precursor $A^*$ by a photochemical process. In case that $\langle A^*\rangle$ was $\delta$-excited, the total rate of its depopulation will be a sum of as much terms as there are contributing processes

$$\frac{df_{A\delta}}{dt} = -\sum k_i f_{A\delta} \tag{29}$$

The $k_i$ may or may not depend on time and/or concentration of unexcited reaction partner. In the general Eq. (27) the total rate is given by Eq. (27.a). In the general Eq. (29) the term $k_j f_{A\delta}$, say, is increasing $\langle B^*\rangle$ at the expense of the precursor. At time $t-\vartheta$ the incremental amount $k_j f_{A\delta}(t-\vartheta)d\vartheta$, is produced from which the remainder which is still excited at time $t$ is got by the factor $f_{B\delta}$, thus

$$\langle B^*\rangle/_{A(\delta)\to B} = \int_0^t k_j f_{A\delta}(t-\vartheta) f_{B\delta}(\vartheta)\, d\vartheta = k_j f_{A\delta} * f_{B\delta} \tag{30}$$

Index$/_{A(\delta)\to B}$ means $B^*$ is produced from $A^*$ which was $\delta$-excited; for this case we solved the problem. In the case of Eq. (27), $k_j = \gamma\left(\frac{n}{t}\right)^{1/2}$ ($\gamma = [B]/[B]_o$). The whole 'production term' is here

$$p_{A(\delta)\to B} = k_j f_{A\delta} = -\left(\frac{df_{A\delta}}{dt} + n f_{A\delta}\right) \tag{31}$$

which means that we take only the term producing $B^*$ from $A^*$. If $A^*$ is excited by general light absorption $I_a(t)$, (direct excitation is the mark of species we denote $A$),

we get as $I_a$ means a sequence of quasi $\delta$-impulses

$$\langle B^* \rangle|_{A(I_a)\to B} = I_a * \langle B^* \rangle|_{A(\delta)\to B} \tag{32}$$

and making use of Eq. (30). Obviously, the production term of $A^*$ is identical with $I_a(t)$

$$p_{(I_a)\to A} = I_a \tag{33}$$

Finally, $B^*$ could be the precursor of $C^*$. Then we find

$$\langle C^* \rangle|A(I_a) \to B \to C = I_a * p_{A(\delta)\to B} * p_{B\to C} * f_{C\delta} = p_C * f_{C\delta} \tag{34}$$

A general straight forward procedure is given in the next section, where the construction of production terms is explained. If backward steps and/or direct excitation of more than 1 species take place, sums of production terms are incorporated.

### *2.2. The basic rules of convolution kinetics*

I) The amount of excited species $X^*$ is found by convolution of its production term $p_X$ with its ideal decay function (= $\delta$-response on direct excitation).

$$\langle X^* \rangle = p_X * f_{X\delta}$$

II) The production term $p_X$ is given by convolution of the $p_{X-1}$ of the precursor $X-1$ with the derivative of its ideal decay function $df_{X-1,\delta}/dt$ omitting the terms not producing $X^*$ from $X^*-1$.

III) The production term $p_A$ of the primary excited species is given by the absorbed excitation flux (density) $I_a$.

If more than 1 species is directly optically excited, $I_a$ must be split. With chemical excitation, branching and backward steps (giving somewhat like loops of production terms) may be incorporated.

Rules I—III are valid in cases of constant coefficients, too, as convolution kinetics are the more general, superimposed procedure. Rule 4 of section 1 which connects fluorescence to the amounts of excited molecules is valid in convolution kinetics without change.

### *2.3. Experimental proofs and applications of convolution kinetics*

The breakdown of ordinary kinetics with time dependent rate factors is most obvious in all types of photostationary experiments to which phase fluorimetry formally belongs, too. On the other hand, discrepancies between convolution kinetics and the old kinetics become smaller the more the excitation is similar to direct $\delta$-excitation which is not possible for excimers and other excited photoproducts. Anyway, time dependent measurements are more conclusive in FES kinetics as a consequence of ambiguity of stationary fluorescence measurements because of *e.g.* static quenching and spurious effects.

2.3.1. The first dynamic test of convolution kinetics [10] was performed with pyrene excimer $(AA)^*$ as the donor and diethylthiacarbocyanine iodide $C$ as the acceptor in ET, whereby the excimer was generated chemically after practically $\delta$-shaped

excitation of the monomer $A$: $I_a = I_{ao} \cdot \delta(0)$ with $I_{ao} = \text{const}$. The concentration $[A] \ll [A]_{1/2}$ was chosen small enough to get a significantly biexponential time dependence of $\langle (AA)^* \rangle$, *cf.* Eq. (13) and list 1.

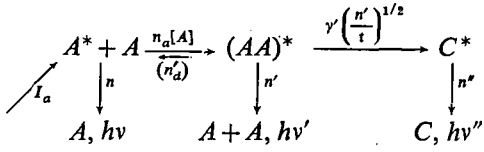


With pyrene excimers, $n'_d \approx 0$ below room temperature. So it is easier to control that direct ET $A^* \rightarrow C$ does not take place. Anyway the acceptor concentration must be small $\gamma = [C]/[C]_o \leqq 0.2$.

Considering the reaction scheme and applying rules I—III we get

$$\begin{aligned}
&a)\ p_A = I_a = I_{ao}\delta(0) && d)\ f_{A\delta} = \exp -(n + n_a[A])t \\
&b)\ p_{AA} = p_A * n_a[A] f_{A\delta} && e)\ p_{AA\delta} = \exp -(n't + 2\gamma'\sqrt{n't}) \\
&c)\ p_C = p_{AA} * \gamma' \left(\frac{n'}{t}\right)^{1/2} f_{AA\delta} && f)\ f_{C\delta} = \exp -n''t
\end{aligned} \tag{35}$$

If $I_a$ were not $\delta$-shaped, one convolution more with $I_a(t)$ would be necessary for constructing the production terms. Finally

$$\begin{aligned}
&a)\ \langle A^* \rangle = I_{ao} f_{A\delta} \\
&b)\ \langle (AA)^* \rangle = I_{ao} n_a[A] f_{A\delta} * f_{AA\delta} \\
&c)\ \langle C^* \rangle = I_{ao} n_a[A] f_{A\delta} * \gamma' \sqrt{n't}\, f_{AA\delta} * f_{C\delta}
\end{aligned} \tag{36}$$

While Eq. (36a) is the same as one gets from the differential equation (since coefficients are constant), one would find for the excimer $AA^*$ by applying usual solving methods of linear differential equations

$$\langle (AA)^* \rangle = I_{ao} n_a[A] \exp -(n't + 2\gamma'\sqrt{n't} \int_{\vartheta=o}^{t} \exp(n'\vartheta + 2\gamma'\sqrt{n'\vartheta} - (n' + n_a[A])\vartheta)\, d\vartheta$$

according to this (wrong) equation the terms $\gamma'$ describing the influence of ET are insignificant except at the very beginning, which could be shown by calculating the integral in closed form. The (correct) Eq. (36b) reads explicitly

$$\langle (AA)^* \rangle = I_{ao} n_a[A] \exp\{-(n - n_a[A])t\} \int_{\vartheta=o}^{t} \exp\left((n + n_a[A])\vartheta - n'\vartheta - 2\gamma'\sqrt{n'\vartheta}\right) d\vartheta \tag{37}$$

In this equation, where also the integral can be calculated in closed form, ET keeps its influence during the whole time of interest. From the above wrong equation, $\langle (AA^*) \rangle$ is proportional to Dawson's function $D(\sqrt{n't} + \gamma')$ which vanishes for large values of the argument, while from Eq. (37) $\langle (AA^*) \rangle$ is really proportional to erf $(\sqrt{n't} + \gamma')$ approaching unity for larger values of the argument.

Altogether, the discrepancies between correct and wrong treatment are not very pronounced with the excimer, mainly because $\gamma' \leqq 0.2$ is rather small. Yet if the excimer quantum efficiency is calculated from

$$\Phi' = \frac{n'_e \int_0^\infty \langle (AA^*) \rangle \, dt}{\int_0^\infty I_a \, dt} \tag{38}$$

using the separately measured kinetic constants and $[A] = 0.02$ M

$$n = 2.9 \times 10^6 s^{-1} \quad n' = 33.8 \times 10^6 s^{-1} \quad n_a = 8.6 \times 10^7 M^{-1} s^{-1}$$

the dependence of $\Phi'$ on $\gamma'$ agrees very well with the theory. (solvent was a cyclohexanol/paraffin oil mixture).

Inserting the constants in the above wrong equation $\Phi'$ is calculated about 30% too large at $\gamma' = 0.18$ (by underestimate of ET).

The disproof of the old kinetics and verification of convolution kinetics become convincingly significant when looking at $C^*$. The production term Eq. (35c)

$$p_C = I_{a0} n_a [A] \exp -(n + n_a[A]) t \cdot 2 \int_{\vartheta=0}^{t} \exp -(n' - n - n_a[A]) \vartheta - 2\gamma' \sqrt{n' \vartheta} \, d\sqrt{n' \vartheta}$$

can also be calculated exactly. As in our case $n' \gg n + n_a[A]$ we get to a good approximation

$$p_C \approx I_{a0} n_a [A] \exp -(n + r_a[A]) t \gamma' \exp \gamma'^2 \sqrt{\pi} [\operatorname{erf}(\sqrt{n' t} - \gamma') - \operatorname{erf} \gamma']$$

With $\gamma' = 0.18$ the term in square brackets becomes $\approx 0.8$ for $t < 2/n' \approx 60$ ns, while the duration of all three responses Eq. (36) are about 300 ns. Making use of the approximation

$$p_C \approx I_{a0} n_a [A] \exp -(n + n_a[A]) t \gamma' \exp \gamma'^2 \sqrt{\pi} \tag{39}$$

we get instead of the exact Eq. (36c)

$$\langle C^* \rangle \approx I_{a0} n_a [A] \sqrt{\pi} \gamma' \exp \gamma'^2 \frac{\exp -(n + n_a[A]) t}{n'' - n - n_a[A]}$$

Analogously to Eq. (38) and making use of $n'' \gg n + n_a[A]$, which was measured $n'' = 6.6 \times 10^8 s^{-1}$, we get for the quantum efficiency of the acceptor $C$ (the cyanine dye)

$$\Phi'' \frac{n''}{n''_e} = \frac{\Phi''}{\Phi''_0} \approx \frac{\sqrt{\pi} \, n_a [A] \gamma' \exp \gamma'^2}{n + n_a[A]} \tag{40}$$

$\Phi''_o = \frac{n''_e}{n''} = \frac{\Phi''}{\Phi''}$ means the quantum yield on direct excitation of $C$, which was determined separately $\Phi''_o = 0.72$.

Eq. (39) as well as Eq. (40) were found in excellent agreement with the experimental results: The slowest preceding process is the decay of excited pyrene monomer

$A^*$ with time law exp $-(n+n_aA)t$, which must be rate controlling for the fast decaying species $C^*$, too. This was clearly observed from the time dependence of $C^*$ fluorescence*** in accordance with Eq. (39) and with the exact Eq. (36c). From the old kinetics applied to the reaction scheme we get

$$\frac{d\langle C^*\rangle}{dt} = -n''\langle C^*\rangle + \gamma'\left(\frac{n'}{t}\right)^{1/2}\langle (AA)^*\rangle$$

Consequently inserting $\langle (AA)^*_\cdot\rangle = \ldots$ from the "wrong companion" of Eq. (37) and tediously solving that differential equation, we get a 30% faster decay. The relative quantum efficiency following with $\gamma'=0.18$ from Eq. (40) is $\Phi''/\Phi''_0=0.11$ while the experimental value was 0.12. In convolution kinetics, quantum efficiency is the same irrespective whether Eq. (40) or the stationary treatment is applied. The experimental evaluation of Eq. (40) needs the areas under the fluorescence time dependences (decay functions) to be compared with integral intensity of the excitation flash, what was practised by direct excitation of $C^*$. With the old kinetics inserting the (wrong) function $\langle C^*\rangle$ which we get from the above differential equation into Eq. (40), we get $\Phi''/\Phi''_0=0.025$ at $\gamma'=0.18$ what is some 100% wrong; calculating the photostationary efficiency gives the totally nonsensical result $\Phi''=0$(!). The reason why the breakdown of the differential equations procedure is more striking with $C^*$ than with the excimer $(AA)^*$ comes from that ET is only moderately diminishing $\Phi'$ of $(AA)^*$, but $\Phi''$ is compared to zero efficiency.

### *2.3.2. Multistep ET.*

In the case of self overlap of the fluorescence spectrum with the absorption spectrum of the same molecule, which is realized *e.g.* with perylene and may fluorescent dyes, $\gamma \approx 1$ and even more is possible.

The reaction scheme is

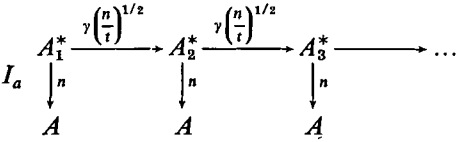


The index $i=1, 2, \ldots$ of $A_i^*$ means ... excited in the first, second, ... step. All ideal decay functions $f_{i\delta}$; $i=1, 2, \ldots$ are the same:

$$f_\delta = \exp -\left(nt + 2\gamma\sqrt{nt}\right) \tag{41}$$

and the term $r$ by which the recursion from $p_i$ to $p_{i-1}$ is given, is also the same for all $p_i$

$$r = \gamma\left(\frac{n}{t}\right)^{1/2} f_\delta = -\left(\frac{df_\delta}{dt} + nf_\delta\right) \tag{42}$$

*** All time dependences of fluorescence were measured with ORTEC single photon counting system

as it follows from Eq. (41). Thus we get from the reaction scheme if $I_a=\delta(0)$

$$\begin{aligned}\langle A_1^*\rangle &= f_\delta \\ \langle A_2^*\rangle &= f_\delta * r \\ \langle A_3^*\rangle &= f_\delta * r * r \\ &\cdots \\ \langle A_i^*\rangle &= f_\delta * r * r * \ldots \\ &\qquad (\mathrm{i}-1 \text{ terms})\end{aligned} \tag{43}$$

Unfortunately, there is no power type notation for repeated convolution of equal terms. The Laplace transform of Eq. (42) reads if we denote $Lf_\delta=g$ and $Lt=x$

$$Lr = -(xg-1+ng) = -g(x+n) \tag{44}$$

The individual $\langle A_i^*\rangle$ cannot directly be measured, however, the sum

$$\langle A^*\rangle = \sum_{i=1}^{\infty} A_i^*$$

With the transform of the sum we obtain with Eqs. (43) and (44)

$$L\langle A^*\rangle = g\sum_{i=1}^{\infty}[1-g(x+1)]^{i-1} = \frac{g}{1-[1-g(x+n)]} = \frac{1}{x+n} \tag{45}$$

The result of the backward transform of the surprisingly simple Eq. (45) is

$$\langle A^*\rangle = L^{-1}\frac{1}{x+n} = \exp -nt \tag{46a}$$

In the corresponding case of multistep collisional transfer with $n_a[A]$ instead of $\gamma\left(\frac{n}{t}\right)^{1/2}$ one gets the same final formula Eq. (45). But ET is very fast over distances shorter than the critical distance which may give raise to random walk of excitation; $\gamma \geqq 1$ means that about 1/3 of excited donors $A^*$ do have 2 or more acceptors $A$ within the critical distance. Quenchers (*e-g.* impurities) without a normal chance of interaction with $A^*$ may act as traps if excitation reaches an $A$ in their neighbourhood; one may speak of a Förster—Galanin exciton (even in homogeneous solutions). Decisive experiments on that field are extremely difficult to realize because many trivial effects may strongly influence the results. Our latest approach was:

*2.3.4. Energy transfer in two steps* [11]

The reaction scheme differs from that of section 2.3.2 so far as the first donor $A$ as well as the first acceptor (=second donor) $B$ and the second acceptor $C$ are different molecules; thus $\gamma\left(=\frac{[B]}{[B]_o}\right)$ and $\gamma'\left(=\frac{[C]}{[C]_o}\right)$ may be chosen arbitratily (within the limits of preventing undesired other effects).

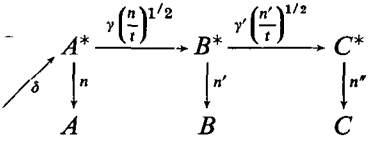


A system which was expected to fulfill the most important prerequisits fairly well is with

$A$=1, 2-Benzofluorene; $1/n$=55 ns

$B$=9, 10-Diphenylanthracene; $1/n'$=8.1 ns

$C$=Dimethyloxacarbocyanine iodide; $1/n''$=0.6 ns

in the solvent cyclohecanol/triethyleneglycol 4:1 with the viscosity 49 cp. The absorption and fluorescence spectra together with properly chosen concentrations, $\gamma$=0,75 and $\gamma' \leqq 0.46$, guarantee direct optical excitation of $A$ only and negligible immediate ET $A^* \rightarrow C$. Trivial reabsorption of $A^*$ fluorescence by $B$ and/or $C$ does not exceed 5%. $B^*$ fluorescence is more strongly reabsorbed by $C$, but this does not influence the time dependence of $\langle B^* \rangle$. As $A$ shows very small self overlap, ET $A^* \rightarrow A \rightarrow B$ and $A^* \rightarrow A \rightarrow C$ are negligible, only $B^* \rightarrow B \rightarrow C$ may have a small influence.

Having some experience with convolution kinetics already and supposing $I_a = I_{ao} \cdot \delta(0)$ we may write down immediately

$$a) \qquad \langle A^* \rangle = I_{ao} \exp -(nt + 2\gamma\sqrt{n}\,t)$$

$$b) \qquad \langle B^* \rangle = \langle A^* \rangle \gamma \left(\frac{n}{t}\right)^{1/2} * \exp -(n't + 2\gamma'\sqrt{n'}\,t) \qquad (46b)$$

$$c) \qquad \langle C^* \rangle = \langle B^* \rangle \gamma' \left(\frac{n'}{t}\right)^{1/2} * \exp -n''t$$

The convolution integral in the kinetically most significant Eq. (46b) must be computed numerically. $\langle C^* \rangle(t)$ was not expected to be very different in shape comparing the differential equations result and that of convolution kinetics, however, its quantum efficiency.

As expected, the over alltime dependences are all similar to $\langle A^* \rangle$ which is rate controlling. A significant feature of $\langle B^* \rangle$, when normalized to equal maximum height with $\langle A^* \rangle$, is an overshoot with Eq. (46b) and in disagreement with the old kinetics. But as regards the most exciting expectation, the quantum efficiency of $C^*$ fluorescence, the experiment was disappointing: As was especially significant with stationary

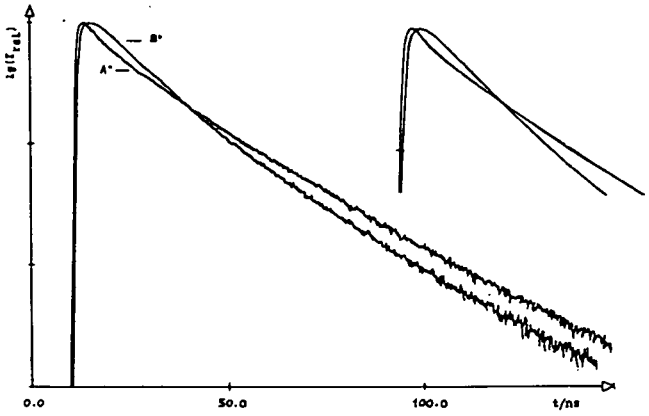


*Fig. 2.* Measured and calculated fluorescence time dependences of $A^*$ and $B^*$; (the old kinetics give practically no overshoot). The time dependence of $C^*$, whichis not shown, is very similar to that of $B^*$. Concentrations $[A]=2.0\cdot10^{-2}$; $[B]=8.8\cdot10^{-3}$; $[C]=1.55$ mol/l, each.

measurements, ET $B^*\rightarrow C$ is strongly violating the adiabaticity principle. This seems to be a very general effect, which we observed with $C$=Trypaflavine, Safranine T, Acridine Yellow, Acridine Red, *etc.* (but not with Uranine in alkaline media). As $B^*$ lifetime is $<10$ ns and the concentrations $[C]<5\times10^{-3}$ M, a static quenching effect must be operative; no significant deviations in the time dependences $\langle B^*\rangle$ and $\langle C^*\rangle$ were observed and, of course, no influences in the absorption spectra. We postulate complexes in the ground state $(BC)$, weak enough not to influence the ET acceptor features of $B$- or $C$-part but preventing emission mainly of $C$ as $[C]\ll[B]$.

This new static quenching effect is also observed if $C$ is excited directly and $B$ is added, even though $B$ absorbes only at much shorter wavelengths.

### *2.2.4. Concluding remarks*

The understanding of FES kinetics with time dependent rate factors should be critically revised on the basis of the new concept presented here. Many conclusions from using Förster—Galanin ET as a spectroscopic ruler have been more or less wrong, as perhaps has been the case with nonstationary diffusion phenomena often obscured as cage effects.

#### References

[1] *Förster, Th.:* Ber. Bunsenges. **73**, 737 (1969).
[2] *Weller, A.:* Progress in Reaction Kinetics, Vol. **1**, 187 (1961). Pergamon Press, Oxford, London.
[3] *Birks, J. B., D. I. Dyson, I. H. Munro:* Proc. Roy. Soc. A **275**, 575 (1963).
[4] *Hauser, M., G. Heidt:* Z. Phys. Chem. N. F. **69**, 261 (1970).
[5] *Förster, Th.:* Ann. Phys. **2**, 55 (1948); Z. Naturforsch. **4A**, 321 (1949). *Galanin, M. D.:* Soviet Physics JETP **1**, 317 (1955); Trudy Fiz. Inst. Akad. Nauk **161**, 255 (1960).[1]

[6] *Hauser, M., U. K. A. Klein, U. Gösele:* Z. Phys. Chem. N. F. **101**, 255 (1976).
[7] *Hauser, M., R. Frey, U. K. A. Klein, U. Gösele:* Acta Phys. et Chem. Szeged **23**, 21 (1972).
[8] *Kubo, R.:* J. Phys. Soc. Japan **12**, 570 (1957).
[9] *Abramowitz, M., I. A. Stegun:* Handbook of Math. Functions, Dover Publ. New York (1965).
[10] *Hauser, M.:* in "Time Dependent Fluorescence Spectroscopy", ASI Plenum, New York (to be published).
[11] *Wagner, W.:* Diplomarbeit, Stuttgart (1982).

## ФЛУОРЕСЦЕНЦИЯ И КИНЕТИКА ВОЗБУЖДЕННЫХ СОСТОЯНИЙ

*М. Хаузер*

В работе описивается четыре основных правила для описания кинетики процессов в первом возбужденном состоянии. Получены обобщенные формулы для исследования систем с одним и двумя родами возбужденных состояний для случая стационарной, фазово-флуорометрической, $\delta$ — образной и для произвольной формы возбуждения.

Доказано неприменимость обычных кинетических представлений в случае коэффициентов скорости зависящих от времени, особенно для случая передачи энергии типа Ферстера-Галанина и для нестационарной диффузии. Приводится новый кинетической приём в трёх правилах, названный кинетической свёрткой. — Сообщается динамическая проверка и примеры для вычисления (эксимер как донор и двухступенчатый перенос энергии).

# ANHARMONIC CONTRIBUTIONS TO VIBRATIONAL THERMODYNAMIC PROPERTIES OF IDEAL RARE-GAS CRYSTALS

By

C. MALINOVSKA-ADAMSKA

Institute of Physics, Technical University of Lódz

*(Received October 1, 1983)*

Using Singh's and Neb's potential, as a model of nearest neighbour central force interactions, the Helmholtz free energy, internal energy and specific heat at constant volume of ideal rare-gas crystals are evaluated in anharmonic approximation. The calculations are extended from the low to high temperatures.

Temperature dependences of the cubic and quartic anharmonic contributions to the thermodynamic functions are showed too.

Obtained results are compared with available experimental and other theoretical data.

## *Introduction*

The rare-gas crystals (RGC) are prototype of molecular crystals [1]. They crystallize in simple close-packed arrangements to be expected for atoms with spherical symmetry [2]. The lattice atoms interact with weak forces principally Van der Waals (V-d-W) attractions [3]. The existence of the V-d-W attraction terms necessitates the consideration of an additional repulsive energy to stabilize the crystal lattice of the spherical atom. This repulsive interaction is short-range and overlap dependent in nature.

Earlier results and theoretical calculations of the short-range repulsion and the long-range attractive portion for a variety of pairwise interactions of atoms in the RGC have been reviewed in the articles by POLLACK [3] and HORTON [4] and in the book of GOODISMAN [5]. Recently the critical analysis of the potential energy curves (PEC) appropriate for the RGC has been given by SINGH and NEB [6] who proposed new model PEC. Singh's and Neb's (S—N) potential consists of the attractive V-d-W force ($r^{-6}$) modified by the three-body interactions arising from the variable induced dipoles and the repulsive Born—Mayer interaction. This model potential used to the calculation of the isothermal elastic constants and some thermodynamical properties of the RGC at temperature $T = O\ K$ gave remarkably good agreement between theoretical and experimental results.

In this paper, using Singh's and Neb's PEC, we explore the temperature dependences of various thermodynamical functions like Helmholtz free energy $F$, internal energy $U$, specific heat at constant volume $C_v$ as well as cubic and quartic contributions to the above thermodynamic quantities in the anharmonic approximation [7, 8].

The computed results in the high and low temperature limits have been compared with available experimental data [9—11] and theoretical results obtained in terms of the renormalized Morse potential in the reduced second-order self-consistent phonon approximation [12] as well as for the Mie—Lennard—Jones potential in the anharmonic approach [13, 14].

*Thermodynamical functions of crystals*

The Helmholtz free energy of a crystal in anharmonic approximation can be written as [14]:

$$F(T) = F_{qh}(T) + F_3(T) + F_4(T), \tag{1}$$

where: $F_{qh}(T)$ is the free energy in the quasi-harmonic approximation,
$F_3(T)$ and $F_4(T)$ are the cubic and quartic anharmonic contributions to the Helmholtz free energy.

As was shown in [7, 8] $F_{qh}$, $F_3$ and $F_4$ in the high ($\theta \gg \omega_L$) and low ($\theta \ll \omega_L$) temperature limits are respectively given by:

$$F_{qh} = 3RT \cdot FO, \tag{2}$$

$$F_3 = -0.056\, N_A \theta^2 G, \tag{3}$$

$$F_4 = N_A K F Q, \quad \theta \gg \omega_L \tag{4}$$

and

$$F_{qh} = N_A FO, \tag{5}$$

$$F_3 = -0.7297\, E_o \gamma G N_A, \tag{6}$$

$$F_4 = 0.75\, N_A E_o K \cdot FQ, \quad \theta \ll \omega_L. \tag{7}$$

The symbols used in Eqs. (2)—(7) have the following meaning:

$$\theta = k_B T$$

$$\omega_L = \sqrt{8\hbar^2 \Phi''(r_e)/m}$$

$$\varphi''(r_e) = (\partial^2 \Phi(r)/\partial r^2)_{r=r_e},$$

$$G = (\Phi^{III}(r_e))^2/(\Phi^{II}(r_e))^3,$$

$$K = \Phi^{IV}(r_e)/(\Phi^{II}(r_e))^2,$$

$$\gamma = \theta\left(\frac{T}{\theta_0}\right)^3.$$

$$\theta_o = \theta_D[1 - 0.04166\, E_h(1.2997\, G - K)].$$

$E_o = E_h(1 - 0.041\,44\, E_h G)$ is the zero-point energy per atom for the mean separation $r_e$ in terms of its value $E_h = 1.0227\, \omega_L$ evaluated at the minimum of the potential energy $\Phi(r)$ in the strict harmonic approximation.

$R$, $N_A$, $k_B$, $\hbar$, $m$ and $\theta_D$ are the gas constant, Avogadro number, Boltzmann constant, Planck constant divided by $2\pi$, mass of atom and Debye temperature in the harmonic approximation, respectively.

The specific heat at constant volume $C_v$ and internal energy $U$ are related to the Helmholtz free energy by [15]:

$$C_v = -T\left(\frac{\partial^2 F}{\partial T^2}\right)_V, \tag{8}$$

$$U = F - T\left(\frac{\partial F}{\partial T}\right)_V. \tag{9}$$

If we substitute Eqs. (1)—(7) into Eqs. (8) and (9) we find immediately that in the high and low temperature limits, respectively, $C_v$ and $U$ are equal to:

$$C_v \approx 3R(1-CH(-0{,}04166\beta^2), \tag{10}$$

$$U \approx 3RT(1-UX) \text{ for } \theta \gg \omega_L, \tag{11}$$

and

$$C_v \approx \frac{12}{5}\pi^4 R\left(\frac{T}{\theta_o}\right)^3(1+CH), \tag{12}$$

$$U \approx N_A E_0(1-UX) \text{ for } \theta \ll \omega_L, \tag{13}$$

where the exact expressions for $FO$, $FQ$, $CH$ and $UX$ for the high and low temperature limits are given in the Appendix.

Applying the results of Eqs. (1)—(13) we obtain the thermodynamic functions of solids if $\Phi(r_e)$ is known. We have chosen here the Singh's and Neb's PEC [6] to represent the interatomic potential between atoms in the rare-gas crystals.

$$\Phi(r_e) = C_1[1+12f(r_e)]/r_e^6 + 12b\exp(r_e/p), \tag{14}$$

$$\text{where: } C_1 = 14.4539\ C,$$

$$f(r_e) = f_o \exp(-r_e/p).$$

$C$ and $b$ are the potential parameters which have been determined by help of the lattice constants and isothermal bulk modulus [6]. The other parameters $p$ and $f(r_e)$ have been expressed from the knowledge of overlap integrals reported by Hafemeister [16]. Numerical values of these parameters are collected in Table I.

*Table I.*

*Singh and Neb potential constants for the pairwise atomic interactions in the RGC*

| Solids | Parameters | | | |
|---|---|---|---|---|
| | $C$ $10^{-67}$ [Jm$^6$] | $b$ $10^{-19}$ [J] | $p$ $10^{-10}$ [m] | $f(r_e)$ |
| Ne | 35.908 | 679.329 | 0.2393 | 0.000 23 |
| Ar | 611.06 | 2021.062 | 0.3056 | 0.001 71 |
| Kr | 1474.60 | 2561.60 | 0.3347 | 0.003 03 |
| Xe | 3334.05 | 3099.70 | 0.3706 | 0.005 82 |

*Numerical results*

Using the values of model parameters, reported in Table I, we have computed the quasi-harmonic ($U_{qh}$), cubic ($U_3$) and quartic ($U_4$) anharmonic contributions to the zero-point energy (Table II). Obtained results are compared with those calculated for the Morse renormalized potential [12] and (12—6) Mie—Lennard—Jones model [14]. Table III shows the comparison of the experimental data for the molar heat at constant volume $C_v$ with calculated in terms of the above mentioned potentials. The experimental values of $C_v$ for Ne, Ar and Kr were obtained from the equation: $C_v = C_p - 9\alpha^2 T/\varkappa\varrho$ using measured data [9—11] for all quantities on the right hand side of the equation in which $C_p$ is the molar heat at constant pressure, $\alpha$-the linear coefficient of thermal expansion, $\varkappa$-the isothermal compressibility, $\varrho$-the density. The calculation $C_v$ for $X_e$ was impossible because of on incomplete experimental data set.

It is evident from Table III that the values of molar heat at constant volume calculated for the S—N model potential are in good agreement with their measured data. Moreover, these results have shown improvements over those obtained by help of the M—L—J potential. This fact together with the results of paper [6] clearly demonstrates that a two-parameter model potential proposed by Singh and Neb is a good representation for the curve of the potential energy of the RGC.

The high temperature $\left(T > \frac{2}{3}\theta_D\right)$ cubic ($\Delta C_v^3$) and quartic ($\Delta C_v^4$) anharmonic contributions to the molar heat at constant volume are listed and compared with the values $\Delta C_v^{3,4} \mathrm{k} - T(\partial^2 F_{3,4}/\partial T^2)_v$ obtained by help of the Feldman and Horton approximation [14] for the Mie—Lennard—Jones and Morse self-consistent potentials in Table IV.

*Table II*

*Quasi-harmonic ($U_{qh}$), cubic ($U_3$) and quartic ($U_4$) anharmonic contributions to the zero-point energy of the RGC using the Singh's and Neb's* (S—N), *renormalized Morse* (M) [12] *and* (12—6) *Mie-Lennard-Jones* (M—L—J) [14] *potentials. The zero static lattice energy $\Phi_0$ is showed for comparison*

| Solids | Potential | Zero-point energy [kJ/mol] | | | |
|---|---|---|---|---|---|
| | | $U_{qh}$ | $-U_3$ | $U_4$ | $\Phi_0$ |
| Ne | S—N | 0.520 | 0.0034 | 0.1094 | 1.9034 |
| | M | 0.503 | 0.014 | | 1.9044 |
| | M—L—J | 0.473 | 0.017 | 0.1210 | 2.4883 |
| Ar | S—N | 0.575 | 0.0015 | 0.0225 | 7.5469 |
| | M | 0.620 | 0.0045 | | 7.3364 |
| | M—L—J | 0.698 | 0.0053 | 0.0363 | 8.4892 |
| Kr | S—N | 0.656 | 0.0007 | 0.0157 | 11.2043 |
| | M | 0.462 | 0.0016 | | 10.8139 |
| | M—L—J | 0.562 | 0.0021 | 0.0141 | 11.7487 |
| Xe | S—N | 0.616 | 0.0005 | 0.0085 | 14.2732 |
| | M | 0.423 | 0.0001 | | 14.6257 |
| | M—L—J | 0.503 | 0.0001 | 0.0071 | 16.5567 |

*Table III*

*Comparison of the experimental data* [9—11] *for the molar heat at constant volume* $C_v$ *of the* RGC *with calculated in terms of the Singh and Neb* (S—N), *selfconsistent Morse* (M) [12] *and Mie-Lennard-Jones* (M—L—J) *potentials*

| Solid | $T$ [K] | $C_V$ [J/mol·K] | | | |
|---|---|---|---|---|---|
| | | Experiment | S—N | M | M—L—J |
| Ne | 8 | 2.4283 | 3.9804 | 3.7480 | 2.6686 |
| | 16 | 11.7858 | 7.9845 | 7.9919 | 9.4773 |
| | 24 | 17.1784 | 13.4341 | 13.0662 | 13.5925 |
| Ar | 10 | 3.2964 | 3.1362 | 4.1458 | 3.5914 |
| | 20 | 12.1218 | 13.0896 | 8.5950 | 12.0462 |
| | 40 | 19.9545 | 15.0810 | 20.2705 | 19.2290 |
| | 60 | 23.2222 | 18.0880 | 22.2754 | 20.7754 |
| | 70 | 25.7181 | 19.8994 | 22.6743 | 20.9500 |
| Kr | 10 | 5.9185 | 7.7716 | 4.5057 | |
| | 20 | 15.6612 | 15.1782 | 16.4822 | 15.6126 |
| | 40 | 21.9231 | 15.9204 | 21.5247 | 21.1495 |
| | 60 | 23.3760 | 18.6740 | 23.1084 | 22.2219 |
| | 80 | 25.5876 | 21.4103 | 23.5830 | 22.3715 |
| | 100 | 27.7751 | 22.6751 | 24.6162 | 22.1720 |
| Xe | 10 | | 7.7867 | 3.5659 | 17.0841 |
| | 20 | | 16.6790 | 17.9579 | 17.0841 |
| | 40 | | 18.5728 | 22.8619 | 21.9974 |
| | 60 | | 19.4523 | 23.6493 | 22.9451 |
| | 80 | | 21.8499 | 23.8445 | 23.0948 |
| | 100 | | 22.9585 | 23.8833 | 23.0199 |
| | 120 | | 23.5680 | 23.8964 | 22.7955 |
| | 140 | | 23.9206 | 23.8642 | 22.5711 |

*Table IV*

*The high temperature cubic* ($\Delta C_V^3$) *and quartic* ($\Delta C_V^4$) *anharmonic contributions to the molar heat at constant volume calculated in terms of the Singh and Neb* (S—N), *renormalized Morse* (M) *and* (12—6) *Mie-Lennard-Jones* (M—L—J) *potentials*

| Solids | $T$ [K] | $\Delta C_{V\,\mathrm{anh}}$ [J/mol·K | | | | |
|---|---|---|---|---|---|---|
| | | $\Delta C_V^3$ | | | $-\Delta C_V^4$ | |
| | | S—N | M | M—L—J | S—N | M—L—J |
| Ne | 16 | 4.180 | 1.945 | 4.350 | 3.975 | 12.770 |
| | 24 | 5.015 | 2.612 | 6.525 | 4.296 | 15.314 |
| Ar | 50 | 0.492 | 1.306 | 2.220 | 4.838 | 4.489 |
| | 60 | 0.812 | 1.885 | 2.663 | 5.840 | 5.387 |
| | 70 | 0.951 | 2.287 | 3.107 | 5.933 | 6.285 |
| Kr | 60 | 1.560 | 1.442 | 1.706 | 3.079 | 3.366 |
| | 80 | 2.080 | 2.032 | 2.274 | 4.105 | 3.927 |
| | 100 | 2.600 | 2.681 | 2.843 | 5.131 | 4.489 |
| Xe | 60 | 0.553 | 0.924 | 1.152 | 1.083 | 2.259 |
| | 80 | 0.737 | 1.279 | 1.536 | 1.445 | 3.012 |
| | 100 | 0.921 | 1.655 | 1.920 | 1.806 | 3.765 |
| | 120 | 1.105 | 2.055 | 2.304 | 2.167 | 4.518 |
| | 140 | 1.289 | 2.481 | 2.688 | 2.519 | 5.271 |

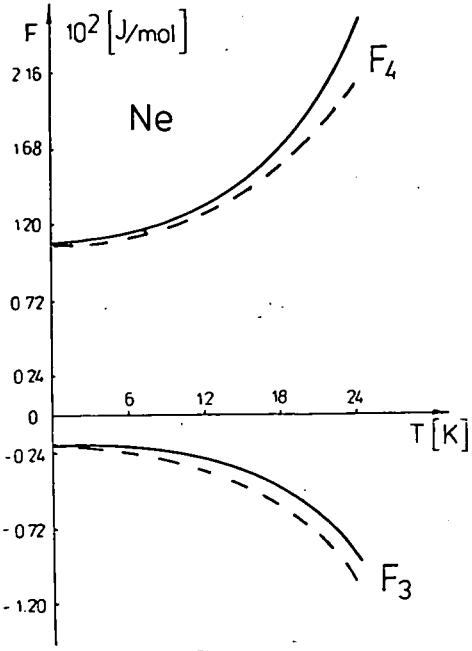


Fig. 1.a.

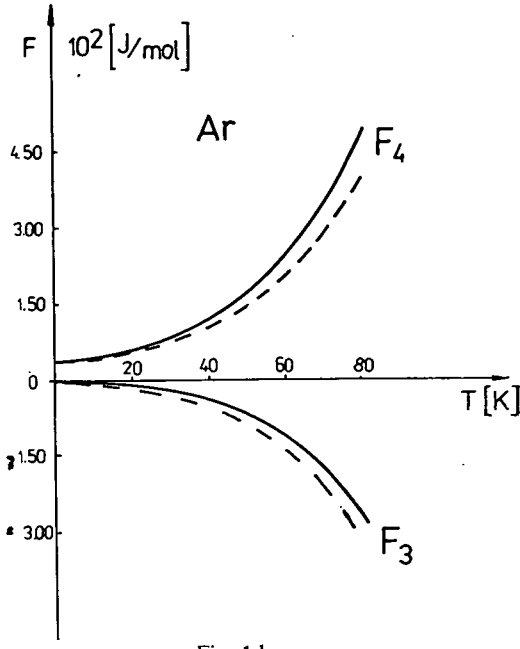


Fig. 1.b.

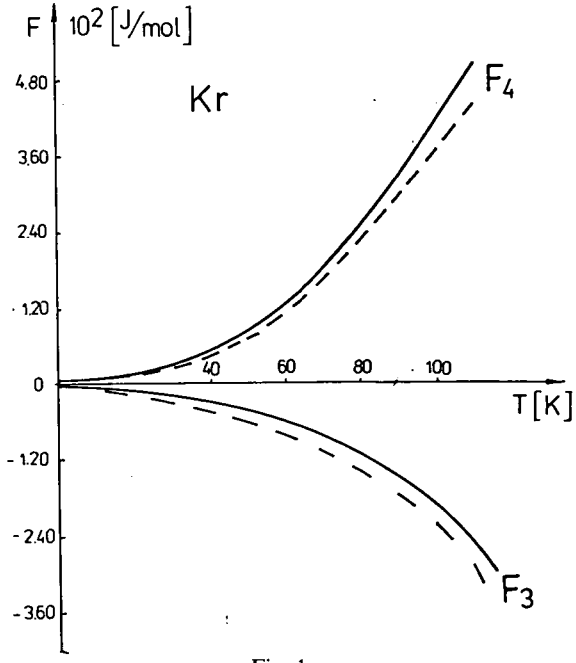


Fig. 1.c.

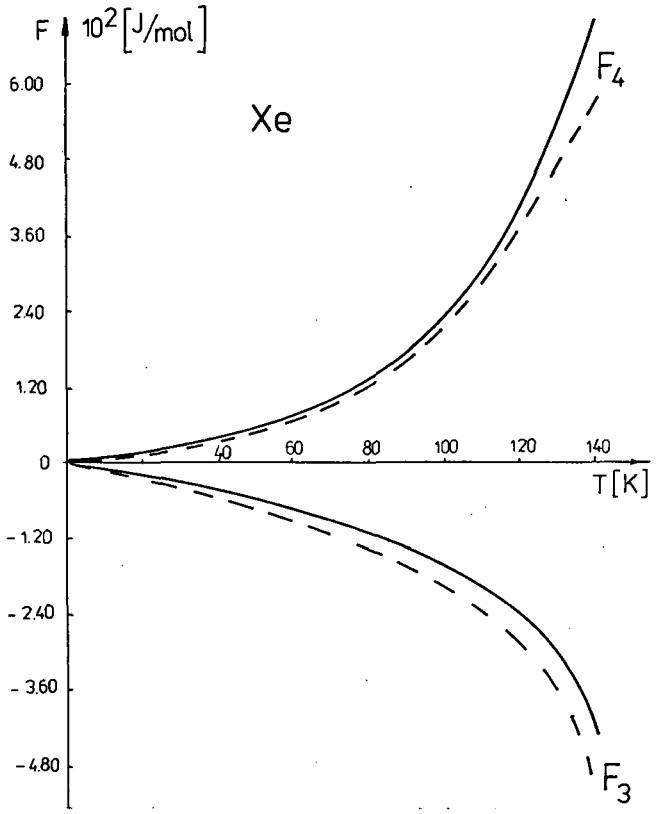


Fig. 1.d.

*Figs. 1 (a, b, c, d)*. The cubic ($F_3$) and quartic ($F_4$) contributions to the free energy. Solid lines represent values obtained for Singh's and Neb's potential. The broken curves are evaluted for Mie—Lennard—Jones potential. (a) Ne; (b) Ar; (c) Kr; (d) Xe

The results calculated in terms of the S—N potential cubic ($F_3$) and quartic ($F_4$) contributions to the free energy (solid lines) as functions of temperature are shown and compared with those obtained for the M—L—J potential (dashed curves) in Figs. 1 (a, b, c, d) for all four solids. From Figs. 1 (a, b, c, d) we see that values $F_3$ and $F_4$ obtained in terms of the Singh and Neb model show the same temperature behaviour as has been found for the Mie—Lennard—Jones potential [13]. At higher temperature it is evident that allowance for thermal expansion has a large effect on the results obtained for Singh and Neb potential.

*Summary and conclusions*

With the approximation given in [7, 8] we have presented numerical calculations of predicted anharmonic contributions to vibrational thermodynamic properties of the inert-gas solids for Singh and Neb model potential (Tables II—IV). In these tables we have listed the thermodynamical quantities evalutaed by help of the approximation made by other workers [13, 14, 17] with the Mie—Lennard—Jones [13, 14] and self-consistent Morse [12] potentials, for comparison. We have made a comparison with available experimental data in order to assess the validity of our potential model. Bearing in mind that a comparison of $C_v$ values (Table III) is a demanding test it appears that the model is a reasonably realistic one for the RGC. A possible improvement in the description of anharmonic crystals is the investigation of effects of phonons in thermodynamic properties from the present model in the self-consistent theory which allows all higher-order terms of lower-order perturbation theory to be taken into account in a S. C. manner [18]. Work in this direction is in progress.

*Appendix*

The quantities $FO$, $FQ$, $CH$ and $UH$ appearing in Eqs. (2), (4), (5), (7) and (10)—(13) for the high and low temperature limits are equal to:

*a)* high temperature limit

$$FO = \ln 0.6505\beta + 0.04166\beta^2.$$

$$FQ = 0.1875\,\theta^2 + 0.0156\,\omega_L^2,$$

$$CH = \theta(0.125\,K - 0.0374\,G),$$

$$UX = 0.5\,CH - 0.04166\beta(0.125\omega_L K + 1/\theta),$$

$$\beta = \frac{\omega_L}{\theta}.$$

*b)* low temperature limit

$$FO = E_o - 0.2\,\pi^4\gamma,$$

$$FQ = 0.028\,E_o + 3.246\,\gamma,$$

$$CH = 0.125\,E_o(0.2997\,G - K)$$

$$UX = 0.0208\,E_o(0.0885\,G - K) - \omega_L E_o^{-1}(0.02177\,\omega_L K - 0.0231\,G).$$

*Acknowledgement*

The author gratefully thanks Professor L. WOJTCZAK, Head of the Department of Solid State Physics, University of Łódź, for helfpul discussions connected with this paper and for reading the manuscript.

## References


[1] *Dobbs, E. R.:* Am . J. Phys. **28**, 243 (1960).
[2] *Kittel, C.:* Introduction to Solid State Physics, PWN, Warsaw 1974 (in Polish).
[3] *Pollack, G. K.:* Rev. Mod. Phys. **36**, (1964).
[4] *Horton, G. K.:* Am. J. Phys. **36**, 93 (1968).
[5] *Goodisman ,J.:* Diatomic Interaction Potential Theory, Vol 1, Academic Press, New York—London, (1973).
[6] *Singh, R. K., D. K. Neb:* phys. stat. sol. **(b) 112,** 735 (1982).
[7] *Maradudin, A. A., P. A. Flin:* Ann. Phys. (USA) **15**, 337, 360 (1961).
[8] *Flinn, P. A., A. A. Maradudin:* Ann. Phys. (USA) **22**, 223 (1963).
[9] *Clusius, K., P. Flubacher, U. Piesbergen, K. Schleich, A. Sperandio:* Z. Naturforsch **15a**, 1 (1960).
[10] *Flubacher, P., A. J. Leadbetter, J. A. Morrison:* Proc. Phys. Soc. **78**, 1449 (1961).
[11] *Beaumont, R. H., H. Chihara, J. A. Morrison:* Proc. Phys. Soc. **78**, 1462 (1961).
[12] *Malinowska-Adamska, C:* Acta Phys. Hung. (1983) (in print).
[13] *Leech, J. W., J. A. Reissland:* J. Phys. **C3**, 975, 987 (1970).
[14] *Feldman, J. L., G. K. Horton:* Proc. Phys. Soc. **92**, 227 (1967).
[15] *Reissland, J. A.,* Physics of Phonons, Izd. Mir, Moscow (1973) (in Russian).
[16] *Hafemeister, D. W.:* J. Phys. Chem. Solids **30**, 117 (1969).
[17] *Plakida, N. M., T. Siklós:* Acta Phys. Hung. **45**, 37 (1978).
[18] *Plakida, N. M., T. Siklós:* phys. stat. sol **39**, 171 (1970).


## ТЕРМОДИНАМИЧЕСКИЕ СВОЙСТВА КРИСТАЛЛОВ ИНЕРТНЫХ ГАЗОВ С УЧЁТОМ КУБИЧЕСКИХ И ВЫСШИХ ПОРЯДКОВ АНГАРМОНИЧЕСКИХ ВКЛАДОВ

*Ц. Малиновска-Адамска*

С использованием модельного потенциала Синга и Неба для парного центрального взаимодействия ближайших соседей исследуется температурная зависимость термодинамических функций кристаллов инертных газов в ангармоническом приближении.

Представлены результаты вычислений температурных зависимостей свободной и внутренней энергии, изохорной теплоёмкости с учётом кубических и высших порядков ангармонических вкладов в термодинамические функции для низких и высоких температур.

В частности, теоретические расчёты хорошо совпадают с экспериментальными данными для аргона, криптона и ксенона.

# BARRIER-HEIGHT AND HOT ELECTRON ATTENUATION LENGTH MEASUREMENTS IN Au—Si, Ag—Si AND Al—Si DIODES BETWEEN 280—350 K

By

B. PELLE[1], J. KISPÉTER[2], J. PEISZNER[3]

*(Received October 31, 1983)*

Schottky barrier diodes were prepared in chemically cleaned, 0.1 ohm·cm, n-type Si by evaporating Au, Ag and Al layers, respectively at $\sim 5.10^{-8}$ mbar. Barrier heights of these diodes have been determined by standard $I-V$, $C-V$ and photoemission threshold measurements at various temperatures between 280—350 K. The same tendency has been observed using the different methods; a slow decrease of barrier height with temperature ($\sim -4.10^{-4}$ eV/K). Special care was taken to determine the correct value of photoemission yield. Photoemission measurements proved to be the most reliable method to determine the barrier height but no significant discrepancies were observed in the results obtained by the photoemission, $I-V$ and $C-V$ methods.

Attenuation length L of hot electrons in Au, Ag and Al has been determined from measurement of the photoemission yield for various metallic layer thicknesses at different temperatures between 280—350 K. For Au layers an empirical relation of $T^{0,23}L(T)=$const seems to be correct for 280—350 K.

## 1. Introduction

Metal-semiconductor contacts are of immense importance in contemporary electronic devices. Recently some interest has been shown in the use of metal-semiconductor barriers realized on Si for detection of infrared radiation and conversion of solar energy. This latter application suggested us to investigate the behaviour of Schottky barriers at temperatures above room temperature until 350 K.

Several authors have determined the electronic barrier height on different metal-silicon contacts by means of standard $I-V$, $C-V$ and photoemission threshold measurements [1, 3, 6, 7, 9, 10] and the hot electron attenuation length in metallic films [2—5, 8] at temperatures ranging between 80—300 K. However, no results have been reported at temperatures below the liquid nitrogen temperature and above room temperature.

[1] Universite des Sciences et de la Technologie d'Oran (Algeria).
[2] College of Food Industry, Szeged, (Hungary).
[3] Institut National Politechnique de Grenoble (France).

## 2. Experimental

The silicon wafers used in our experiments were of 0.1 ohm·cm, *n*-type ($N_D \sim 7 \cdot 10^{16}\,cm^{-3}$), (111) oriented. They were etched in $HNO_3$—HF (20:1) mixture, then immersed in cc. $HNO_3$ for a short time, rinsed in deionized $H_2O$ and dried in $H_2$ flow. Oxide was removed from the bottom side with cc. HF, then the wafers were rinsed and dried again. Contacts were made by evaporating Al film then the wafers were tempered at 673 K in the vacuum system. For barrier preparation the front side of the wafers was rinsed in cc. HF to turn the surface into hydrophobic just before inserting the wafers into the vacuum system. Thin Au, Ag, or Al films were evaporated from W-boat through a stainless-steel mask having circular holes with diameters of 2 mm or 0.7 mm, respectively, at a pressure of $5 \cdot 10^{-8}$ mbar. Film thickness was monitored during deposition by a quartz crystal microbalance calibrated previously by Talystep and interference microscope.

For each evaporation process both a $10 \times 20\ mm^2$ Si wafer and a $10 \times 20\ mm^2$ fused silica plate were inserted to measure optical transmission, reflectivity and resistivity of the deposited metallic layers.

During $I-V$, $C-V$ and photoemission yield measurements at various temperatures (from 280 to 350 K) the slices were placed onto a gold plated vacuum thermochuck. Its temperature was regulated by a Temptronic electronic temperature controller. For the measurements a P.A.R. point probe assembly was used equipped with an $X-Y-Z$ micromanipulator. The vacuum thermochuck and the point probe assembly with the manipulator were inserted into a measuring box with removable cover, in which an optical window of Infrasil quality fused silica was mounted for photoemission measurements. For voltage supply a highly isolated voltage source was provided with 1.2 V Hg—Cd batteries and 10 turn precision Helipot potentiometers.

For $I-V$ measurements the applied voltage was monitored by a Keithley Mod 191 digital voltmeter and the current was measured by a Keithley Mod 616 digital electrometer (Fig. 1.). The $C-V$ characteristics were measured by a P.A.R Mod

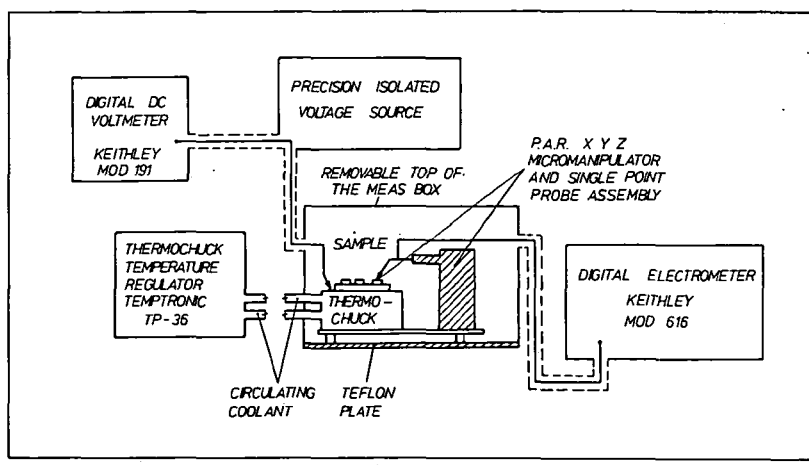


*Fig. 1.* Electrical circuit for $I-V$ characteristics measurements

410 hf $C-V$ plotter assembly operating at 1 kHz and were recorded by a SEFRAM TGM 164 $x-y$ recorder (Fig. 2.).

Measuring circuitry and optical arrangement used for photoemission yield measurements are shown in detail in Fig. 3.

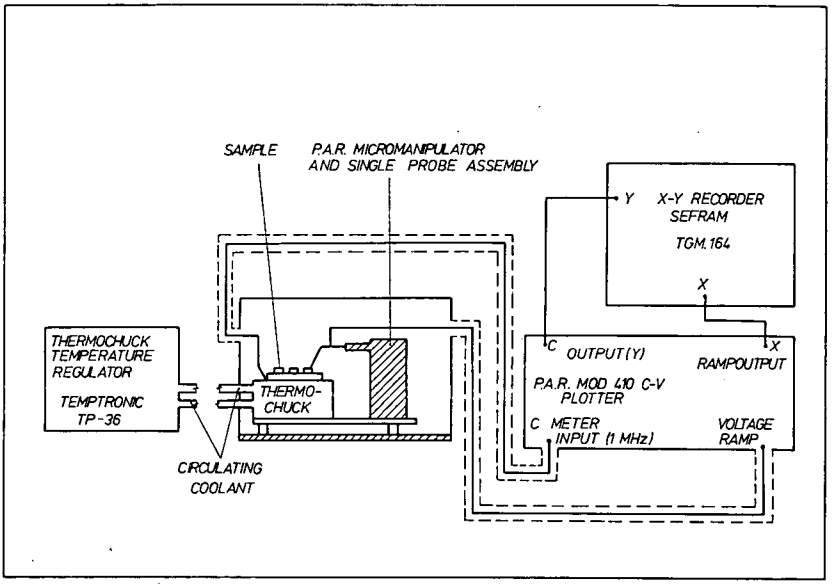


*Fig. 2.* Electrical circuit for $C-V$ characteristics measurements

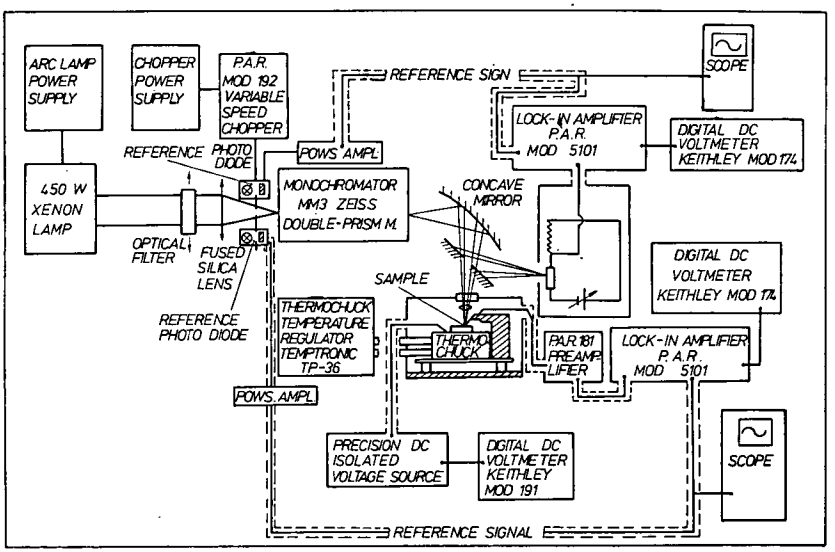


*Fig. 3.* Experimental arrangement for photoyield measurements

Since the photocurrents generated were relatively small ($10^{-12}-10^{-8}$A). and thermoemission currents are in the range of $10^{-9}-10^{-8}$ A at room temperature even at slight reverse bias (—0.5 V) applied for photoemission measurements, a.c. locking technique was used instead of a.c. measurements with electrometer. Light was chopped by a P.A.R Mod 192 chopper at 239 Hz and the photocurrents were detected with P.A.R. Mod 5101 lock-in amplifier equipped with a P.A.R. Mod 181 current sensitive preamplifier. Currents ranging between $10^{-12}$ to $10^{-8}$ A could easily be detected by this assembly.

As a light source 450 W Xe arc lamp was used which was followed by a Zeiss MM3 double prism monochromator to select wavelengths. The chopped monochromatic light was focused onto the sample by a concave reflecting mirror and a fused silica lens. A part of the light was reflected onto the surface of a PbS detector. Photocurrent and incident photon flux could be measured at the same time by this assembly calibrated previously, so the photoresponse could be determined directly as a function of wavelength (or photon energy).

## 3. Experimental results

### *Barrier height determination*

Schottky barrier heights were determined in three ways:

*a)* "forward current $I-V$ method": by plotting the logarithm of the forward current density versus applied bias, the barrier height was found from the intercept of the extrapolated current density curve on the current density axis.

*b)* "$C-V$ method": by plotting the reciprocal of the square of the differential capacitance $C^{-2}$ versus applied reverse bias, barrier height was found from the intercept on the voltage axis.

*c)* "photoresponse measurement": by plotting the square root of the photoelectric response (yield) $Y^{1/2}$ as a function of photon energy (Fowler-plot), the barrier height was found from the intercept of the extrapolated photoresponse curve on the photon energy axis.

### *Barrier height determination from $I-V$ characteristics*

For semiconductors with low doping concentration ($N_D$; $N_A<10^{17}\,\mathrm{cm}^{-3}$) the $I-V$ characteristics in forward direction between 280—350 K with $V>3\,kT/q$ can be given as

$$I = A^{**}T^2 \exp\left(\frac{-q\Phi_{Bo}}{kT}\right)\exp\left(\frac{q(\Delta\Phi+V)}{kT}\right), \tag{1}$$

where $I$ is the current density, $A^{**}$ is the effective Richardson-constant, $q\Phi_{Bo}$ is the zero field asymptotic barrier height, $\Delta\Phi$ is the Schottky barrier lowering, $V$ is the applied bias. $q\Phi_{Bo}$ was determined by plotting the $I-V$ characteristics, with $I$ in logarithmic scale.

The extrapolated value of current density to zero voltage gives the saturation current $I_s$:

$$I_s = A^{**} T^2 \exp\left(\frac{-q\Phi_{Bo}}{kT}\right) \tag{2}$$

and the barrier height can be given as

$$q\Phi_{Bo} = kT \ln\left(\frac{A^{**} T^2}{I_s}\right) \tag{3}$$

$A^{**} = 105\ \mathrm{Acm^{-2}\,K^{-2}}$ was assumed throughout this work.
In reality, the diode equation is as follows:

$$I = I_s\left\{\exp\left(\frac{qV}{nkT}\right) - 1\right\}, \tag{4}$$

where $n$ is the "ideality factor" which can be determined from

$$n = \frac{q}{kT}\frac{\partial V}{\partial(\ln I)}. \tag{5}$$

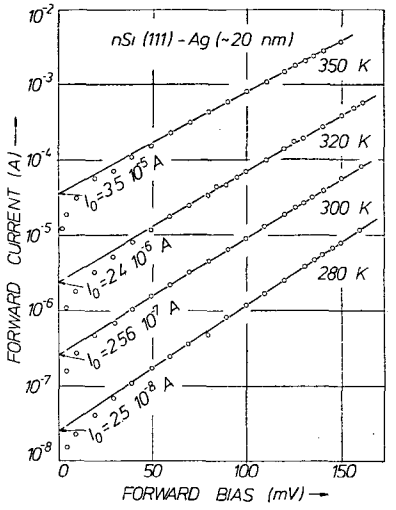


*Fig. 4.* Forward current-voltage characteristics of nSi(111)—Au (20 nm) diodes for various temperatures (280, 300, 320 and 350 K)

Figs. 4, 5 and 6 represent our experimental $I-V$ curves obtained at various temperatures between 280—350 K for nSi (111)—Au, *n*Si (111)—Al and *n*Si (111)—Ag diodes fabricated with chemically cleaned Si-surfaces.

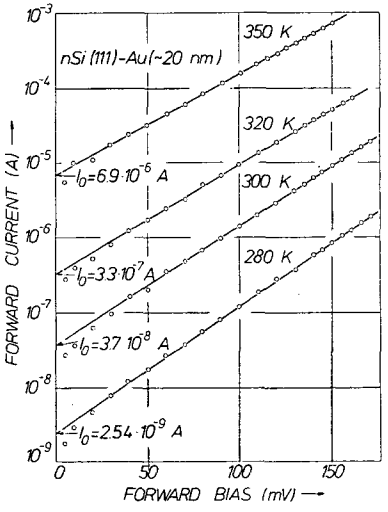


*Fig. 5.* Forward current-voltage characteristics of nSi(111)—Al (25 nm) diodes for 280, 300, 320 and 350 K

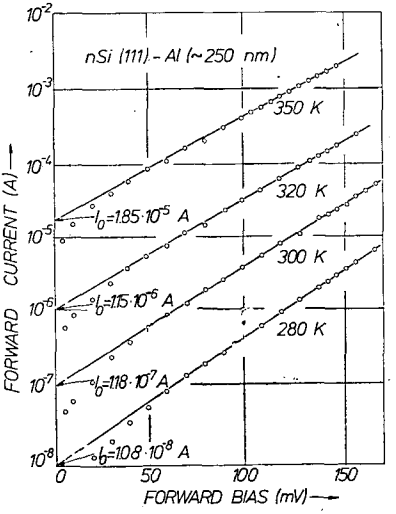


*Fig. 6.* Forward current-voltage characteristics of n—Si(111)—Ag (20 nm) diodes at 280, 300, 320 and 350 K

*Table I*

*Barrier heights of n type* Si (111) — *metallic layer diodes with* $N_D = 7 \cdot 10^{16}$ cm$^{-3}$ *from* $I-V$ *measurements at various temperatures*

| Temperature (K) | Au—Si $q\Phi_{Bo}$ (eV) | Al—Si $q\Phi_{Bo}$ (eV) | Ag—Si $q\Phi_{Bo}$ (eV) |
|---|---|---|---|
| 280 | 0.78 | 0.74 | 0.72 |
| 300 | 0.77 | 0.74 | 0.72 |
| | (0.81) [13] | (0.73) [14] | (0.72) [15] |
| 320 | 0.76 | 0.73 | 0.71 |
| 350 | 0.75 | 0.72 | 0.70 |

The ideality factor $n$ was between 1.01—1.03. However, since no characteristic variation was observed in the nature of the diodes with temperature, $n=0.01$ as a permanent value was accepted throughout the evaluation of the real barrier height.

The values of the barrier height $q\Phi_{Bo}$ are listed in Table *I* for the diodes at different temperatures.

*Barrier height determination from* $C-V$ *characteristics*

Barrier heights have also been determined by capacitance measurements with applied voltage.

The $C^{-2}-V$ plots obtained exhibit excellent linearity. From the intercept $V_i$ on the voltage axis the barrier height $q\Phi_{Bn}$ was found using the relation

$$q\Phi_{Bn} = qV_i + qV_n + kT, \tag{6}$$

where $qV_n$ is the distance between Fermi-level and the conduction band edge in bulk Si:

$$qV_n = E_c - E_F = kT \ln \frac{N_C}{N_D}. \tag{7}$$

This expression was calculated for 280, 300, 320, 350 and 370 K, respectively with $N_D = 7 \cdot 10^{16}$ cm$^{-3}$.

Values of $q_{V_n}$ and $k$T are listed in Table II.

The temperature dependence of the $C^{-2}-V$ characteristics for Si—Au diodes is presented in Fig. 7.

The $C^{-2}-V$ characteristics of Si—Au, Si—Al and Si—Ag diodes at room temperature are plotted in Fig. 8.

Finally the $C-V$ relationship of a chemically cleaned ("real barrier") Ag—Si interface is compared in Fig. 9 to that of an "intimate barrier" Ag—Si diode prepared in ultra high vacuum (UHV) with a clean Si surface.

The barrier height values obtained from $C-V$ measurements are shown in Table III.

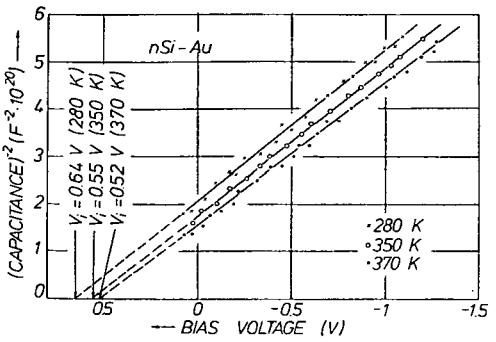


*Fig. 7.* $C^{-2}-V$ characteristics of nSi(111)—Au contacts at 280, 350 and 370 K

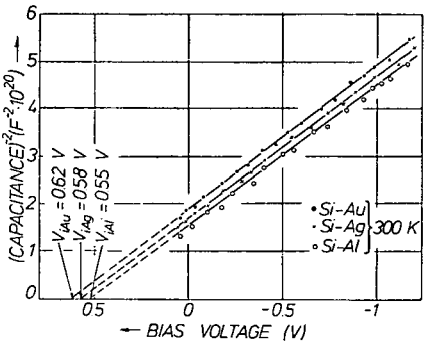


*Fig. 8.* Comparison of $C^{-2}-V$ characteristics measured on nSi(111)—Au, nSi(111)Ag and nSi(111)—Al contacts at 300 K

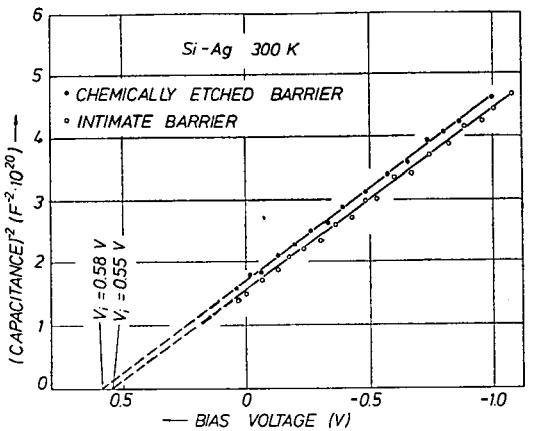


*Fig. 9.* Comparison of $C^{-2}-V$ characteristics measured on nSi(111) contacts prepared on "chemically cleaned" Si surfaces and on nSi(111)—Ag diodes with "intimate barrier" (prepared by vacuum deposition of Ag on clean Si surface at $5\cdot10^{-10}$ mbar)

*Table II*

*Properties of the n type* Si *samples with* $N_D = 7\cdot10^{16}$ cm$^{-3}$

| Temperature (K) | $N_b$ (cm$^{-3}$) | $qV_n$ (eV) | $qV_n+kT$ (eV) |
|---|---|---|---|
| 280 | $2.52\cdot10^{19}$ | 0.141 | 0.165 |
| 300 | $2.80\cdot10^{19}$ | 0.156 | 0.182 |
| 320 | $3.08\cdot10^{19}$ | 0.170 | 0.198 |
| 350 | $3.53\cdot10^{19}$ | 0.187 | 0.217 |
| 370 | $3.84\cdot10^{19}$ | 0.202 | 0.234 |

*Table III*

*Barrier heights of n type* Si ($N_D = 7 \cdot 10^{16}$ cm$^{-3}$) *from C – V measurements at various temperatures*

| Temperature (K) | nSi—Au $q\Phi_{Bn}$ (eV) | nSi—Al $q\Phi_{Bn}$ (eV) | nSi—Ag $q\Phi_{Bn}$ (eV) | |
|---|---|---|---|---|
| | | | "REAL BARRIER" | "INTIMATE BARRIER" |
| 280 | 0.80 | — | — | — |
| 300 | 0.80 | 0.73 | 0.76 | 0.73 |
| 320 | 0.78 | — | — | — |
| 350 | 0.77 | 0.70 | 0.72 | — |
| 370 | 0.75 | — | — | — |

*Barrier height determination from photoemission yield measurements*

By definition, quantum yield $Y$ is the ratio of the number of photoelectrons and that of the absorbed photons:

$$Y(h\nu) = \frac{I_{ph}(h\nu)/q}{W_a(h\nu)/h\nu}, \tag{8}$$

where $I_{ph}$ is the measured photocurrent, $h\nu$ is the energy of a photon of frequency $\nu$, $W_a$ is the absorbed energy.

Since the absolute values of the yield are not necessary to know, the knowledge of the relative $W_a(h\nu)$ function is sufficient. As a result $Y(h\nu)$ is presented in arbitrary units in Figs. 10—12.

In several papers $Y$ is calculated on the incident radiation power basis only. This gives obviously incorrect results, as reflection, transmission and absorption of light by metallic layers depend on the layer thickness and on the wavelength of light.

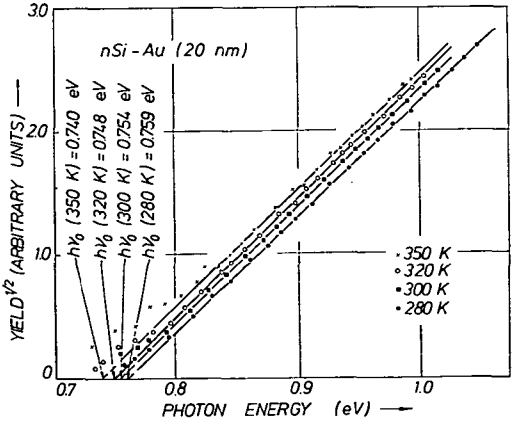


*Fig. 10.* Photoemission yield-photon energy ("Fowler plots") on nSi(111)—Au barriers at 280, 300, 320 and 350 K

This fact was always taken into consideration throughout this work with rigorous calculation of the air-metal-silicon optical layer system. Reflection $R(d, \lambda)$, transmission $T(d, \lambda)$ and absorption $A(d, \lambda)$ were either directly measured or calculated from optical constants found in the literature. In our photoemission experiments monochromatic light was focused onto the metal side of the diodes but checking measurements were also performed with light transmitted

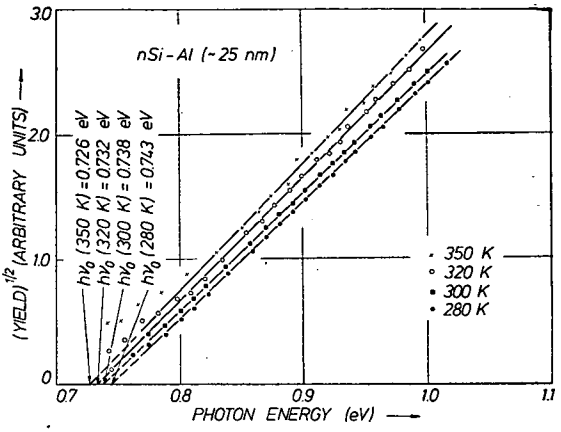


*Fig. 11.* "Fowler-plots" of nSi(111)—Al diodes at 280, 300, 320 and 350 K

through the silicon towards the metal layer. The fact that no significant deviation was observed for results obtained by the different ways of illumination, verified that the "optical model" used was correct. For metallic layers of thickness $d > 50$ nm, $W_a \approx \{1 - R(d)\} W_i$ is a good approximation for yield calculations, where $W_i$ is the incident energy.

Fig. 10 shows the "Fowler plots" ($Y^{1/2}$ *versus* $h\nu$) between 280—350 K for nSi—Au diodes at various temperatures.

For nSi—Al and nSi—Ag diodes the Fowler plots are shown in Fig. 11

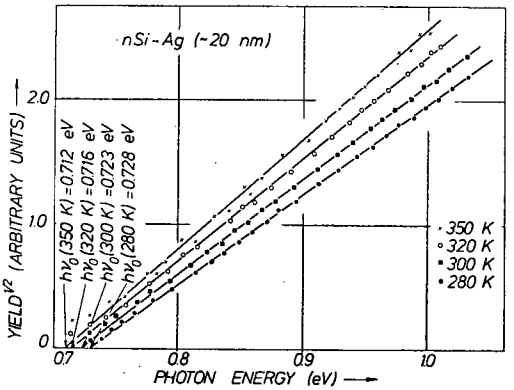


*Fig. 12.* "Fowler-plots" of nSi(111)—Ag diodes (prepared on "chemically cleaned" nSi) at 280, 300, 320 and 350 K

*Table IV*

*Barrier heights of* nSi—Au, nSi—Al *and* nSi—Ag *diodes at various temperatures from photoemission threshold analysis*

| Temperature (K) | nS—Au $q\Phi_{Bn}$ (eV) | nSi—Al $q\Phi_{Bn}$ (eV) | nSi—Ag $q\Phi_{Bn}$ (eV) |
|---|---|---|---|
| 280 | 0.76 | 0.74 | 0.73 |
| 300 | 0.75 | 0.74 | 0.72 |
| 320 | 0.75 | 0.73 | 0.72 |
| 350 | 0.74 | 0.73 | 0.71 |

and Fig. 12, respectively, at 280, 300, 320, and 350 K temperatures measured by a.c. technique with light chopped at 239 Hz. Table IV shows the barrier height data obtained from photoemission threshold analysis for *n*Si—Au, *n*Si—Al, and *n*Si—Ag diodes at various temperatures.

### *Calculation of the attenuation length of hot electrons in metallic layers from thickness dependence of the photoemission yield*

The range (or attenuation length) $L(h\nu)$ of hot electrons is defined as follows: When monochromatic light of energy $h\nu$ is incident upon the surface of the metallic layer of thickness $d$, it can be found both experimentally and theoretically that the number of electrons escaping over the metal-semiconductor barrier at the opposite side of the layer is proportional to $\exp\left\{-\frac{d}{L(h\nu)}\right\} \cdot L(h\nu)$ can be determined from the thickness dependence of the external photoemission yield. When $d > 30$ nm, the penetration depth of light is relatively small comparing to thickness, and $L(h\nu)$ can be determined by comparing photoemission yields obtained for thicknesses $d_1$ and $d_2$ respectively:

$$L(h\nu) = \frac{d_2 - d_1}{\ln \frac{Y(h\nu, d_1)}{Y(h\nu, d_2)}} \tag{9}$$

if $d_2 > d_1 \cdot Y(h\nu, d_i)$ is the ratio of the number of emitted electrons and absorbed photons of energy $h\nu$ by the layer of thickness $d_i$.

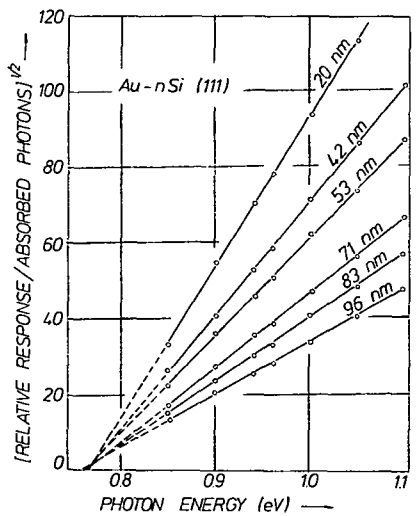


*Fig. 13.* The dependence of photoresponse on photon energy for 6 different thicknesses (20 nm, 42 nm, 53 nm, 71 nm, 86 nm, 96 nm) of Au deposited on "chemically cleaned" nSi(111) surfaces

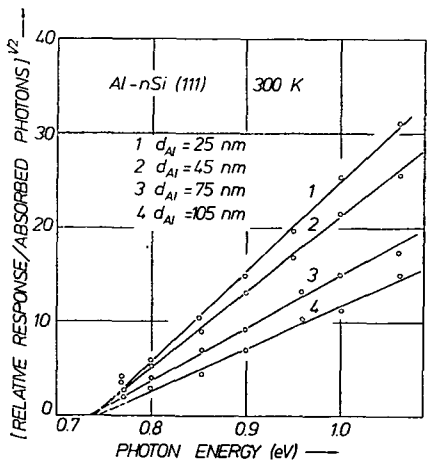


*Fig. 14.* The dependence of photorespones on photon energy for 4 different thicknesses (25 nm, 45 nm, 75 nm, 105 nm) of Al deposited on "chemically cleaned" nSi (111) surfaces

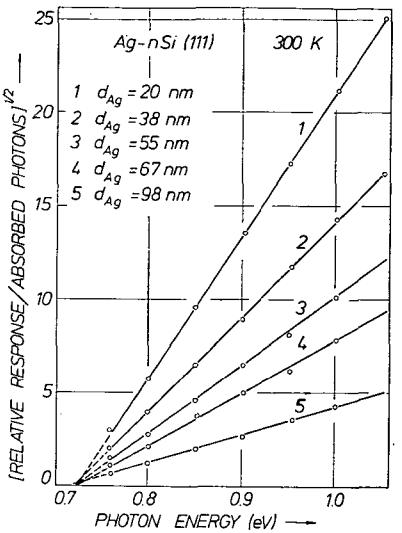


*Fig. 15.* The dependence of photoresponse on photon energy for 5 different thicknesses (20 nm, 38 nm, 55 nm, 67 nm, 98 nm) of Ag deposited on "chemically cleaned" nSi(111) surfaces

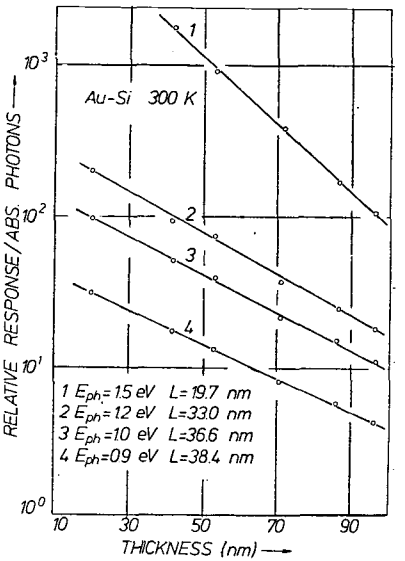


*Fig. 16.* The photoresponse as a function of the Au film-thicknesses measured at 0.9 eV, 1.0 eV, 1.2 eV and 1.5 eV photon energies for Au—nSi (111) Schottky diodes prepared on "chemically cleaned" Si surfaces

Fig. 13 shows the photoemission yield of *n*Si—Au diodes with various layer thickness (20, 42, 53, 71, 86 and 96 nm) measured at room temperature.

The photoemission yield for *n*Si—Al diodes is presented in Fig. 14 for various layer thicknesses (25, 45, 75 and 105 nm) at 300 K.

Fig. 15 shows the photoemission yield for *n*Si—Ag diodes with various layer thicknesses (20, 38, 55, 67, and 98 nm) at 300 K.

The graphical determination of $L(h\nu)$ is shown in Fig. 16 at 300 K, for the results plotted in Fig. 14. The same procedure was used to determine graphically the attenuation length $L(h\nu)$ for *n*Si—Al diodes and *n*Si—Ag diodes at 300 K.

*Table V*

*Attenuation length $L(h\nu)$ in metallic layers from photoemission measurements for* nSi—Au, nSi—Al *and* nSi—Ag *diodes at various temperatures*

| Temperature (K) | Range of hot electrons $L(h\nu)$ [nm] | | | | | | | |
|---|---|---|---|---|---|---|---|---|
| | Au | | Al | | | Ag | | |
| | 0.9 eV | 1.0 eV | 0.8 eV | 0.9 eV | 1.0 eV | 0,8 eV | 0,9 eV | 1.0 eV |
| 280 | 39.0 | 37.2 | 56.6 | 51.9 | 50.2 | 26.4 | 25.1 | 24.5 |
| 300 | 38.4 | 36.6 | 55.8 | 51.0 | 49.4 | 25.8 | 24.7 | 24.1 |
| 320 | 37.9 | 36.1 | 55.0 | 50.2 | 48.6 | 25.0 | 24.3 | 23.8 |
| 350 | 37.0 | 35.3 | 53.7 | 49.5 | 47.6 | 24.7 | 23.7 | 23.3 |

Thickness dependence of the photoemission yield was also measured at 280, 320 and 350 K for *n*Si—Au, *n*Si—Ag and *n*Si—Al diodes. Results of these measurements and attenuation lengths $L(h\nu)$ for *n*Si—Au, *n*Si—Ag, and *n*Si—Al diodes are assemblied in Table V giving the temperature dependence of $L(h\nu)$ for Au, Ag and Al layers.

## 4. Discussion

Photoemission threshold measurements have been accepted as the most reliable and direct method of determining Schottky-barrier heights. By the use of lock-in detection method, leakage effects caused by tunneling and thermal excitation can be eliminated [9, 11]. A rigorous calculation of the power absorbed by the thin films proved to also be necessary.

Using photoemission, the knowledge of the diode area is not necessary in opposition to the current-voltage ($I-V$) method. The discrepancy obtained between the results of the photoemission and $I-V$ methods can be due to the presence of tunneling current for higher temperature and that of generation — recombination currents for lower temperature [7] and the choice of the effective Richardson — constant $A^{**}$. However, no significant discrepancy was observed in the experiments which can be explained by the fact that for the relatively high temperature range (280—350 K) thermoemission proves to be the determinant component of the observed current.

Precision of capacitance-voltage ($C-V$) measurements can be considered quite good for "intimate barriers" prepared in UHV and by sophisticated cleaning technique [10] but seemed to be inferior in precision comparing to the photoemission and even to the $I-V$ method in our experiments when diodes were prepared with chemically cleaned Si-surfaces and an intermediate very thin dielectric layer was always present between the metal layer and the semiconductor.

Comparing the barrier height values collected in Tables I, II, and IV, it can be observed that the barrier heights determined by $I-V$ and $C-V$ methods are 0.02 and 0.04 eV respectively larger than those obtained by the photoemission method. However, the results concerning the temperature dependence of barrier height were consistent; $I-V$, $C-V$ and photoemission experiments show the same tendency, i.e. decreasing barrier height values with increasing temperature. The slope $\frac{q\Phi_{Bo}}{\Delta T} = -4 \cdot 10^{-4}$ eV/K is in good agreement with the similar slopes of $-3 \cdot 2 \cdot 10^{-4}$ eV/K and $-3 \cdot 4 \cdot 10^{-4}$ eV/K obtained by photoemission measurements and reported in [9] and [11], respectively.

The values obtained for attenuation length $L(h\nu)$ of hot electrons for Au are in good agreement with those published in [4, 5] but are smaller than those given in [3].

This discrepancy is obviously due to the fact that in [3] the optical absorption, transmission and reflection values were obtained for Au layers deposited on glass substrates: however in the present work and in [4, 5, 8] Au layers were prepared on Si.

The experimentally determined attenuation length $L$ can be expressed by

$$\frac{1}{L} \approx \frac{1}{l_{ee}} + \frac{1}{l_{eph}} \tag{10}$$

if Si is moderately doped, where $l_{ee}$ is the mean free path of electron-electron scattering and $l_{eph}$ is the mean free path of electron-lattice (electron-phonon) interaction.

$l_{ee}$ is independent of temperature but $l_{eph}$ shows strong temperature dependence, and it is proportional to $\frac{1}{T}$ above ~20 K. In the temperature range of 280—350 K an empirical relation of $T^{0,23}L(T)=\text{const}$ seems to be correct for Au layers.

* * *

*Acknowledgement*

The authors wish to acknowledge the assistance of Mr. I. BARSONY.

*List of symbols*

$A$: absorption coefficient
$A^{**}$: Richardson constant (amp cm$^{-2}$ K$^{-2}$)
$C$: differential capacitance ($F$)
$d$: layer thickness (cm)
$E_c$: energy level of conduction band (eV)
$E_F$: Fermi level (eV)
$h\nu$: photon energy (eV)
$I$: current density (amp cm$^{-2}$)
$I_{ph}$: photoelectric current (amp)
$I_s$: saturation current (amp)
$k$: Boltzmann's constant (joule/K)
$L$: attenuation length (range/cm)
$N_A$: acceptor concentration (cm$^{-3}$)
$N_D$: donor concentration (cm$^{-3}$)
$q$: charge of electron (coul)
$qV_n$: distance between Fermi-level and conduction band (eV)
$q\Phi_{Bo}$: zero field asymptotic barrier height (eV)
$q\Phi_{Bn}$: Schottky barrier height on n-type semiconductor (eV)
$R$: reflection coefficient
$T$: absolute temperature (K)
$T$: transmission coefficient
$V$: bias voltage (V)
$W_a$: absorbed energy (eV)
$W_i$: incident energy (eV)
$Y$: photoelectric response (yield)
$\Delta\varphi$: Schottky barrier lowering (V)

**References**

[1] *Mead, C. A.:* Solid-State Electron, **9**, 1023 (1966).
[2] *Crowell, C. R., W. G. Spitzer, L. E. Howarth, L. E. Labate:* Phys. Rev. **127**, 2006 (1962).
[3] *Sze, S. M., J. L. Moll, T. Sugano:* Solid-State Electron. **7**, 509 (1964).
[4] *Joshea, R. W., R. C. Lucas:* Phys. Rev. **138**. 1182 (1965).
[5] *Sensik, M., J. M. Seiler:* C. R. Acad. Sc. Paris **267**, 1439 (1968).
[6] *Yu, A. Y.:* Solid-State Electron. **13**, 97 (1970).
[7] *Thanailakis, A.:* J. Phys. C.: Solid State **8**, 655 (1975).

[8] *Seiler, J. M., M. Sensik:* C. R. Acad. Sc. Paris **273**, 123 (1971).
[9] *Anderson; C. L., C. R. Crowell, T. N. Kao:* Solid-State Electron. **18**, 705 (1975).
[10] *van Otterloo, J. P., L. J. Gerritsen:* J. Appl. Phys. **49**, 723 (1978).
[11] *Rideout, V. L.:* Thin Solid Films **48**, 261 (1978).
[12] *Stuart, K., F. Wooten, W. E. Spicer:* Phys. Rev. **135**, A 495 (1964).
[13] *Turner, T., E. H. Rhoderick:* Solid-State Electron. **11**, 291 (1968).
[14] *Strutt, A. K.:* Appl. Phys. Lett. **21**, 405 (1972).

## ИЗМЕРЕНИЕ ВЫСОТЫ БАРЬЕРА И ЗАТУХАЮЩЕГО ПУТИ ГОРЯЧЕГО ЭЛЕКТРОНА НА ДИОДАХ Au—Si, Ag—Si И Al—Si В ТЕМПЕРАТУРНОМ ИНТЕРВАЛЕ 280—350 К

*Б. Пелле, Й. Кишпетер, Я. Пейснер*

Изготавливались Шоттки барьерные диоды с испарением Au—, Ag— и Al-ых слоев на химически очищенном Si типа (*n*) с проводимостью 0,1 ом.см при давлении $5 \cdot 10^{-8}$ мбар. Высота барьера диодов определялась стандартным методом I—V, C—V и методом измерения фотоэмиссионного порога в температурном интервале 280—350 К.

Разными методами измерения определялась одинаковая тенденция. Высота барьера с повышением температуры несколько уменьшается ($-4 \cdot 10^{-4}$ эВ/К). Особое внимание уделили определению точного значения фотоэмиссионной эффективности. Фотоэмиссионные измерения являлись наилучшим методом определения высоты барьера, однако, между результатами полученными фотоэмиссионным методами I—V, C—V нет значительных расхождений. Затухающий путь горячих электронов L в серебряном и алюминиевом материалах определялся из результатов измерений фотоэмиссионной эффективности при разных толщинах металлических слоев в температурном интервале 280—350 К. При использовании золотых слоев в температурном интервале 280—350 К установили следующую функциональную зависимость: $T^{0,23} \cdot L(T) = \text{const}$.

# THE TEMPERATURE DEPENDENCE OF ELECTRIC CONDUCTANCE OF POLAR LIQUID DIELECTRICS

By

L. HORVÁTH

Technical High School, Subotica, Yugoslavia

*(Received November 20, 1983)*

Continuous measurements were performed for conductivity and permittivity of some polar liquid dielectrics in the wide temperature range from the melting to the critical point in a closed measuring cell under saturated vapor pressure of their own. The measurements were made on methyl alcohol, ethyl alcohol, acetone and sulphur dioxide at a frequency of 1591.5 Hz.

## *Introduction*

The electric conductance of pure liquid polar dielectrics, which arises from autodissociation of their molecules, depends to a great extent on temperature, due to its influence on the number of ions, their mobility and some physical characteristics of liquids. The electric conductance of sufficiently purified polar liquid dielectrics whose dielectric constant is relatively high, can be considered as a characteristic constant liquids. The electric conductance of sufficiently purified polar liquid dielectrics whose dielectric constant is relatively high, can be considered as a characteristic constant of the substance.

In this work electric conductance measurement has been carried out from the melting temperature to the critical temperature, *i.e.* in the temperature interval in which the liquids can exist under saturated vapor pressure. The measurements were carried out on methyl alcohol, ethyl alcohol, acetone and sulphur dioxide. Data on electric conductivity of these substances can be found in the literature by various authors [1—9], but they dealt with particular temperatures or temperature ranges only and the purity of used substances, for the most of these measurements, can be questioned. We want to make perfectly clear the importance of the possibility of simultaneously measuring the conductivity and permittivity and we think that a continuous measurement of these data will give us more reliable values than separate measurements.

*Experimental technique*

The conductivity and permittivity were measured by means of a bridge method. The capacity and the conductance of the condenser were measured with a Wayne—Kerr B 331 Mk II Autobalance Precision Bridge, at the frequency 1591.5 Hz ($\omega = 10^4$ 1/s).

The measurement range of the bridge for capacity is from 100 aF to 1 F and for conductivity from 1 pS to 10 kS. The bridge error was 0.01%. The bridge enables simultaneous measurement of resistance as well as capacity.

For the continuous regulation of temperature in the interval of $-80\,°C$ $-+180\,°C$ the "Materialprüfkammer" type VMT II from Vötsch was used. The temperature above 180 °C was achieved in an oil bath, while under $-80\,°C$ in a dish recooled by liquid oxygen. The temperature measurement was carried out by means of a copper-constantan thermocouple. The error in temperature determination was estimated at 0.1 °C [10, 11].

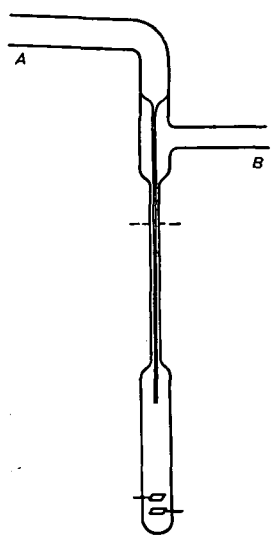


*Fig. 1. The measuring cell*

The measuring cell used in the experiment, made of Pyrex glass, is presented in Fig. 1. The cell was at part *A* connected to the reservoir filled with the purfied substance, while at part *B* it was connected to the recipient which could be evacuated. The investigated substance was introduced into the cell in gaseous state, where it was transformed into liquid state by intensive recooling. The cell was filled to the volume, which corresponds to the critical volume of the investigated substance. After filling the cell was melted with flame and closed at the indicated line and separated from its upper part, while the lower part was cooled and protected by an asbestos card-board. The cell was calibrated by the method which is recommended in the literature [12, 13]. Each cell was examined before measurement in the temperature interval in which it was used, with air as dielectric. The change of cell capacity, obtained by this measurement, enabled a certain error correction which appears due to thermic deformation.

To obtain pure methyl alcohol, ethyl alcohol and acetone the deionisation method and the fractional vacuum distillation were used. This way a substance of very low conductivity was obtained [14, 15]. Sulphur dioxide was obtained and purified by the method recommended in the literature [16]. Before measurement in the cell five fractional vacuum distillations were carried out, using the middle fraction only till constant conductivity was achieved.

*Result*

The measured conductivity values as a function of temperature are given in *Table I* and Fig. 2. Table I contains the average of three measurements. The error was at about 5% at low and high temperatures, room temperature it was under 2%.

The permittivity *vs.* temperature curves can be fitted with the following third order power laws:

for methyl alcohol $\varepsilon_{(T)}=1.99\cdot 10^2-1.17T+2.79\cdot 10^{-3}T^2-2.45\cdot 10^{-6}T^3$
for ethyl alcohol $\varepsilon_{(T)}=1.34\cdot 10^2-7.08\cdot 10^{-1}T+1.50\cdot 10^{-3}T^2-1.19\cdot 10^{-6}T^3$
for acetone $\varepsilon_{(T)}=58.3-1.40\cdot 10^{-1}T+5.39\cdot 10^{-5}T^2+9.42\cdot 10^{-8}T^3$
for sulphur dioxide $\varepsilon_{(T)}=88.5-5.14\cdot 10^{-1}T+1.20\cdot 10^{-3}T^2-1.08\cdot 10^{-6}T^3$

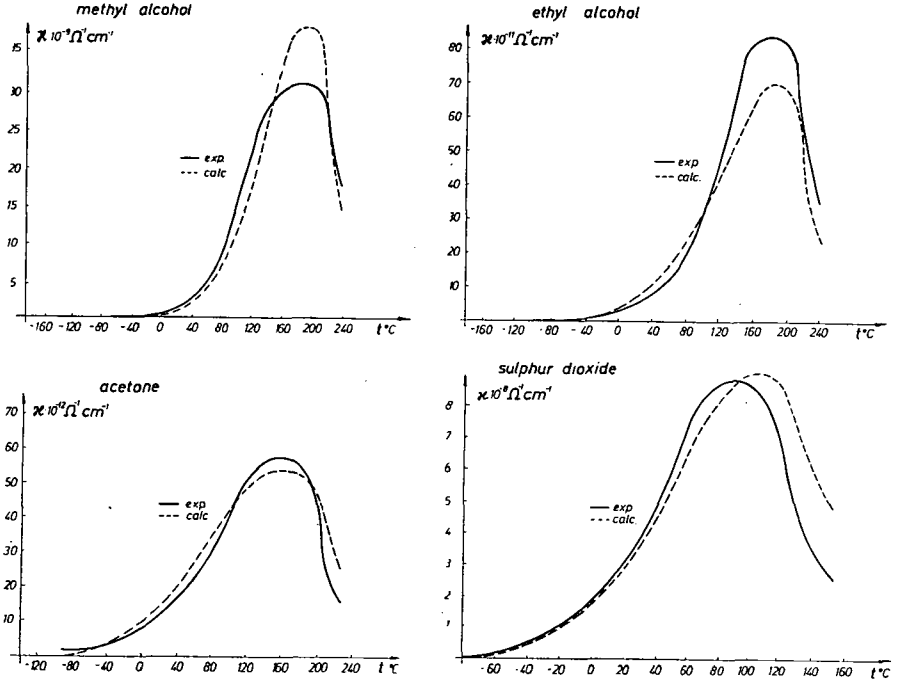


*Fig. 2.* Conductivity of methyl alcohol, ethyl alcohol, acetone and sulphur dioxide as a function of temperature

The conductivity maximum appears for methyl alcohol at about 195 °C, for ethyl alcohol at about 190 °C, for acetone at about 162 °C, and for sulphur dioxide at about 93 °C. The maxima are in the same areas, if they are expressed by the reduced temperature $T_r=T/T_c$, where $T_r$ is a reduced temperature, and $T_c$ is the critical temperature. The reduced temperature of the maximum for methyl alcohol is 0.91, for ethyl alcohol 0.90, for acetone 0.85 and for sulphur dioxide 0.85. The transition into gaseous state is not followed by a jump either in electric conductivity or permittivity.

*Table I*

*Conductivity of methyl alcohol, ethyl alcohol, acetone and sulphur dioxide as a function of temperature*

| t°C | Methyl alcohol $\varkappa \cdot 10^{-1} \Omega^{1-} cm^{-1}$ | Ethyl alcohol $\varkappa \cdot 10^{-10} \Omega^{-1} cm^{-1}$ | Acetone $\varkappa \cdot 10^{-12} \Omega^{-1} cm^{-1}$ | Sulphur dioxide $\varkappa \cdot 10^{-1} \Omega^{-1} cm^{-1}$ |
|---|---|---|---|---|
| −110 | — | 0.11 | — | — |
| −100 | — | 0.14 | — | — |
| −90 | 0.057 | — | 1.30 | — |
| −80 | 0.068 | 0.24 | 1.72 | — |
| −70 | — | — | — | 0.13 |
| −60 | 0.11 | 0.42 | 2.54 | 0.19 |
| −40 | 0.18 | 0.77 | 3.19 | 0.49 |
| −20 | 0.29 | 1.31 | 5.22 | 0.99 |
| 0 | 0.51 | 2.21 | 7.35 | 1.87 |
| 20 | 1.12 | 3.87 | 11.2 | 2.90 |
| 40 | 2.25 | 6.87 | 15.3 | 4.82 |
| 60 | 5.01 | 11.3 | 21.1 | 7.60 |
| 80 | 8.63 | 18.6 | 29.2 | 9.08 |
| 100 | 15.2 | 31.1 | 39.1 | 8.82 |
| 120 | 22.1 | 47.2 | 49.8 | 7.63 |
| 130 | — | — | — | 5.09 |
| 140 | 27.7 | 67.4 | 55.1 | 3.80 |
| 150 | — | — | — | 2.94 |
| 160 | 30.2 | 81.0 | 56.8 | 2.54 |
| 180 | 30.9 | 85.3 | 54.9 | — |
| 200 | 31.0 | 84.1 | 48.2 | — |
| 210 | — | — | 37.3 | — |
| 220 | 28.7 | 58.8 | 19.3 | — |
| 230 | 21.8 | 46.7 | 15.1 | — |
| 240 | 18.1 | 35.4 | — | — |

## *Discussion*

In the result analysis we have started form the liquid model which supposes a molecule arrangement on the short distances. In such a liquid due to the action of dipoles strong local fields appear and in the potential field of this type the movement of dipoles and of ions formed by autodissociations was quite limited. Started from this model [17—21], the quantitative expression for conductivity can be found,

$$\varkappa = \frac{c_o Z^2 e^2 \Delta l^2 \bar{\nu}}{6kT} \exp\left\{-\frac{U_o}{RT}\right\}, \tag{1}$$

where $\varkappa$ is the conductivity, $c_o$ — the concentration of ions, $e$ — the elementary charge, $\Delta l$ — the medium distance value between two next free places for the movement of ions, $\bar{\nu}$ — the medium frequency value of a breaking out attempt of a potential barrier, $k$ — Boltzmann constant, $U_o$ — the activation energy of process, and $T$ — the thermodynamic temperature.

For the smaller temperature interval, neglecting the change of the preexponential terms in relation to the exponential term, we obtain

$$\varkappa = A \exp\left\{-\frac{U_o}{RT}\right\} \tag{2}$$

This equation has often been proposed as an expression describing the temperature dependence of the conductivity. Using the experimental data we tried to bring the physical values in equation (1) to a qualitative connection with the values which we measured. The average ion speed, approximately equal to the average molecule speed, can be expressed as

$$\bar{v} = \frac{\Delta l}{\Delta t} \tag{3}$$

where $\Delta t$ is the time travelling of distance $\Delta l$. Substituting $l/\Delta t$ with the frequency of jump attempt of the potential barrier, we have

$$\bar{v} = \bar{v}\Delta l \text{ respectively } \bar{v}\Delta l = \bar{v}\Delta l^2 \tag{4}$$

With decreasing density the number of free spaces increases reducing there by the distance between next free spaces, while the average speed is proportional to the root of thermodynamic temperature:

$$\bar{v}\Delta l^2 = \varrho\sqrt{T} \tag{5}$$

The ion concentration is proportional to the concentration of the nondissociated molecules, *i.e.* to the density and to the dissociation degree. In the first approximation it can be assumed that dissociation degree will be proportional to the permittivity as a factor determining the Coulomb interaction force. The change of thermal energy will influence the degree of dissociation as a direct cause of dissociation, while the energy is proportional to the thermodynamic temperature. The ion concentration could be connected to the values in the simplest from:

$$c_o = \frac{N}{M}\varrho\alpha = \frac{N}{M}\varrho\varepsilon T \tag{6}$$

Eq. (1) can consequently be expressed as

$$\varkappa = \frac{Z^2 e^2 N p \varepsilon T \varrho \sqrt{T}}{6kTM} \exp\left\{\frac{U_o}{RT}\right\} \tag{7}$$

or in more condensed form

$$\varkappa = K\varepsilon\varrho^2\sqrt{T}\exp\left\{-\frac{U_o}{RT}\right\} \tag{8}$$

The constant $K$ contains the physical quantities which do not change with temperature and proportionality factors. Using the permittivity data in the whole temperature interval and the available data on density from the temperature interval and the available data on density from the literature [22—27], the calculated results were presented according to Eq. (8). The reproducibility of the course of the experimental curve can be satisfactory, taking into consideration the semi-quantitative character of Eq. (8). The application of Eq. (8) for the determination of the conductivity of water, for which we have the experimental data [27—30] on conductivity, density and permittivity, gave us similar results. Eq. (8) predicts the maximum of conductivity of water on the temperature cca. 270 °C, what is an agreement with some experimental data and with the course of experimental curve. The reduced temperature of the maximum of water is 0.84, expressed according to the Eq. (8).

## *Conclusions*

The experimental results show that the conductivity of the investigated substances as a function of temperature goes through a maximum. Observations point out that this is a general feature of all polar liquid dielectrics. We consider that the cause of the decreasing conductivity is the declining number of ions at higher temperatures and the suddenly declining density approaching the critical temperature. The thermal energy as a direct cause of dissociation increases more slowly than the above mentioned factors decrease in this temperature interval causing a maximum in $\varkappa = f(t)$.

### References

[1] *Evers, E. C., A. G. Knox:* J. Am. Chem. Soc. **73**, 1739 (1951).
[2] *van Dyke, R. E.:* J. Am. Chem. Soc. **72**, 2823 (1950).
[3] *Cady, H. P., R. Taft:* J. Phys Chem. **29**, 1075 (1925).
[4] *Walden, P.:* Das Leitvermögen der Lösungen (Akademische Verlagsgesellschaft m.b.H. Leipzig, 1924).
[5] *Landolt—Börnstein:* Zahlenwerte und Funktionen (Springer Verlag, Berlin Göttingen—Heidelberg, 1964).
[6] *Briere, G.:* Ann. Phys. **9**, 73 (1964).
[7] *Barret, S., G. Briere , N. Felici, G. Pierre:* C. R. Acad. Sc. Paris, 4400—4403 (1965).
[8] Ullmanns Encyklopedie der technischen Chemie, III Auflage, Urban Schwarzenberg, Berlin (1960).
[9] *Dannhauser, W.:* J. phys. Chem **68**, 2007 (1964).
[10] *Dulić, N. ,L. Horváth:* Acta Phys. et Chem. Szeged, **4**, 451 (1978).
[11] *Dulić, N., L. Horváth:* Bulletin de la société chimique Beograd **45** 358 (1980).
[12] *Kohlrausch, F.:* Praktische Physik (Teubner Verlagsgesellschaft, Stutgart, 1955).
[13] *Mecke, R., R. Joeckle, G. Klingenberg:* Z. für Elektrochemie, **66**, 239 (1962).
[14] *Felici, N. J.:* Brit. J. Appl. Phys. **15**, 801 (1964).
[15] *Inczédy, J.:* Ioncserélők analitikai alkalmazása (Műszaki Könyvkiadó, Budapest, 1962).
[16] *Müller G., G. Gnauck:* Reinste Gase (VEB Deutscher Verlag der Wissenschaften, Berlin, 1965).
[17] *Frenkel J.:* Kinetic Theory of Liquids (Clarendon Press, Oxford, 1946).
[18] *Szkanavi, I. G.:* Dielektrikumok fizikája (Akadémiai Kiadó, Budapest, 1953).
[19] *Hirschfelder, J. O., C. F., Curtiss, R. B. Brid:* Molecular Theory of Gases and Liquids (J. Wiley et Sons, Inc. New York, 1964).
[20] *Fröhlich, H.:* Theory of Dielectrics (Clarendon Press, Oxford, 1968).
[21] *Rost, A.:* Messungen dielektrischer Stoffeigenschaften, (Viewege, Braunschweig, 1978).
[22] *Young, S.:* Sci. Proc. Roy. Soc. Dublin N. S. XII. 374 (1909—10).

[23] *Lange, A.:* Z. angew. Chem. 275, (1899).
[24] *Herz, A., E. Neukrich:* Z. Phys. Chem. **104**, 433 (1923).
[25] *Cardoso, E., E. Sorrentino:* J. Chim. Phys. **24**, 77 (1927).
[26] *Brewer A. D., J. E. C. Hutchins:* Nature, London, **210**, 1257 (1966).
[27] *Wright, J. M. jun., W. T. Lindsay, T. R. Druga:* WAPD—TM—204 U.S.A.C. (June 1961).
[28] *Wilde, B. E.:* Electrochimica Acta, **12**, 737 (1967).
[29] *Akerlof, G. C., H. J. Oshry:* J. Am. Chem. Soc. **72**, 2844 (1950).
[30] *Fairbrother, F.:* J. Chem. Soc. 1051 (1948).

## ТЕМПЕРАТУРНАЯ ЗАВИСИМОСТЬ ЭЛЕКТРИЧЕСКОЙ ПРОВОДИМОСТИ ЖИДКИХ ПОЛЯРНЫХ ДИЭЛЕКТРИКОВ

*Л. Хорват*

Проведены непрерывные измерения проводимости и диэлектрической проницаемости некоторых жидких полярных диэлектриков, в широком температурном интервале от точки плавления до критической точки, в закрытой измерительной ячейке при давлении насыщенных паров. Измерения проводились метиловым и этиловым спиртами, ацетоном и двуокисью серы при частоте 1591,1 Гц.

# STUDIES OF SPECTRAL BEHAVIOUR OF COPPER(II) COMPLEXES OF AROMATIC SCHIFF BASES AND OF SECONDARY AMINES

By

J. CSÁSZÁR

Institute of General and Physical Chemistry, Attila József University, Szeged, Hungary

*(Received 20th October, 1983)*

A series of amines of the type $C_6H_4(OH).CH_2.NH.(CH_2)_n.NH.CH_2.C_6H_4(OH)$ (n = 2—7 9, 10) were prepared by $NaBH_4$ reduction of salicylidene anilines, and their copper(II) complexes too were prepared. From the results of u.v., i.r. spectral and magnetic moment investigations it is probable that these secondary amines form monomeric, square-planar CuL-type chelate complexes with Cu(II) ions.

Compounds of bivalent copper are known to exhibit different coordination states, some being four-coordinate, whereas others are five-, or occasionally six-coordinate; a weaker ligand field generally leads to an increased coordination number [1]. In an earlier paper [2] we described the spectra of secondary amines obtained by $NaBH_4$ reduction of salicylidene anilines and also the spectra of their copper(II) complexes. As an extension of this work we have prepared a series of amines of type $C_6H_4(OH).CH_2.NH(CH_2)_nNH.CH_2.C_6H_4(OH)$ (Structure 1) ($n$=2−7, 9, 10), in

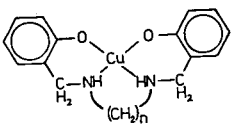


a similar way as previously, together with their copper chelates. In the present paper we report on the u.v. and visible spectral behaviour of these compounds, and compare the spectra of some copper chelates of the corresponding tetradentate parent Schiff bases ($n$=2, 4, 6, 10) with those of their adducts with phenol derivatives.

## *Experimental*

*Preparation of amines.*

A two-fold molar amount of $NaBH_4$ was added in portions to a methanolic solution of the Schiff base, and the mixture was refluxed for fifteen minutes. The amines were liberated from the colourless solutions on addition of distilled water; the products were recrystallized from aqueous ethanol. All the amines prepared are white solids, practically insoluble in water, but readily soluble in organic solvents. The analytical data are listed in Table I.

*Table I*

*Analytical data on secondary amines and their copper(II) complexes*

| n | C% | | H% | | M. p.* | C% | | Cu% | |
|---|---|---|---|---|---|---|---|---|---|
| | Calcd. | Found | Calcd. | Found | | Calcd. | Found | Calcd. | Found |
| 2 | 70.56 | 70.48 | 7.40 | 7.34 | 121.5—121.7 | 57.56 | 57.65 | 19.03 | 18.80 |
| 3 | 71.30 | 71.22 | 7.74 | 7.78 | 107.2—107.4 | 58.69 | 58.56 | 18.26 | 18.09 |
| 4 | 71.97 | 71.96 | 8.05 | 8.00 | 119.5—119.8 | 59.73 | 59.48 | 17.56 | 17.44 |
| 5 | 72.58 | 72.51 | 8.33 | 8.31 | 98.5—98.7 | 60.70 | 60.65 | 16.90 | 16.80 |
| 6 | 73.13 | 73.09 | 8.59 | 8.48 | 110.6—110.8 | 61.59 | 61.70 | 16.29 | 16.11 |
| 7 | 73.64 | 73.60 | 8.83 | 8.75 | 98.0—98.8 | 62.43 | 62.49 | 15.73 | 15.60 |
| 9 | 74.55 | 74.55 | 9.25 | 9.27 | 99.5—99.7 | 63.94 | 63.70 | 14.71 | 14.62 |
| 10 | 74.96 | 74.29 | 9.44 | 9.40 | 106.7—106.9 | 64.62 | 64.56 | 14.24 | 14.09 |

* Uncorrected values.

*Preparation of copper(II) chelates.*

To a mixture of a warm aqueous solution of copper(II) acetate monohydrate (0.01 mole) and a slight excess of secondary amine in methanol, was added 0.01 mole NaOH in water. From the green solutions, crystalline products separated out immediately or after 24 hours. The products were filtered off, and washed with ethanol and ether. The complexes are deepgreen; they are soluble in polar organic solvents, but their solubility decreases as the length of the methylene chains increases. The analytical data are given in Table I.

*Preparation of adducts.*

A mixture of CuBHSAL-en* and the corresponding phenol derivative in 1:1 mole ratio was warmed above the m.p. of the phenol component; immediate formation of a violet addition compound occured. The mass was washed with chloroform or chloroform-benzene to remove the excess of phenol. The analytical data prove the formation of 1:1 adducts.

* N,N-ethylenebis(salicylaldimine)copper(II)

*Spectral measurements.*

The u.v. and visible spectra were measured at 295 K on a SPECORD UV—VIS spectrofotometer, using spectrograde solvents. The reflection spectra were measured without dilution, against a MgO standard on a BECKMAN DU spectrophotometer, in KBr discs and in chloroform solution.

## *Results and Discussion*

*U.v. spectra of secondary amines.*

The spectral data on the secondary amines studied are presented in Table II; typical spectra are shown in Fig. 1.

*Table II*

*U.v. spectral data on secondary amines in different media*

| n= | Solvent* | nm and log ε | n= | Solvent* | nm and log ε |
|---|---|---|---|---|---|
| 2 | M | 205(4.18) ~218 274(3.59) | 6 | M | 206(4.33) ~215 277(3.74) |
| | A | 203(4.18) 216(4.08) 278(3.73) | | A | 202(4.21) 217(4.05) 276(3.63) |
| | B | 213(4.25) 241(4.20) 293(3.85) | | B | 212(4.32) 241(4.27) 293(3.80) |
| 3 | M | 207(4.20) ~216 277(3.64) | 7 | M | 203(4.32) ~218 277(3.48) |
| | A | 203(4.22) 216(4.15) 276(3.80) | | A | 202(4.23) 216(4.11) 276(3.67) |
| | B | 212(4.29) 241(4.15) 293(3.79) | | B | 212(4.30) 241(4.15) 294(3.71) |
| 4 | M | 206(4.27) ~215 276(3.69) | 9 | M | 203(4.33) ~218 277(3.64) |
| | A | 202(4.21) 216(4.08) 277(3.73) | | A | 202(4.29) 216(4.13) 277(3.79) |
| | B | 212(4.32) 241(4.21) 293(3.85) | | B | 211(4.43) 241(4.29) 292(3.93) |
| 5 | M | 203(4.27) ~218 277(3.59) | 10 | M | 203(4.35) ~218 278(3.56) |
| | A | 202(4.25) 216(4.16) 276(3.82) | | A | 202(4.28) 216(4.06) 277(3.73) |
| | B | 211(4.33) 241(4.18) 293(3.81) | | B | 211(4.38) 241(4.21) 293(3.84) |

* M: methanol; A: 0.1 mol $dm^{-3}$ $H_2SO_4/CH_3OH$; B: 0.1 mol $dm^{-3}$ $NaOH/CH_3OH$

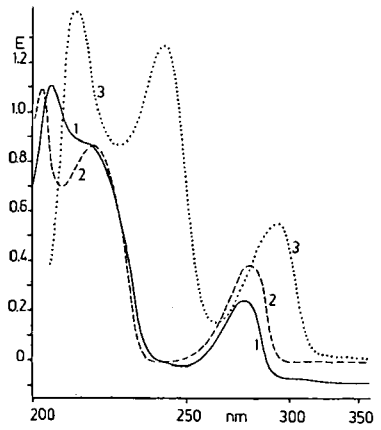


*Fig. 1.* U. v. spectra of N,N'-ethylenebis(o-hydroxybenzylamine). **1**: in methanol, $c = 7.7.10^{-4}$ mol/$dm^3$; **2**: in 0.1 $H_2SO_4/CH_3OH$, $c = 7.3.10^{-4}$ mol/$dm^3$; **3**: in 0,1 $NaOH/CH_3OH$, $c = 8.1.10^{-4}$ mol/$dm^3$. d = 0.1 cm; T = 295 K

The structures of the u.v. spectra of the amines are completely similar. The methanolic solutions show two characteristic bands, at 202—206 and 274—278 nm, with a shoulder at about 218 nm; the bands are interpreted as $\pi^* \leftarrow \pi$ bands. The intensity of the first band increases with increasing methylene chain length. In acidic solution a band appears at 216—218 nm, too; we assumed that this band corresponds to the protonated form of the amine molecule. In basic media the band intensities increase and the maxima show a red shift. It is interesting that the energy of the bands shows no dependency on $n$, but the intensity is higher for odd $n$.

*Visible spectra of copper chelates.*

The relevant features of the solution spectra of the complexes studied are summarized in Table III; a typical set of curves is given in Fig. 2.

The reflection spectra of copper(II) chelates are characteristic of square-planar complexes; a band is found in the range 600—650 nm. It may be noted that a plot of $\lambda_{max}$ *vs.* the number of carbon atoms in the alkyl chain is zigzag in shape; $\lambda_{max}$ is generally higher for an odd number of C atoms. In chloroform solution a medium-intensity and a flat band ($\varepsilon \sim 700$—1600) appear at about 660—580 and 380—420 nm, respectively. Dissolution of green CuBHSAL-en in chloroform or in glacial acetic acid results in a purple solution; the phenomena were interpreted by adduct formation [3, 4]. A similar colour change is not observed for the complexes of secondary amines. There is a marked spectral difference between the two types of complexes having bands of significantly higher intensity ($\varepsilon \sim 8000 - 12\,000$) in the region 380—420 nm.

WATERS et al. [5, 6] proposed that the green copper complexes possess an effective coordination number exceeding four, due either to intermolecular association or to adduct formation with LEWIS bases, while the brown or violet complexes contain four-coordinate copper(II). The green complexes generally absorb less in the 500 nm region and more in the 700 nm region than do the brown or violet complexes.

For copper(II) ions, theory predicts that three or four transitions should occur within the 3d orbitals, depending on the symmetry involved [7, 8]. In most cases the spectra of planar copper(II) complexes display only a single band, making assignment of individual electronic transitions difficult. The CD spectra of optically active copper(II) complexes indicate the presence of three transitions [7]; these have been

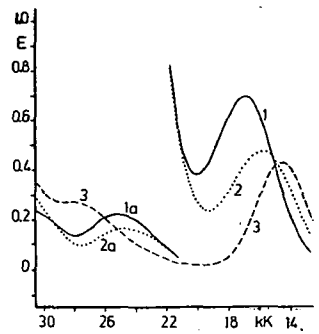


*Fig. 2.* Visible spectra of N,N'-ethylenebis(o-hydroxybenzylamine)copper(II). **1**: in chloroform, $c = 2.2.10^{-3}$ mol/dm³; **2**; in pyridine, $c = 2.1.10^{-3}$ mol/dm³; **3**: in glacial acetic acid, $c = 2.4.10^{-3}$ mol/dm³. d=for 1, 2, 3: 1.0 cm, for **1a**, **2a**: 0.1 cm,: t=295 K

*Table III*

*Visible spectral data on copper(II) chelates of secondary amines and of Schiff bases*

| n= | Solvent a) | nm and ε | | | |
|---|---|---|---|---|---|
| | | Chelates of sec. amines | | Chelates of Schiff bases | |
| 2 | Chl. | 595(325) | 396(1150) | 573(380) | 371(10 965) |
| | Py | 638(235) | 406(810) | 601(282) | 369(10 720) |
| | HAc | 683(190) | ~358 | 568(365) | 351( 9 120) |
| 3 | Chl. | 658(130) | 396(1100) | | |
| | Py | 611(225) | 401(815) | | |
| | HAc | 683(248) | ~370 | | |
| 4 | Chl. | b) | | 644[c] | 382[c] |
| | Py | 635(180) | ~385 | 661[c] | 382[c] |
| | HAc | 687(186) | ~365 | 687(148) | 357( 8 710) |
| 5 | Chl. | ~625 | 420(730) | | |
| | Py | 661(178) | 408(863) | | |
| | HAc | 687(195) | ~358 | | |
| 6 | Chl. | ~618 | 433(1230) | ~617 | 399( 9 550) |
| | Py | 641(225) | 414(975) | 613(167) | 368( 9 330) |
| | HAc | 683(218) | ~365 | 683(177) | 357( 7 908) |
| 7 | Chl. | ~625 | 420(1410) | | |
| | Py | 668(163) | 388(870) | | |
| | HAc | 676(220) | 347(226) | | |
| 9 | Chl. | ~628 | 417(1462) | | |
| | Py | 672(164) | 391(900) | | |
| | HAc | 691(196) | 353(265) | | |
| 10 | Chl. | ~632 | 395(1088) | ~617 | 368(11 750) |
| | Py | 676(175) | ~385 | 625(130) | 365(11 220) |
| | HAc | 687(205) | 352(196) | 687(182) | 355( 9 120) |

[a] Chl.: chloroform; Py: pyridine; HAc: glacial acetic acid;
[b] Very low solubility; [c] Saturated solution at room temperature.

assigned to $d_{z^2} \leftarrow d_{xy}$, $d_{x^2-y^2} \leftarrow d_{xy}$ and probably $d_{xz} \leftarrow d_{xy}$ in the sequence of increasing energy under $C_2$ symmetry.

The spectra of the complexes recorded in Table III show a pronounced absorption in the 580—660 nm region; this band can be assigned as a d—d band. The *cis*-acentric copper(II) chelates generally have d—d-bands of higher intensity than those of the related *trans* chelates [9]. Our results show that the chelates of secondary amines have bands with intensities of $\varepsilon \sim 150$—350, so the possibility of a polymeric structure is not excluded. CuBHSAL-en, containing *cis*-planar moieties, has a band of higher intensity ($\varepsilon = 380$) in this region (Fig. 3).

Interpretation of the medium-intensity band found in the range 380—420 nm for chelates of secondary amines is difficult. According to YAMADA et al. [10], this band is closely related to a copper-copper interaction, but on the basis of our experimental data it may only be stated that the 380—420 and 580—660 nm bands are of completely different origins.

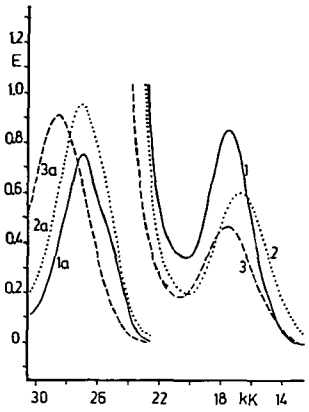


*Fig. 3.* Visible spectra of N,N'-ethylenebis(salicylidene-iminato) copper(II). **1**: *in* chloroform, $c = 2.2.10^{-3}$ mol/dm³; **2**: *in* pyridine, $c = 2.1.\ 10^{-3}$ mol/dm³; **3**: in glacial acetic acid, $c = 2.4.10^{-3}$ mol/dm³; d = for 1—3: 1.0 cm; curves **1a**—**3a** are illustrated with an arbitrary scale

In pyridine the bands are shifted by ca. 20—50 nm towards lower energy, and the spectra of the products crystallized from pyridine are the same as those of the original compounds. The experimental results demonstrate that no adduct formation takes place, similarly as for CuBHSAL-en [11]. In glacial acetic acid the bands are shifted further to lower energy. In N-bases (pyridine, 2- and 4-picoline, 2,4,6-collidine) the two groups of chelates behave similarly; with increase in pK the visible bands shift to higher energy and their intensities increase, too.

The magnetic measurements of LEWIS and WALTON [11] indicate that there is no significant exchange interaction between the copper atoms in the case of CuBHSAL-en. The copper(II) derivatives of tetradentate ligands of BHSAL-en type exhibit a decrease in ligand field strength as the number of $CH_2$ groups increases; this decrease is coupled with a small increase in magnetic moment [12]: BM for $n = 2$: 1.84, $n = 3$: 1.89, $n = 4$: 1.94. This change is interpreted as being indicative of an increasing distortion from planarity towards tetrahedral geometry [12]. CuBHSAL-hxmda* is an exception (BM = 1.74 [12]; its structure is probably polymeric, as can be seen in Structure 3 [13]. Our preliminary magnetic measurements show that the magnetic moments of chelates of secondary amines fall in the range 1.85—2.05 BM, and no relation can be found between the BM values and the chain length. These values probably correspond to a square-planar arrangement, and they indicate no magnetic interaction between the atoms, if we assume a polymeric structure.

There are important differences between the i.r. spectra of the complexes of the two types. The NH strething frequency can be found at around 3100 $cm^{-1}$, its position being almost independent of the alkyl chain length. Several frequencies are absorbed in the interval 1200—1600 $cm^{-1}$, corresponding to vibrations of the aromatic systems. We assigned the 1270—1280 $cm^{-1}$ band to the $\nu C-O$ vibration. On the basis of the i.r. spectra the coordination of acetate ion can be excluded, in contrast with the aniline derivatives discussed earlier [2].

* N,N'-hexamethylenediaminebis(salicylaldimine) copper(II)

X-ray determinations [14, 15] have shown that CuBHSAL-en is dimeric (Structure 2), with copper-to-oxygen bridges joining the two units of the dimer, in which

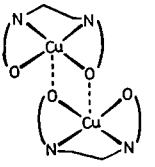

the copper(II) ions are in an essentially square-pyramidal environment. A basically similar structure is found [16] for the trimethylene-bridged analogue, too. Unfortunately, there is no structural information on chelates of secondary amines, so we can present only suppositions in connection with the stereochemical arrangement.

Besides the experimental results already discussed the following must also be taken into account. In one respect, an additional methylene group would allow the donor atoms to move out of square-planar coordination positions. On the other hand, with increasing length of the polymethylene chain there would be an increasing tendency for the potentially tetradentate ligand to bind two copper(II) ions, each in a bidentate fashion (Structures 3, 4).

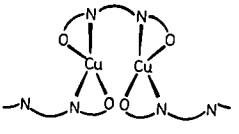

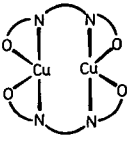

On the basis of the data available in this study it is not possible to determine unambiguously the stereochemistry of these chelates. We consider it most likely that monomeric square-planar molecules are formed (at least in solution), independently of the length of the methylene chains (Structure 5). The results of osmometric measurements also suggest monomeric species.

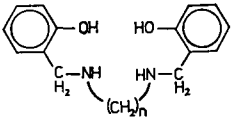

*Comparison of spectral and other behaviour of CuBHSAL-en and CuBEBA.** The spectral data measured in different organic solvents are listed in Table IV. The long-wave band of CuBHSAL-en appears at 560—600 nm ($\varepsilon \sim 320-450$) and no correlation can be found between $\lambda_{max}$ and the dielectric constants $\varepsilon$; however, a plot of $\lambda_{max}$ *vs.* the donor number DN [17, 18] gives a linear relationship. The 350—360 nm band has a very high intensity, $\varepsilon \sim 9000$—12 000. The visible band of CuBEBA is shifted by ca. 10—40 nm to lower energy ($\varepsilon \sim 150$—300); the $\lambda_{max}$ *vs.*

* N,N'-ethylenebis(o-hydroxybenzylamine) copper(II)

*Table IV*

*Spectral data on CuBHSAL-en and CuBEBA in different solvents*

| Solvents | ε | λ/nm of bands | | | |
|---|---|---|---|---|---|
| | | Chelates of Schiff bases | | Chelates of sec. amines | |
| DMSO | 46.68 | 580 | 365 | 618 | 392 |
| Acetonitrile | 37.50 | 573 | 362 | 604 | 392 |
| DMFA | 36.71 | 578 | 365 | 612 | 395 |
| Nitromethane | 35.87 | 570 | 364 | 586 | 394 |
| Nitrobenzene | 34.80 | 571 | — | 594 | — |
| Acetone | 20.70 | 575 | 366 | 607 | 395 |
| Pyridine | 12.40 | 601 | 369 | 641 | 407 |
| MeOH | 32.70 | 565 | 356 | 592 | 391 |
| EtOH | 24.55 | 568 | 360 | 583 | 394 |
| n-PrOH | 20.33 | 568 | 362 | 586 | 395 |
| $CH_2Cl_2$ | 8.93 | 573 | 368 | 591 | 399 |
| $CHCl_3$ | 4.806 | 573 | 371 | 597 | 397 |
| Benzene | 2.275 | 574 | 374 | 590 | 404 |
| Cl-Benzene | | 578 | 374 | 595 | 395 |
| p-Xylene | 2.2699 | 586 | 373 | insol. | |
| Dioxane | 2.209 | 587 | 370 | 599 | 398 |
| Glac. ac. acid | 6.15 | 568 | 351 | 688 | ~360 |

DN plot also gives a straight line. The 380—400 nm band has a lower intensity ($\varepsilon \sim 800$—$2000$) than that for CuBHSAL-en.

One marked difference between the two complexes is that CuBHSAL-en reacts with metal halides or perchlorates to form bi- and trinuclear complexes [12, 19, 20], while for CuBEBA this is not observed.

TANAKA [4] has reported that CuBHSAL-en forms an adduct with general formula CuBHSAL-en.B with chloroform, glacial acetic acid and phenol derivatives. X-ray determinations have shown [5] that these adducts are monomeric, four-coordinate and essentially planar; the above molecules are bound to the oxygen donor atoms and not to the metal [16, 21]. We have prepared and investigated a series of CuBHSAL-en. n-X-phenol-type adducts (n-X: H, 2-$CH_3$, 2-Cl, 2-OH, 2-$NO_2$, 4-$CH_3$, 4-Cl, 4-OH, 4-$NO_2$). With the exception of the 2-$NO_2$-phenol derivative (green) all the adducts are violet solids soluble in chloroform. Their reflection spectra show a broad band at about 560—580 nm, while in chloroform two bands are found, at 560—570 and 360—370 nm, respectively. The substituents X have no significant effect on the band positions. Similar adduct formation was not observed for any chelate of secondary amines.

Our further detailed investigations are in progress.

## References

[1] *Freeman, H. C.:* The Biochemistry of Copper., Ed. J. Peisach, P. Aisen, W. E. Blumberg, Acad. Press, New York, 1966.
[2] *Császár, J.:* Acta Phys. et Chem., Szeged, **29**, 139 (1983).
[3] *Pfeiffer, P., E. Breith, E. Lübbe, T. Tsumaki:* Ann. **503**, 84 (1933).
[4] *Tanaka, T.:* Bull. Chem. Soc. Japan **29**, 93 (1956), **31**, 4108 (1958).

[5] *Baker, E. N., D. Hall, T. N. Waters:* J. Chem. Soc. **A**, 400 (1970).
[6] *Waters, T. N., D. Hall:* J. Chem. Soc. 1200, 1203 (1959).
[7] *Belford, R. L., W. A. Yeramos:* Mol. Phys. **6**, 121 (1963).
[8] *Downing, R. S., F. L. Urbach:* J. Amer. Chem. Soc. **91**, 5977 (1969).
[9] *Belford, R. L., T. S. Piper:* Mol. Phys. **5**, 251 (1962).
[10] *Yamada, S., H. Nakamura, R. Tsuchida:* Bull. Chem. Soc. Japan, **31**, 303 (1958).
[11] *Lewis, J., R. A. Walton:* J. Chem. Soc. **A**, 1559 (1966).
[12] *Gruber, S. J., C. M. Harris, E. Sinn:* J. Inorg. Nucl. Chem. **30**, 1805 (1968).
[13] *Kirson, B., H. Sechter:* Bull. Soc. Chim. France 2743 (1965).
[14] *Fackler, K., M. von Stackelberg:* Z. anorg. allg. Chem. **305**, 286 (1960).
[15] *Hall, D., T. N. Waters:* J. Chem. Soc. 2644 (1960).
[16] *Llewellyn, F. J., T. N. Waters:* J. Chem. Soc. 2639 (1960).
[17] *Gutmann, V.:* Coordination Chemistry in Non Aqueous Solutions., Springer Vlg. ,Vienna, New York, 1968.
[18] *Gutmann, V., A. Scherhaufer:* Mh. Chem. **99**, 335 (1968).
[19] *Harris, C. M., E. Sinn:* J. Inorg. Nucl. Chem. **30**, 2723 (1968).
[20] *Kokot, S., C. M. Harris, E. Sinn:* Austr. J. Chem. **25**, 45 (1972).
[21] *Clark, G. R., D. Hall, T. N. Waters:* J. Chem. Soc. **A**, 223 (1968).

## ИЗУЧЕНИЕ СПЕКТРОСКОПИЧЕСКИХ СВОЙСТВ КОМПЛЕКСОВ МЕДИ (II) С АРОМАТИЧЕСКИМИ ОСНОВАНИЯМИ ШИФА И ВТОРИЧНЫМИ АМИНАМИ

*Й. Часар*

Натрий боргидридным восстановлением салицилидене-анилинов синтезирована серия аминов типа $C_6H_4(OH)CH_2NH(CH_2)NHCH_2C_6H_4$ (OH)(n=2–7, 9–10) и их комплекса с медью(II). На основании УФ- и ИК-спектроскопии и данных по магнитным моментам соединений можно предположить, что эти вторичные амины образуют плоские квадратные хелатные комплексы типа CuL с ионами меди (II).

# STUDY OF 5-$NO_2$-2-FURALDEHYDE DERIVATIVES, I. U. V., I. R. AND $^1H$ NMR SPECTRAL INVESTIGATIONS OF SCHIFF BASE COMPOUNDS

By

J. CSÁSZÁR

Institute of General and Physical Chemistry, Attila József University, Szeged

*(Received 20th October, 1983)*

Schiff base derivatives of 5-$NO_2$-2-furaldehyde were prepared and their u.v., i.r. and $^1H$ NMR spectra were examined.

Several investigations have been reported on the bacteriological properties of certain furan compounds [1—3]. DODD and STILLMAN [4] stated that the presence of a $NO_2$ group in position 5 of the furan ring conferred appreciable bacteriostatic action. Thus, the 5-$NO_2$-furan derivatives generally exhibited considerable antibacterial activity, primarily *in vitro* against gram-negative and gram-positive organisms. Some compounds of this type, *e.g.* Nitrofurazol, Nitrofurantoin and Furazolidon, are applied therapeutically in the treatment of bacterial infections of the urinary tract. TANAKA and USUI [5—8] described in several papers the preparation and antibacterial activity of 2-derivatives of 5-$NO_2$-furan, while MASSARINI et al. [9, 10], SZARVAS [11] and SPENCER et al. [12] investigated a number of Schiff base derivatives of 5-$NO_2$-2-furaldehyde (**NFA**).

As a continuation of our previous investigations on the spectral behaviour of aromatic Schiff bases [13], we have prepared and studied several Schiff base derivatives of NFA; in this paper we report on the spectral behaviour of the following Schiff bases.

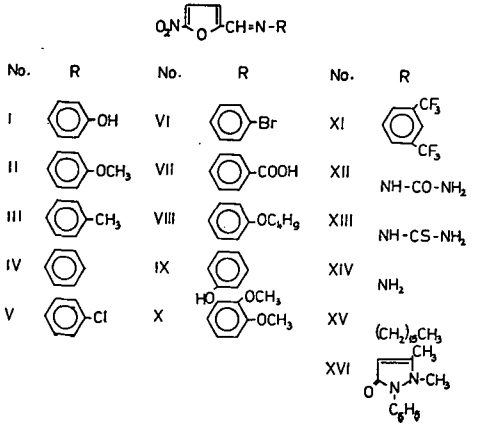

## *Experimental*

The Schiff bases were prepared by the following general procedure. A methanolic solution of 0.01 mol NFA was treated with an alcoholic solution of 0.01 mol of the appropriate amine. The mixtures were acidified with 0.001 mol cc. $H_2SO_4$. The crystalline products separated immediately or after removal of half of the solvent. The products were recrystallized from an ethanol/benzene mixture. The compositions were checked *via* the m.p.s and C and H analysis; these data are given in Table I.

The u.v. spectra were measured on a SPECORD UV—VIS spectrophotometer, in spectroscopically pure solvents at room temperature; the records were begun 2.5 min after dissolution. The $^1H$ NMR spectra were obtained in $CDCl_3$-DMSO-$d_6$ solution with a JEOL 60 MHz spectrometer, and the chemical shifts in ppm were determined using TMS as internal standard. The i.r. spectra were taken on a ZEISS UR—10 spectrophotometer, in KBr discs.

The disappearance of Schiff bases was followed spectrophotometrically at 298 K in unbuffered 50% aqueous methanol solution. All kinetic runs were carried out in the time interval between $t=0$ and $t=360$ min. The preliminary rate constants were calculated by the GUGGENHEIM method.

*Table I*

*Analytical data on Schiff bases*

| No. | M. p. | C% | | H% | |
|---|---|---|---|---|---|
| | | Calcd. | Found | Calcd. | Found |
| I | 181—4 | 56.85 | 56.78 | 3.47 | 3.39 |
| II | 124—6 | 58.48 | 58.45 | 4.01 | 5.01 |
| III | 130—3 | 62.54 | 62.44 | 4.38 | 4.31 |
| IV | 125—8 | 61.34 | 61.24 | 3.28 | 3.16 |
| V | 155—8 | 52.67 | 52.63 | 2.82 | 2.75 |
| VI | 156—7 | 44.73 | 44.70 | 2.39 | 2.34 |
| VII | 145* | 55.39 | 55.28 | 3.10 | 3.12 |
| VIII | 137—40 | 62.49 | 62.41 | 5.59 | 5.47 |
| IX | 145* | 56.85 | 56.74 | 3.47 | 3.52 |
| X | 126—8 | 56.52 | 56.48 | 4.38 | 4.35 |
| XI | 104—6 | 44.34 | 44.28 | 1.72 | 1.70 |
| XII | 239—42 | 36.34 | 36.19 | 3.05 | 3.11 |
| XIII | 250* | 33.61 | 33.54 | 2.82 | 2.75 |
| XIV | 251—2 | 38.68 | 38.61 | 3.25 | 3.21 |
| XV | 170—1 | 69.20 | 69.17 | 9.96 | 9.90 |
| XVI | 265—9 | 58.84 | 58.80 | 4.32 | 4.27 |

* decomposed

## *Results and discussion*

*U.v. spectra.* The spectral data on the Schiff bases in methanol and benzene are presented in Table II; several spectra are shown in Fig. 1.

The $NO_2$ group exhibits two bands in the u.v. range, at 210 ($\varepsilon=15\,850$) and 270 nm ($\varepsilon=20$); both bands are assigned as $\pi^* \leftarrow \pi$ bands [14]. The characteristic

*Table II*

*U.v. spectral data on the Schiff bases studied*

| No. | Solvent | Band maxima (nm and ε) | | |
|---|---|---|---|---|
| **NFA** | MeOH | 225 (3 800) | 308(11 220) | |
| | $C_6H_6$ | | 303 (9 770) | |
| **I** | MeOH | 222(15 490) | 294(15 130) | 397(22 900) |
| | $C_6H_6$ | | 294(10 000) | 396(16 600) |
| **II** | MeOH | 222(14 800) | 290(15 130) | 390(20 900) |
| | $C_6H_6$ | | 296(15 130) | 400 (25120) |
| **III** | MeOH | 213(17 780) | 284(15 130) | 360(23 990) |
| | $C_6H_6$ | | 287(12 880) | 380(20 890) |
| **IV** | MeOH | | 279(12 020) | 357(19 050) |
| | $C_6H_6$ | | 283(10 000) | 364(15 850) |
| **V** | MeOH | 232(14 800) | 282(14 450) | 360(23 990) |
| | $C_6H_6$ | | 287(10 230) | 371(16 600) |
| **VI** | MeOH | 232(11 480) | 283(11 480) | 361(18 620) |
| | $C_6H_6$ | | 284(11 220) | 370 (18 200) |
| **VII*** | MeOH | 219 (9 550) | 289(17 380) | |
| **VIII** | MeOH | 223(14 450) | 294(14 790) | 394(21 880) |
| | $C_6H_6$ | | 298(14 120) | 402(23 440) |
| **IX** | MeOH | 217(19 050) | 300(15 850) | 394(17 780) |
| | $C_6H_6$ | | 304(11 480) | 404(19 050) |
| **X*** | MeOH | 207(19 950) | 300(14 790) | 402(15 850) |
| **XI** | MeOH | 233(17 380) | ~280 | 340(25 120) |
| | $C_6H_6$ | | | 346(19 050) |
| **XII*** | MeOH | ~238 | 264(14 450) | 364(22 910) |
| **XIII*** | MeOH | 240 (7 940) | 288(11 480) | 382(19 500) |
| **XIV** | MeOH | 233 (4 470) | | 373(16 600) |
| | $C_6H_6$ | | 282 (6 920) | 373(26 300) |
| **XV** | MeOH | 225(13 490) | 324(15 850) | |
| | $C_6H_6$ | | 239(16 980) | |
| **XVI** | MeOH | 234(12 590) | 291(13 180) | 404(18 620) |
| | $C_6H_6$ | | 294(14 790) | 408(18 200) |

* practically insoluble in benzene

bands of furan, 2-furaldehyde and **NFA** are found at 250 nm ($\varepsilon$=6400), at 230 and 275 nm ($\varepsilon$=3500 and 13 750) and at 225 and 310 nm ($\varepsilon$=8250 and 11 600) [15, 16], respectively. The longwave band of **NFA**, which is a superposition of the absorption of furaldehyde and that of the nitro group, shows a bathochromic shift of ca. 30 nm, and the intensity of this band is decreased, relative to the situation for 2-furaldehyde.

Both Fig. 1 and Table II show that the u.v. spectra of the Schiff bases studied are very similar to one another. In general, three well-defined bands can be found, at 210—240, 280—310 and 350—400 nm, respectively; these bands can be assigned in all

likelihood to $\pi^* \leftarrow \pi$ transitions. The structure of the spectra and the band positions show no appreciable differences in polar and in apolar solvents. It is interesting that for the 4-X-aniline derivatives the energy of the second band is the highest (279 nm) for the compound with $X$=H, while for the other derivatives — independently of the electron-repelling or — attracting effect of $X$ — this band is shifted towards lower energy; a plot of $\lambda_{max}$ *vs.* $\sigma_p$ gives a minimum curve (Fig. 2). The interpretation of this result is difficult at present.

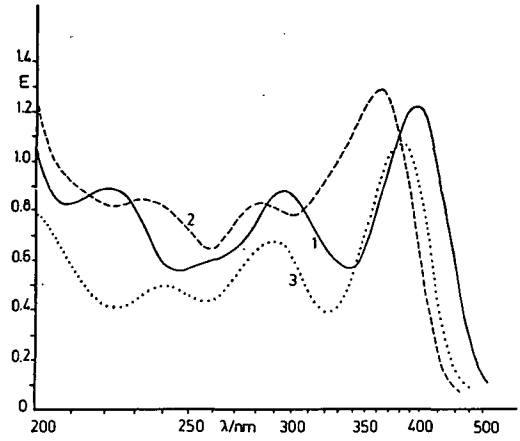


*Fig. 1.* U.v. spectra of I (curve 1), V (2) and XIII (3) in methanol. c = $5.10^{-4}$ mol $dm^{-3}$; d = 0.1 cm

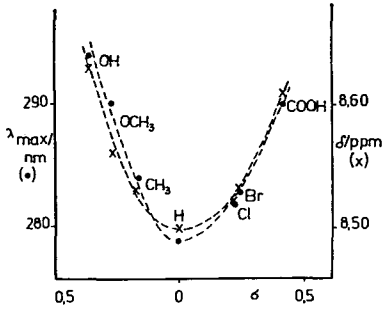


*Fig. 2.* Plots of $\lambda_{max}$ and $\delta$/ppm *vs.* $\sigma_p$ for the 4-X-aniline derivatives

The u.v. spectra seem relatively simple. However, if we take into account that these Schiff bases include three, or perhaps four chromophores, the unambiguous assignment of the bands is at least problematic. It can be unquestionably established that the spectra of the Schiff bases do not consist only of the absorption of aldehyde and amine moieties; in the range 360—400 nm a new high-intensity band appears due (probably) to the azomethine group formed and to the increased conjugated system, too.

All the spectra show considerable change with time, in particular in the presence of water; a set of curves is given in Fig. 3. Five isosbestic points can be seen, at ca. 206, 226, 246, 295 and 320 nm, which indicates that there is no accumulation of intermediates. Our preliminary investigations suggest that first-order or pseudo-first-order kinetics can be proposed on the basis of the initial rates. There is a linear relationship between $t_{1/2}$ and the $\sigma_p$ value of $X$; the reaction rate is higher for electron-donating substituents and it seems that the basicity of the parent amine also plays an important role.

It may be suggested that the transformation takes place *via* the carbinolamine intermediate, the decomposition of which results in aldehyde and the corresponding amine. The limiting curve is identical with the calculated one, as can be seen in Fig. 4. We have observed that the solvolysis rate in non-aqueous solvent is at least 100—500 times lower than in water-containing solvent, so the influence of methanolysis can be

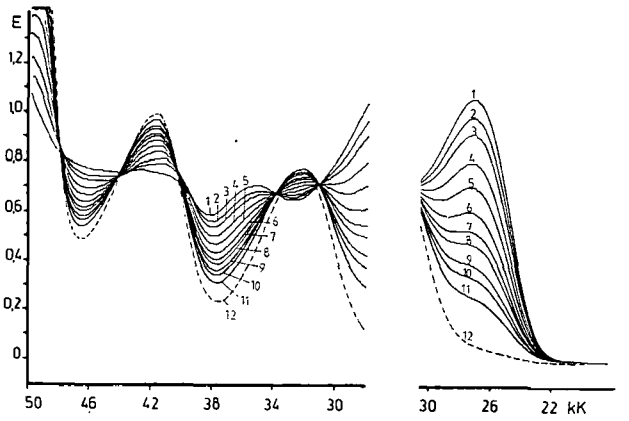


*Fig. 3.* Spectral change of $CH_3OH/H_2O$ 1:1 solution of V with time at 298 K. $c=6.4.10^{-4}$ mol $dm^{-3}$; d=0.1 cm. Times from above downwards: 0, 10, 20, 40, 60, 90, 120, 150, 210, 270 and 390 min and 24 hours

neglected in our systems [see also *e.g.* 17] . The interpretation of the mechanism requires still further detailed experiments.

*I. r. spectra.* The main frequencies and the assignments are presented in Table III. The very intense C=N stretching can be found at 1570—1630 $cm^{-1}$. The $<1600$ $cm^{-1}$ values for **X**, **XII**, **XIII** and **XVI** are noteworthy; these are interpreted by the completely different structures of the molecular moieties bound to the azomethine nitrogen. The $\nu_{as}NO_2$ and $\nu_sNO_2$ frequencies appear with very high intensities at around 1500—1540 and 1340—1360 $cm^{-1}$, respectively. For the 4-X-aniline derivatives the above two frequencies lie closer to each other; the wave-number differences are approximately linearly correlated with $\sigma_p$. In spite of the fact that the

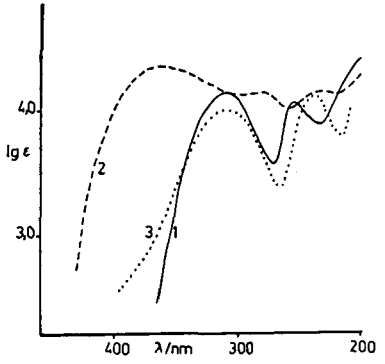


*Fig. 4.* Spectra of **V**. 1: calculated curve; 2: curve measured in methanol; 3: curve measured in methanol/water mixture after 24 hours.

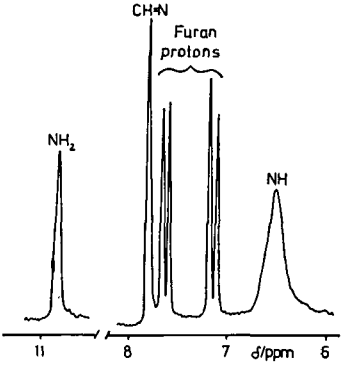


*Fig. 5.* A part of the $^1H$ NMR spectrum of **XII**

4-X-phenyl ring is far from the $NO_2$ group, it still seems that it forms a unified electron system; due to the effect of $X$, the O-N-O angle decreases gradually with increasing $\sigma_p$.

The different skeletal vibrations of the furan ring can be found among the other frequencies in the ranges 1300—1500 and 1000—1070 $cm^{-1}$.

*Table III*

*Main i.r. frequencies for the Schiff bases*

| No. | νC=N | $\nu_{as}NO_2$ | $\nu_s NO_2$ | νC—N | γ=CH | |
|---|---|---|---|---|---|---|
| I | 1621 m | 1506 s | 1350 s | 1170 s | 817 s | 1015 m |
| II | 1614 m | 1505 s | 1352 s | 1180 m | 805 m | 1010 m |
| III | 1621 m | 1504 s | 1357 s | 1179 m | 817 m | 1026 m |
| IV | 1617 s | 1499 s | 1359 s | 1181 m | 735 m | 1021 m |
| V | 1614 m | 1490 s | 1357 s | 1180 s | 810 m | 1021 m |
| VI | 1614 m | 1487 s | 1359 s | 1177 s | 810 m | 1022 m |
| VII | 1618 s | 1508 s | 1353 s | 1178 m | 855 m | 1020 m |
| VIII | 1617 s | 1507 s | 1358 s | 1177 m | 820 m | 1017 m |
| IX | 1624 m | 1527 s | 1355 s | 1150 m | 760 m | 1020 m |
| X | 1585 m | 1510 s | 1347 s | 1130 m | 846* m | 1020 m |
| XI | 1621 m | 1511 s | 1355 s | 1178 s | 827 m | 1020 m |
| XII | 1577 m | 1508 s | 1347 s | 1195 s | | 1016 m |
| XIII | 1595 s | 1534 s | 1355 s | 1186 m | | 1027 m |
| XIV | 1634 m | 1534 s | 1350 s | 1167 m | | 1027 m |
| XV | 1612 s | 1510 s | 1350 s | 1167 m | 820 m | 1020 m |
| XVI | 1575 m | 1500 s | 1390 s | 1183 m | | 1016 m |

* complex band; s: strong; m: medium-intensity band

*Table IV*

$^1H$ *NMR data** (δ/ppm) *on the Schiff bases***

| No. | δOH | $\delta NH_2$ | δCH=N | δNH | $\delta OCH_3$ | $\delta CH_3$ | $\delta CH_2$ |
|---|---|---|---|---|---|---|---|
| I | 14.56 | | 8.63 | | | | |
| II | | | 8.56 | | 3.83 | | |
| III | | | 8.53 | | | 2.38 | |
| IV | | | 8.50 | | | | |
| V | | | 8.53 | | | | |
| VI | | | 8.51 | | | | |
| VII | | | 8.61 | | | | |
| VIII | | | 8.36 | | | 3.92 | 0.98 |
| | | | | | | | 1.66 |
| IX | ? | | 8.83 | | | | |
| X | | | 8.41 | | 3.79 | | |
| XI | | | 8.41 | | | | |
| XII | | 10.89 | 7.84 | 6.56 | | | |
| XIII | | 11.92 | 8.06 | 7.92 | | | |
| XIV | | ? | 8.79 | | | | |
| XV | | | 8.20 | | | 3.61 | 1.25 |

* in $CDCl_3$+DMSO 1:1 mixture

** XVI is practically insoluble in the solvent used

*$^1H$ NMR spectra.* The main resonance frequencies of the Schiff bases are reported in Table IV. It seems that the different proton signals are generally well distinguishable, except for **XVI**, where then ppm values are uncertain because of the low solubility. In the spectra of **I—VI**, **IX**, **X** and **XVI** a very complicated band system can be found between 6 and 7.5 ppm, which is the superposition of the proton signals of the furan and those of the substituted phenyl ring. The characteristic two doublets of the furan protons in the spectra of **XII—XIV** (see e.g. Fig. 5) appear at 7.10—7.30 and 7.40—7.70 ppm. The ring proton signals shift systematically toward higher ppm values in the sequence **XII—XIII—XIV**, while at the same time the distance between the doublets decreases. The positions of the azomethine proton signals depend on the character of the substituent *X* in **I—VI**; the plot of $\delta CH=N$ *vs.* $\sigma_p$ is totally analogous to the $\lambda_{max}$ vs. $\sigma_p$ relationship (Fig. 2).

## References


[1] *McGuigan, H.:* J. Pharmacol. **21**, 65 (1923).
[2] *Kaufman, H. P.:* Ber. pharm. Ges. **33**, 132 (1923).
[3] *Phatak, N. M., C. D. Leake:* J. Pharmacol. **56**, 265 (1936); **58**, 155 (1936).
[4] *Dodd, M. C., W. B. Stillman:* J. Pharmacol. Exptl. Therap. **82**, 11 (1944).
[5] *Tanaka, A., T. Usui, S. Yoshina:* Heterocycles, **3**, 1087 (1975); Heterocyclic Chem. **15**, 555 (1978); **16**, 493 (1979).
[6] *Yamamoto, K., A. Tanaka:* J. Heterocyclic Chem. **16**, 1293 (1979).
[7] *Tanaka, A., T. Usui:* Chem. Pharm. Bull. **26**, 3576 (1978); J. Heterocyclic Chem. **16**, 1409 (1979).
[8] *Tanaka, A., T. Usui:* Chem. Pharm. Bull. **27**, 3078 (1979); **28**, 1604 (1980).
[9] *Massarini, E., et al.:* J. Med. Chem. **14**, 633 (1971).
[10] *Nardi, D. et al.:* J. Med. Chem. **14**, 635 (1971).
[11] *Szarvasi, E.:* J. Med. Chem. **16**, 281 (1973).
[12] *Spencer, C. F. et al.:* J. Med. Chem. **16**, 953 (1973).
[13] *Császár J. et al.:* Acta Phys. et Chem. Szeged, **24**, 473 (1978); **25**, 129, 137 (1979); **27**, 47 (1981); **28**, 135 (1982).
[14] *Jaffe, H. H., M. Orchin:* Theory and application of ultraviolet spectroscopy., Wiley and Sons, New York, 1962.
[15] *Raffauf, R. F.:* J. Amer. Chem. Soc. **72**, 753 (1950).
[16] *Giller, C. A., N. O. Szaldobolsz:* Izv. Akad. Nauk CCCP Ser. Fizicseszkaja, **17**, 708 (1953).
[17] *Bellobono, I. R., G. Favini:* Tetrahedron **25**, 57 (1969).


## ИССЛЕДОВАНИЕ ПРОИЗВОДНЫХ 5-$NO_2$-2-ФУРАЛЬДЕГИДА, I. УФ— ИК— И $^1$Н ЯМР-СПЕКТРОСКОПИЧЕСКОЕ ИЗУЧЕНИЕ СОЕДИНЕНИЙ ТИПА ОСНОВАНИЙ ШИФА

*Й. Часар*

Синтезированы основания Шифа производные 5-$NO_2$-2-фуральдегида и изучены их ультрафиолетовые, инфракрасные и протонно ядерно-магнитно резонансные спектры.

# STUDY OF 5-$NO_2$-2-FURALDEHYDE DERIVATIVES, III*. SCHIFF BASES FORMED WITH UREA AND SEMICARBAZIDE DERIVATIVES

By

J. CSÁSZÁR

Institute of General and Physical Chemistry, Attila József University, Szeged

*(Received 20th October, 1983)*

The Schiff base derivatives of 5-$NO_2$-2-furaldehyde with urea, thiourea, their derivatives, and semi- and thiosemicarbazide were prepared and their u.v. and visible spectral properties were studied. The equilibrium of semi- and thiosemicarbazide derivatives in alkaline solution is discussed.

In previous papers we have described the synthesis of several 5-$NO_2$-2-furaldehyde (**NFA**) derivatives, obtained in reactions with aniline derivatives [1] and sulphonamides [2], and discussed their spectral behaviour and the antibacterial activity of the latter compounds. The pharmacological activity of thiourea [3—5] and thiosemicarbazide [6] derivatives has been reported in the literature. The semicarbazide derivative, Nitrofurazon, is widely used in therapy for local injury treatment and as an antiseptic agent against skin and mucous inflammation. We have prepared ten derivatives of **NFA**, with structures analogous to that of Nitrofurazon and discussed their u.v. and visible spectral characteristics. The Schiff bases studied are as follows.

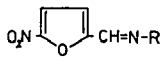

| | | | |
|---|---|---|---|
| **1** | R = OH | **6** | R = $NH.C(S)NH_2$ |
| **2** | = $NH_2$ | **7** | = $C(O)NH.CHCHCH_3$ |
| **3** | = $C(O)NH_2$ | **8** | = $C(S)NH.CHCHCH_3$ |
| **4** | = $C(S)NH_2$ | **9** | = $C(O)NH.C_6H_5$ |
| **5** | = $NH.C(O)NH_2$ | **10** | = $C(S)NH.C_6H_5$ |

* Part II: Császár, J., J. Morvay, O. Herczeg: J. Pharm. Hung., in press.

## *Experimental*

The Schiff bases were prepared by the reaction of **NFA** and the corresponding amine components in 1:1 mole ratio in methanol solution. The products separated out after heating of the solutions at about 310—315 K, and were recrystallized from an ethanol/benzene mixture. The analytical data are given in Table I.

*Table I*

*Analytical data on NFA derivatives*

| No. | R | C% | | H% | |
|---|---|---|---|---|---|
| | | Calcd. | Found | Calcd. | Found |
| 1 | OH | 38.47 | 38.40 | 2.58 | 2.65 |
| 2 | $NH_2$ | 38.68 | 38.61 | 3.25 | 3.21 |
| 3 | $C(O)NH_2$ | 39.35 | 39.28 | 2.75 | 2.70 |
| 4 | $C(S)NH_2$ | 36.18 | 36.14 | 2.53 | 2.47 |
| 5 | $NH.C(O)NH_2$ | 36.34 | 36.19 | 3.05 | 3.11 |
| 6 | $NH.C(S)NH_2$ | 33.61 | 33.54 | 2.82 | 2.75 |
| 7 | $C(O)NH.CHCHCH_3$ | 48.43 | 48.30 | 4.06 | 4.01 |
| 8 | $C(S)NH.CHCHCH_3$ | 45.20 | 45.08 | 3.79 | 3.66 |
| 9 | $C(O)NH.C_6H_5$ | 55.60 | 55.51 | 3.50 | 3.51 |
| 10 | $C(S)NH.C_6H_5$ | 52.36 | 52.19 | 3.30 | 3.26 |

The u.v. and visible spectra were recorded on a SPECORD UV—VIS spectrophotometer at room temperature, with purified solvents. The equilibrium measurements were performed at $298 \pm 0.5$ K in $NaOH/CH_3OH$ solution; the NaOH concentration varied in the range $2.10^{-3}-150.10^{-3}$ mol $dm^{-3}$. The Schiff base concentration was $5.5.10^{-4}$ mol $dm^{-3}$; $d = 1.0$ cm, and the spectral changes were monitored between 300 and 700 nm.

## *Results and discussion*

The u.v. and visible spectral data on the Schiff bases in methanol and in acidic and basic solutions are presented in Table II; the spectra of the semi- and thiosemicarbazide derivatives are shown in Figs. 1 and 2.

The spectral structures of the compounds studied are similar to one another; characteristic bands appear at around 202—206, 228—250, 260—290 and 310—340 nm, while at 400—450 nm there is a low-intensity inflexion, too. These spectra are similar to those of a methanolic solution of **NFA**, where two high-intensity bands can be found, at 225 and 303 nm; the absorbance of the amine components exerts only a small effect. The unambiguous assignment of the bands is difficult, because at least six chromophores are present and the measured spectra result from the complicated superposition of individual absorbances. Theoretical calculations to determine the possible electronic transitions are in progress.

No marked change can be observed in acidic solution; the general tendency is for the intensities of the bands to increase, but the energies of the transitions remain

almost unchanged. A totally different picture is obtained in alkaline medium. New bands appear between 370 and 450 nm, and the whole spectrum shows a bathochromic shift, except in the case of the semi- and thiosemicarbazide derivatives.

The greatest change occurs upon alkali addition to a solution of **5** or **6** (see Figs. 1 and 2). In response to alkali, both compounds give a very intense brickred colour and high bands appear at 372, 452 and 451 nm in the spectra. For the semicarbazide derivative the 364 nm band shifts to 372 nm and a new band appears at 452 nm, while the 382 nm band of the thiosemicarbazide shifts to 451 nm. For both compounds the spectral change depends on the alkali concentration; the set of curves measured unambiguously indicate an equilibrium system (Fig. 3). Isosbestic points are

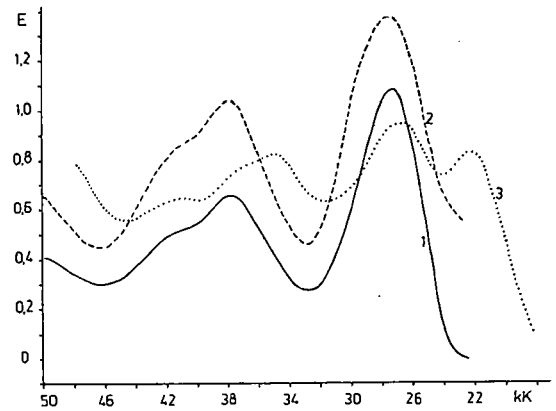


*Fig. 1.* Spectra of $O_2N.C_4H_2O.CHNNHC(O)NH_2$; 1: in methanol, $c=2.0\cdot10^{-4}$; 2: in 0.1 mol $dm^{-3}$ $H_2SO_4/CH_3OH$, $c=1.06\cdot10^{-3}$; 3: in 0.1 mol $dm^{-3}$ $NaOH/CH_3OH$, $c=9.59\cdot10^{-4}$ mol $dm^{-3}$; d=0.1 cm

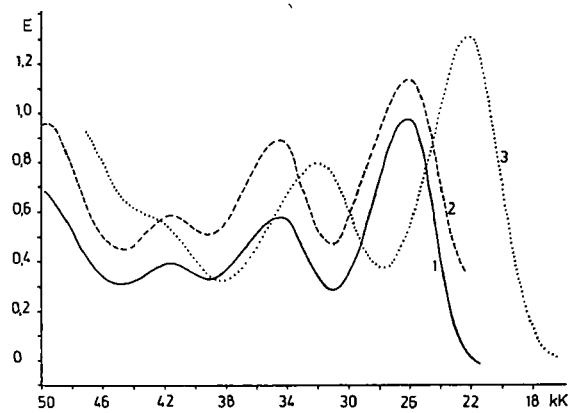


*Fig. 2.* Spectra of $O_2N.C_4H_2O.CHNNHC(S)NH_2$; 1: in methanol, $c=5.0\cdot10^{-4}$; 2: in 0.1 mol $dm^{-3}$ $H_2SO_4/CH_3OH$, $c=9.34\cdot10^{-4}$; 3: in 0.1 mol $dm^{-3}$ $NaOH/CH_3OH$, $c=7.0\cdot10^{-4}$ mol $dm^{-3}$; d=0.1 cm

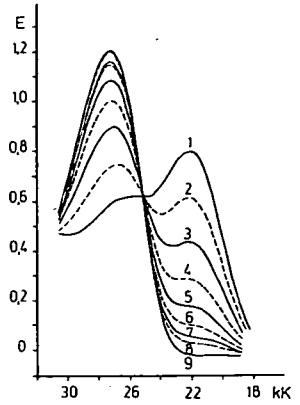


*Fig. 3.* Changes in the spectrum of $O_2N.C_4H_2O.CHNNHC(O)NH_2$ with the NaOH concentration: $c_{Schiff b.} = 6.7 \cdot 10^{-4}$ mol dm$^{-3}$, $c_{NaOH}$ = 1: $150 \cdot 10^{-3}$; 2: $90 \cdot 10^{-3}$; 3: $54 \cdot 10^{-3}$; 4: $32.4 \cdot 10^{-3}$; 5: $19.4 \cdot 10^{-3}$; 6: $11.7 \cdot 10^{-3}$; 7: $7.0 \cdot 10^{-3}$; 8: $4.2 \cdot 10^{-3}$ mol dm$^{-3}$; 9: in methanol; d = 0.1 cm

*Table II*

*U. v. spectral data on the Schiff bases*

| No. | Solvent* | U.v. band maxima (nm and ε) | | | | |
|---|---|---|---|---|---|---|
| 1 | $CH_3OH$ | 234 (8 910) | ~256 | | 337(12 880) | |
| | Acid | 233(11 750) | ~256 | | 337(21 380) | |
| | Base | ~238 | 267 (7 240) | | 392(12 880) | |
| 2 | $CH_3OH$ | 233 (4 470) | ~290 | | 373(16 600) | |
| | Acid | 235 (4 570) | ~286 | | 370(12 590) | |
| | Base | ~241 | ~286 | | 370 (6 760) | |
| 3 | $CH_3OH$ | 203(21 380) 228(13 180) | | 313(33 110) | | |
| | Acid | ~228 | | 309 (8 710) | | |
| | Base | | 273 (7 760) | 313 (7 760) | ~385 | |
| 4 | $CH_3OH$ | 203(18 650) 243(15 150) | | 311 (7 120) | ~380 | |
| | Acid | 203(13 810) 242(11 480) | | ~303 | ~385 | |
| | Base | 243(40 740) | | ~303 | ~385 | |
| 5 | $CH_3OH$ | ~238 | 264(14 450) | | 364(22 910) | |
| | Acid | ~244 | 264 (9 770) | | 365(16 220) | |
| | Base | ~244 | 286 (8 510) | | 372(10 000) | 452 (8 790) |
| 6 | $CH_3OH$ | 240 (7 940) | 288(11 480) | | 382(19 500) | |
| | Acid | 202(10 470) 240 (6 310) | 291 (9 550) | | 382(16 980) | |
| | Base | ~233 | 313(11 480) | | | 451(18 620) |
| 7 | $CH_3OH$ | 205 (8 130) ~228 | | 317 (8 910) | | |
| | Acid | ~228 | | 311 (8 510) | | |
| | Base | ~230 | 282(11 480) | ~323 | ~385 | |
| 8 | $CH_3OH$ | 204(12 020) 251 (8 130) | | 311 (7 080) | ~400 | |
| | Acid | 202(12 020) ~244 | | 311 (6 170) | ~390 | |
| | Base | ~244 | | 317 (6 920) | ~385 | |
| 9 | $CH_3OH$ | 204(38 020) 240(33 880) | | 313(11 750) | | |
| | Acid | 203(41 690) 238(26 300) | | 311 (8 910) | | |
| | Base | 238(14 450) | ~270. | | 385 (2 820) | |
| 10 | $CH_3OH$ | 204(41 690) ~240 | 266(32 360) | | | |
| | Acid | 203(42 660) ~238 | 265(25 180) | | | |
| | Base | ~241 | 265(42 660) | | | |

* Acid: 0.1 mol dm$^{-3}$ $H_2SO_4/CH_3OH$; Base: 0.1 mol dm$^{-3}$ $NaOH/CH_3OH$.

present at 398 and 408 nm. The changes in absorbance at two different wavelengths are shown in Fig. 4.

It was possible to calculate the equilibrium constants *via* the following equation:

$$K = \frac{E_i - E}{E - E_f} \frac{1}{[\mathrm{NaOH}]_{eq}}$$

where $E_i$, $E$ and $E_f$ are the absorbances of the solution without NaOH, at different NaOH concentrations and at a high NaOH concentration where no further spectral change can be obtained. $[\mathrm{NaOH}]_{eq}$ is obtained from the equation

$$[\mathrm{NaOH}]_{eq} = [\mathrm{NaOH}]_{total} - \frac{E_i - E}{E - E_f} c_{SB}$$

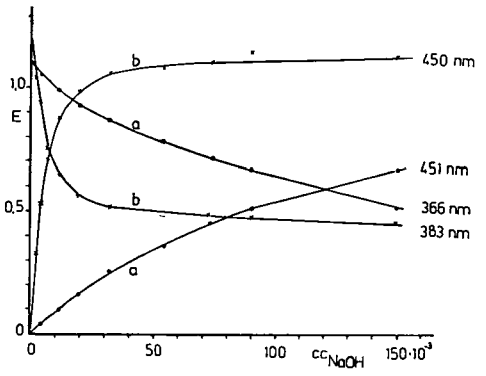


*Fig. 4.* Changes in the absorbance of semicarbazide (a) and thiosemicarbazide derivatives (b) with the NaOH concentration, at two different nm values

As regards the spectral change, there is a marked difference between the structurally analogous compounds. Two species of identical absorbance are present in the equilibrium systems of semi- and thiosemicarbazide derivatives at $120.10^{-3}$ and $7.5.10^{-3}$ mol dm$^{-3}$ NaOH concentration, respectively. The equilibrium constants computed for the two compounds are $8.2 \pm 0.4$ and $226 \pm 1.5$, respectively.

The interpretation of the equilibrium systems is difficult. We presume that, on the action of NaOH, the Schiff base molecule (a) undergoes an electronic rearrangement to give the conjugated system (b).

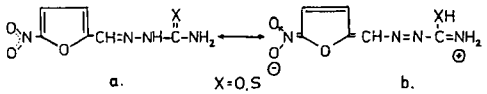


This supposition is supported by the preliminary NMR investigations, but an unambiguous interpretation of the equilibrium systems requires still further theoretical and experimental investigations.

## References

[1] *Császár, J.:* Acta Phys. et Chem. Szeged, **30,** 71 (1984).
[2] *Császár, J., J. Morvay:* Acta Pharm. Hung. **53,** 121 (1983).
[3] *Astwood, E. B.:* J. Pharmacol. **78,** 79 (1943).
[4] *Astwood, E. B., A. Bissell, A. M. Hughes:* Endocrinology **37,** 456 (1945).
[5] *May, J. D., J. L. McNaughton:* Poult. Sci. **59,** 893 (1980).
[6] *Mostafa, M. M., A. M. Shallaby, A. A. El-Asmy:* Trans. Metal. Chem. **6,** 303 (1981); J. Inorg. Nucl. Chem. **43,** 2998 (1981).

# ИССЛЕДОВАНИЕ ПРОИЗВОДНЫХ 5-$NO_2$-2-ФУРАЛЬДЕГИДА, III. ОСНОВАНИЯ ШИФА, ОБРАЗУЮЩИЕСЯ С МОЧЕВИНОЙ И ПРОИЗВОДНЫМИ СЕМИКАРБАЗИДА

*Й. Часар*

Синтезированы основания Шифа производные 5-$NO_2$-2-фуралъдегида и мочевины, тиомочевины и их производных, а также семи- и тиосемикарбазидов. Изучены ультрафиолетовые и видимые спектры полученных соединений. Обсуждены состояния равновесия производных семи- и тиосемикарбазидов в щелочных растворах.

# ON THE THERMAL DECOMPOSITION OF PROPENE IN THE PRESENCE OF 1,3-BUTADIENE. THE ROLE OF DIELS-ALDER REACTION

By

T. KÖRTVÉLYESI, M. GÖRGÉNYI AND L. SERES

Institute of General and Physical Chemistry, Attila József University, Szeged

*(Received December 12, 1983)*

The thermal decomposition of propene in the presence of 1,3-butadiene was studied in the temperature range 745—809 K. 45 products were identified, and the initial rates of formation were determined from gas-chromatographic analysis of the products. It was concluded that radical chain processes and molecular reactions contribute to product formation.

From the initial rates of formation of 4-methylcyclohexene and toluene, the rate coefficient of the reaction

$$C_3H_6 + 1,3\text{—}C_4H_6 \rightarrow \text{4-methylcyclohexene}$$

was determined as

$\log (k_{DA}/dm^3\ mol^{-1}\ s^{-1}) = 7.74 \pm 0.29 - (129.3 \pm 6.1)\ kJ\ mol^{-1}/2.303\ RT$

The results obtained support the concerted nature of the Diels—Alder reaction.

## *Introduction*

Since some of the products of the thermal decompositions of olefins are more reactive than the parent compounds themselves, these products may influence even the formation of the major products. Thus, the roles of the different reaction paths in the formation of a given product may change considerably with increasing conversion.

In an attempt to clarify the routes of formation of some of the products of the thermal decomposition of propylene (**P**), the reaction was studied in the presence of different amounts of 1,3-butadiene (**B**).

The thermal decomposition of **P** has been studied under various experimental conditions (see *e.g.* [1—5]), whereas reaction of **B** has not been investigated so extensively [6—8]. In the reaction of **P** in the presence of **B**, the formation of aromatic products (benzene, toluene) was examined under industrial conditions [9—10]. The improvement of the analytical techniques made possible the identification of a great number of products, and an effort is made here and in a forthcoming publication to describe in more detail the effect of **B** on the pyrolysis of **P**.

**P** has long been known to inhibit the decomposition of many hydrocarbons. In the addition and abstraction reactions of both saturated alkyl radicals and H atoms, these species are converted into relatively less reactive radicals, decreasing the rates of

accumulation of different products. In the presence of **B**, a significant increase was expected in the overall rate of addition to **B**, since these reactions yield resonance-stabilized radicals and are essentially irreversible, while the similar reactions of **P** are not.

## *Experimental*

### *Apparatus*

The experiments were carried out in a conventional static system. Pyrex and quartz reaction vessels 0.146 $dm^3$ ($S/V = 0.114\ dm^{-1}$) and 0.139 $dm^3$ ($S/V = 0.109\ dm^{-1}$) in volume were used. The reaction temperature was kept constant within ± 0.5 K over the temperature range 745—809 K.

Mixtures of the reactants were prepared in a temperature-controlled spherical vessel. Efficient mixing was ensured by convection, brought about by warming a side-arm of the mixing vessel for two hours.

When **B** was decomposed alone, $CO_2$ diluent was used at nearly the same partial pressure as that of **P** in the **P**+**B** mixtures.

Pressure measurements were made with a precision pressure gauge (Texas Instruments, Inc.) in the range 0—80 kPa. The products of the reaction were expanded into a pyrex vessel containing a known amount of a gas standard (2-methyl-1--butene, FLUKA AG, 99.9% purity). The rest of the reaction mixture was frozen into $2.5 \cdot 10^{-4}$ $dm^3$ solvent (decane, FLUKA AG, 99.9% purity, or *sec*-butylbenzene, 98% purity) containing a precisely measured internal standard (2,2,3,3-tetramethylbutane, FLUKA AG, 99.9% purity).

The $C_1$—$C_4$ products were analyzed in the gas sample and the $C_5$—$C_8$ products in the solution.

### *Materials*

The **P** (Tisza Chemical Works) and **B** (FLUKA AG) used in the experiments were of high purity. Both reactants were subjected to repeated low-temperature bulb-to-bulb distillation and were degassed before admission into the storage vessels. After this procedure the main impurities were 0.02% ethane+ethene and 0.13% propane in **P** (99.85% purity) and 0.49% $C_5$ olefins in **B** (99.51% purity).

The gas-chromatographic identifications were made with chemicals of high purity (FLUKA AG, 99.9% purity, and CHEMICAL SAMPLES, 99.9% purity).

### *Analysis*

The reaction products were analyzed with Hewlett—Packard 5750G and 5734A gas-chromatographs equipped with FID. The quantitative analysis of the products was performed with a Hewlett—Packard 3380S integrator.

The $C_1$—$C_4$ products were separated on a Chromosorb P (80/100 mesh) column coated with 20% BMEA (bis(2-methoxyethyl)-adipate); column length: 6.1 m, ∅ 0.22 cm. The operating temperature was 298 K.

1-Butene and isobutene were separated on the former column connected to a Durapak column 0.9 m in length, with ∅ 0.22 cm. The operating temperature was 298 K. The carrier gas was $N_2$ and a flow rate of $2 \cdot 10^{-2}$ dm³ min$^{-1}$ was applied. These columns were purified by means of the "back flush" method at 353 K.

Ethane and ethene were separated at 363 K on an alumina column 1 m in length, while the $C_5$—$C_8$ compounds were analyzed on a DC—550 SCOT capillary column 30 m long, at 298—353 K. The flow rate of the carrier gas was $2.5 \cdot 10^{-3}$ dm³ min$^{-1}$ and the split ratio was 1/10. The analysis was not continued beyond the appearance of the peak of styrene since the combined area of the subsequent peaks amounted to less than 2% of the total peak area of all the other products.

The products were identified *via* retention times, Kovats retention indices [11], selective olefin and aromatic absorption [12] and mass-spectrometry (FINNIGAN 1015 S/L).

## *Results*

### *Pressure measurements*

Figure 1 shows the total pressure *vs.* time plots at different $[\mathbf{B}]_o/[\mathbf{P}]_o$ ratios. In the early stages of the reaction, the rate of negative pressure change increases with increasing $[\mathbf{B}]_o$.

From the expression

$$-\frac{dp_T}{dt} = \text{const.}\,[B]_o^{\beta}$$

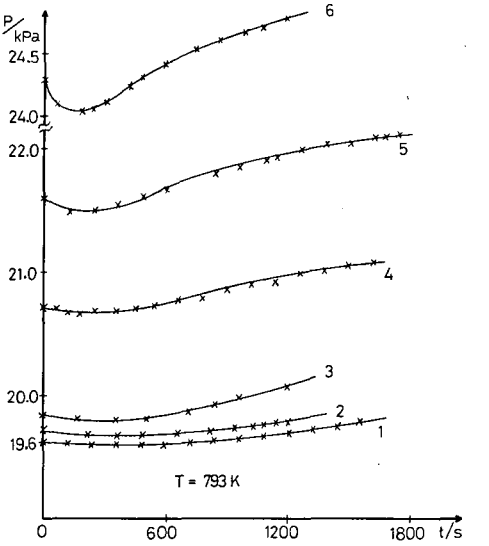


*Fig. 1.* Total pressure *vs.* time plots at $[\mathbf{P}]_o = 2.93 \cdot 10^{-3}$ mol dm$^{-3}$ at $[\mathbf{B}]_o/[\mathbf{P}]_o$ ratios of 1/99 (1), 1/74 (2), 1/49 (3), 1/19 (4), 1/9 (5) and 1/4 (6) at 793 K

where $p_T$ is the pressure at temperature T, values of $\beta$ (768 K) = 1.22±0.04 and $\beta$ (793 K) = 1.24±0.06 were calculated at $[\mathbf{P}]_o = 2.93 \cdot 10^{-3}$ mol dm$^{-3}$, clearly indicating the role of **B** in the oligomerization processes.

### *Analytical results*

The experiments were performed at ten different temperatures in the interval 745—908 K, while $[\mathbf{P}]_0$ and $[\mathbf{B}]_0$ were in the ranges $0-3.21 \cdot 10^{-3}$ mol dm$^{-3}$ and $0-8.08 \cdot 10^{-4}$ mol dm$^{-3}$, respectively. The conversion was 3.0—20.1% for P, and 1.3—68.0% for **B**.

In the analytical study of the pyrolysis of **P** in the presence of **B**, 45 products were identified. The identification results are summarized in Table I, where the products are listed according to decreasing rates of formation. Further, a comparison is given to specify the products identified in the detailed studies on **P** decomposition

*Table I*

*Identified products of the P + B reaction*

| Products | Method of identification [a] | Ref. [b] [8, 13, 14] |
|---|---|---|
| methane | GC | + |
| ethene | GC | + |
| 1-butene | GC | + |
| t-2-butene | GC | + |
| c-2-butene | GC | + |
| cyclopentene | GC, MS | + |
| 1,3-cyclopentadiene | GC, MS | + |
| 4-methyl-1-pentene | GC, MS | + |
| 3-methyl-1-pentene | GC, MS | + |
| c-1,3-pentadiene | GC | + |
| 3-methylcyclopentene | GC, MS | + |
| 4-methylcyclopentene | MS | |
| 5-methyl-1,3-cyclopentadiene | MS | |
| 1,4-cyclohexadiene | MS | |
| cyclohexene | GC, MS | |
| 1,3-cyclohexadiene | GC, MS | |
| 4-methylcyclohexene | GC, MS | + |
| hydrogen | GC | + |
| benzene | GC, MS | + |
| 1-hexene | GC, MS | + |
| 1,5-hexadiene | GC, MS | + |
| toluene | GC, MS | + |
| propane | GC | + |
| ethane | GC | + |
| 3-methyl-1-butene | GC | + |
| 1-pentene | GC, MS | + |
| 1,4-pentadiene | GC | + |
| t-2-pentene | GC, MS | + |
| c-2-pentene | GC, MS | + |
| isobutene | GC | + |
| 2-methyl-1,3-butadiene | GC, MS | + |
| $C_5$-olefin | MS | + |
| 2-methyl-1-pentene | MS | |
| 4-vinylcyclohexene | GC | |
| 1-methyl-1,4-cyclohexadiene | GC | |
| ethylbenzene | MS | |
| 1,3-dimethylbenzene | GC, MS | |
| 1,2-dimethylbenzene | GC, MS | |
| styrene | MS | |
| 2-methyl-1-butene | GC, MS | |
| 2-methyl-2-pentene | GC, MS | + |
| 1,3-hexadiene | GC | + |
| 1-methylcyclopentene | GC, MS | + |
| 1-methylcyclohexene | GC, MS | + |
| 2-methyl-1,5-hexadiene | MS | |

[a] GC: identification with gas-chromatography
MS: identification with mass-spectrometry

[b] The sign + designates compounds identified in earlier investigations of the thermal decomposition of P [1, 13, 14].

by KALLEND et al. [1] and SIMON and BACK [13, 14]. The products of the **P**+**B** reaction are very similar to those of the **P** reaction under similar conditions. At high conversions of **P** in the reaction of the pure reactant, and also at higher $[B]_o/[P]_o$ ratios some further products appeared, but their combined amount was negligible.

The products can be classified into two groups, according to their accumulation patterns. The concentrations of some products continually increase throughout the reaction, while those of others reach maxima and subsequently decrease. Among the more important products of the first group are $CH_4$ (Fig. 2), $C_2H_6$, $C_2H_4$, $C_3H_8$, butenes, 5-methyl-1,3-cyclopentadiene, benzene (Fig. 3) and toluene, while those in the second group include cyclopentene+1,3-cyclopentadiene, 1-hexene+1,5-hexadiene (Fig. 4), cyclohexene+1,3-cyclohexadiene (eluted together), 3- and 4-methyl-

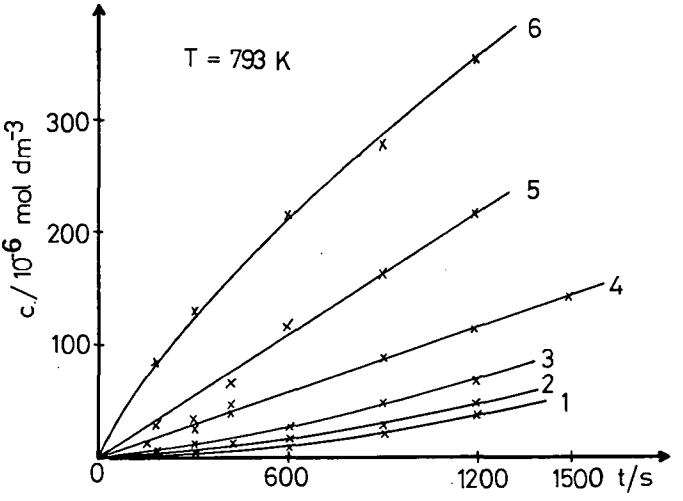


*Fig. 2.* Yields *vs.* time plots of methane at $[P]_o = 2.93 \cdot 10^{-3}$ mol dm$^{-3}$ at $[B]_o/[P]_o$ ratios of 0 (1), 1/99 (2), 1/49 (3), 1/19 (4), 1/9 (5) and 1/4 (6) at 793 K

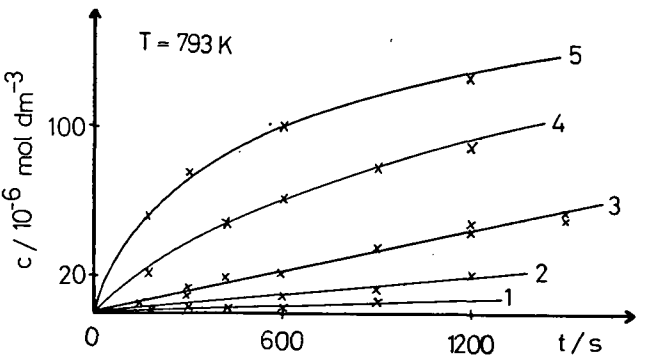


*Fig. 3.* Yields *vs.* time plots of benzene at $[P]_0 = 2.93 \cdot 10^{-3}$ mol dm$^{-3}$ at $[B]_0/[P]_0$ ratios of 1/99 (1), 1/49 (2), 1/19 (3), 1/9 (4) and 1/4 (5) at 793 K

cyclopentenes, 4-methylcyclohexene (Figs. 5 and 6) and 1,4-cyclohexadiene. While the initial rates of product accumulations can be determined quite reliably for the first group of products, the values calculated for the second group are only semi-quantitative in nature. The amounts of allene and butane were too small to be detected in the present investigation. These products are formed in more substantial amounts in reactions carried out at higher temperatures [15, 16]. In contrast to the result obtained by BACK and SIMON [13, 14], 1-methyl-cyclopentene and 2-hexene were not found to be major products of the reaction of pure **P**. Similarly, 1,3-hexadiene and 1,4-hexadiene, identified as major reaction products by KALLEND et al. [1], were not found in our measurements. The shapes of the product accumulation curves indicate that some products (methane, ethene, butenes, cyclopentene + 1,3-cyclopentadiene, 3-and 4-methylcyclopentenes and cyclohexadienes) are formed mostly in secondary reactions in the reaction of pure **P** [1, 5, 13, 14]. With increase in $[\mathbf{B}]_o$ these curves became more linear.

After the early stages of the reactions, the relative yields of the unsaturated $C_5$- and $C_6$-membered cyclic products increase.

The effect of **B** on the initial rates of formation of the products can be illustrated by the apparent reaction orders with respect to **B**. Table II contains these values for some important products at 748 and 793 K.

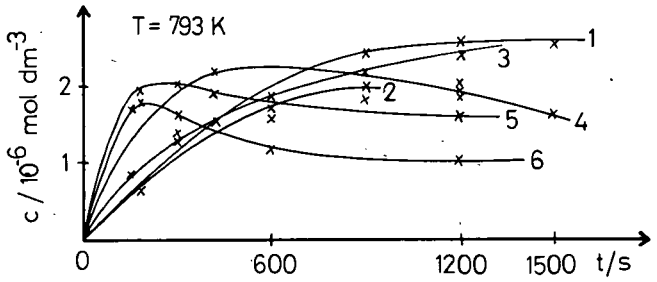


*Fig. 4.* Yield *vs.* time plots of 1-hexene + 1,5-hexadiene at $[\mathbf{P}]_o = 2.93 \cdot 10^{-3}$ mol dm$^{-3}$ at $[\mathbf{B}]_o/[\mathbf{P}]_o$ ratios of 0 (1), 1/99 (2), 1/49 (3), 1/19 (4), 1/9 (5) and 1/4 (6) at 793 K

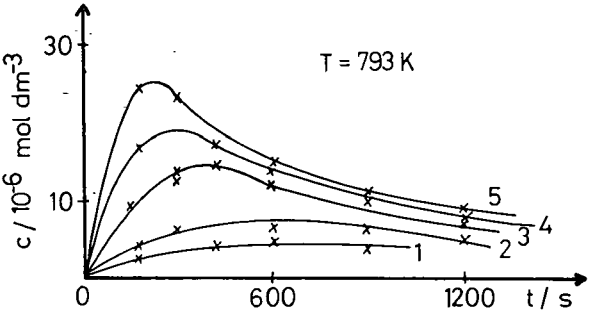


*Fig. 5.* Yield *vs.* time plots of 4-methylcyclohexene at $[\mathbf{P}]_o = 2.93 \cdot 10^{-3}$ mol dm$^{-3}$ at $[\mathbf{B}]_o/[\mathbf{P}]_o$ ratios of 1/99 (1), 1/49 (2), 1/19 (3), 1/9 (4) and 1/4 (5) at 793 K

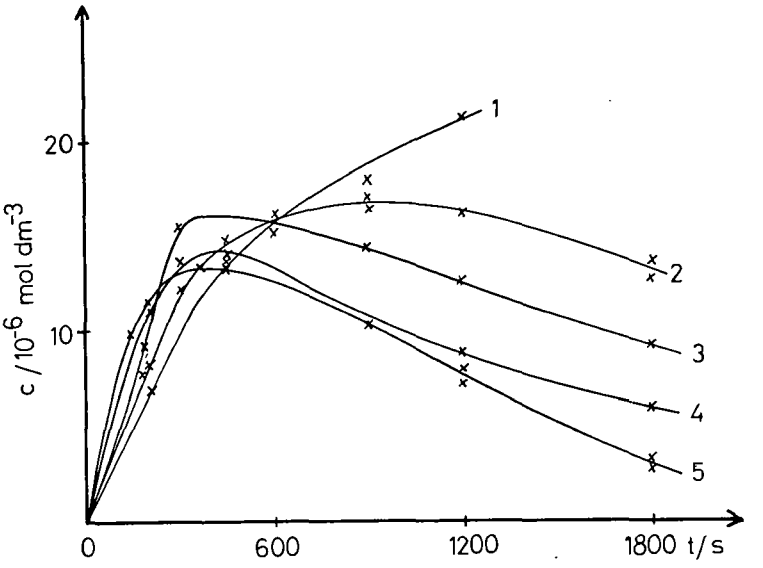


*Fig. 6.* Yields *vs.* time plots of 4-methylcyclohexene at $[P]_o = 2.93 \cdot 10^{-3}$ mol dm$^{-3}$, $[B]_o = 1.56 \cdot 10^{-3}$ mol dm$^{-3}$ at 753 K (1), 768 K (2), 775 K (3), 782 K (4) and 793 K (5)

*Table II*

*The apparent order of formation of some products with respect to* **B** *at 768 and 793 K*

| T/K | 768 | 793 |
|---|---|---|
| methane | 0.96 ± 0.07 | 0.96 ± 0.04 |
| ethane | 0.96 ± 0.04 | 1.06 ± 0.07 |
| ethene | 0.90 ± 0.05 | 0.94 ± 0.05 |
| 1-butene | 1.05 ± 0.12 | 0.97 ± 0.09 |
| t-2-butene | 0.88 ± 0.08 | 0.98 ± 0.07 |
| c-2-butene | 0.93 ± 0.07 | 0.94 ± 0.10 |
| cyclopentene | 1.10 ± 0.06 | 0.90 ± 0.05 |
| 1,3-cyclopentadiene | | |
| 1-hexene | 0.49 ± 0.07 | 0.28 ± 0.10 |
| 1,5-hexadiene | | |
| 3-methylcyclopentene | 0.62 ± 0.04 | 0.57 ± 0.02 |
| 4-methylcyclopentene | 0.60 ± 0.04 | 0.21 ± 0.02 |
| cyclohexene | 1.17 ± 0.08 | 1.06 ± 0.10 |
| 1,3-cyclohexadiene | | |
| 1,4-cyclohexadiene | 1.38 ± 0.09 | 1.22 ± 0.11 |
| benzene | 1.22 ± 0.12 | 1.16 ± 0.09 |
| 4-methylcyclohexene | 0.90 ± 0.07 | 0.51 ± 0.07 |
| toluene | 1.58 ± 0.06 | 1.49 ± 0.07 |
| $cC_6$—R cyclic compounds [a] | 1.11 ± 0.05 | 1.05 ± 0.07 |
| toluene + 4-methylcychlohexene | 1.04 ± 0.09 | 0.97 ± 0.06 |

[a] R ≡ H or $CH_3$.

Since there are no predominant oligomeric products of the reactions (a number of major products are formed in similar quantities), the **P**+**B** reaction seems to be a rather complicated process. In spite of this, the apparent order of reaction for **B** is nearly unity (within narrow error limits) for most of the compounds (listed in Table II). **B** is apparently a common precursor of most of the products, even in the thermal decomposition of pure **P**.

## *Discussion*

As will be demonstrated below, reactions of both radical chain and molecular characters are involved in the thermal decomposition of **P** in the presence of **B**. Since the order of reaction with respect to **B** was found to be close to unity for most of the products, the two kinds of processes must exhibit a similar dependence on $[\mathbf{B}]_0$. An attempt is made below to clarify the role of molecular processes. Other aspects of the reaction will be discussed elsewhere.

As concluded earlier, **B** is obviously a precursor of most of the products formed, if even moderate amounts of **B** are added to **P** initially. The large amounts of methane, ethene, ethane and some other products clearly indicate that radical processes are of major importance in the overall reaction.

It is well known, however, that molecular processes of the Diels—Alder (DA) [17] and ene reaction types [18] are common in systems similar to ours. These processes may yield some of the products observed in our system in a straightforward manner and may be the predominant source of these compounds. The major DA reaction in the B-influenced reaction of **P** is

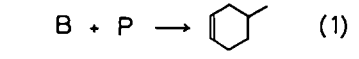


(1)

Since the products (4-methylcyclohexene (4MCH), methylcyclohexadienes (MCHD) and toluene (T) formed from 4MCH) of this reaction sequence are present in negligible concentrations in the early stages of the reaction, the reaction is irreversible at $t \approx 0$, and so reaction (1) is rate-determining. The products formed *via* the DA reaction might also be formed in radical reactions *via* addition of radical **A** to **B**, *e.g.*

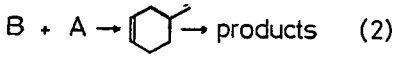


(2)

A: allyl radical

If the kinetic role of reaction (2) in the formation of 4MCH and T is not negligible, the Arrhenius parameters calculated from the initial rates of accumulation of these products are too low.

The rate coefficient of the DA reaction was calculated from the equation

$$k_{DA} = \frac{r_o(4\mathrm{MCH}) + r_o(T)}{[\mathbf{P}]_o[\mathbf{B}]_o}$$

*Table III*

*Experimentally determined rate constants of* **P+B** *DA reaction*

| T/K | $[P]_o$ / $10^{-3}$ M[a] | $[B]_o$ / $10^{-4}$ M | $r_o(4MCH)+r_o(T)$ / $10^{-9}$ M s$^{-1}$ | $k_{DA}$ / M$^{-1}$s$^{-1}$ | $\bar{k}_{DA,T}\pm\sigma$[b] / M$^{-1}$s$^{-1}$ |
|---|---|---|---|---|---|
| 753 | 2.93 | 0.296 | 3.017 | 0.03479 | 0.05655 ± 0.03077 |
| 753 | 2.93 | 1.56 | 35.79 | 0.07831 | |
| 761 | 2.93 | 0.296 | 6.202 | 0.07151 | 0.08221 ± 0.01513 |
| 761 | 2.93 | 1.56 | 42.47 | 0.09291 | |
| 768 | 2.56 | 0.523 | 11.12 | 0.08309 | |
| 768 | 2.56 | 2.85 | 77.09 | 0.1057 | |
| 768 | 2.56 | 6.44 | 137.5 | 0.08341 | |
| 768 | 2.93 | 0.296 | 7.156 | 0.08251 | |
| 768 | 2.93 | 0.602 | 15.03 | 0.08521 | |
| 768 | 2.93 | 1.56 | 52.33 | 0.1145 | 0.09246 ± 0.01891 |
| 768 | 2.93 | 3.29 | 121.6 | 0.1260 | |
| 768 | 2.93 | 7.37 | 172.8 | 0.08002 | |
| 768 | 3.21 | 0.655 | 14.48 | 0.06889 | |
| 768 | 3.21 | 3.57 | 129.9 | 0.1133 | |
| 768 | 3.21 | 8.08 | 193.0 | 0.07443 | |
| 775 | 2.93 | 0.296 | 8.155 | 0.09402 | 0.1126 ± 0.02629 |
| 775 | 2.93 | 1.56 | 59.96 | 0.1312 | |
| 782 | 2.93 | 0.296 | 10.05 | 0.1158 | 0.1275 ± 0.01648 |
| 782 | 2.93 | 1.56 | 63.59 | 0.1391 | |
| 788 | 2.93 | 0.296 | 14.21 | 0.1638 | 0.1640 ± 0.000282 |
| 788 | 2.93 | 1.56 | 75.03 | 0.1642 | |
| 793 | 2.56 | 0.523 | 28.70 | 0.2144 | |
| 793 | 2.56 | 2.85 | 133.4 | 0.1829 | |
| 793 | 2.56 | 6.44 | 256.9 | 0.1558 | |
| 793 | 2.93 | 0.296 | 16.30 | 0.1880 | |
| 793 | 2.93 | 0.399 | 15.07 | 0.1289 | 0.1586 ± 0.02781 |
| 793 | 2.93 | 0.602 | 23.99 | 0.1360 | |
| 793 | 2.93 | 3.29 | 142.0 | 0.1473 | |
| 793 | 2.93 | 7.37 | 297.1 | 0.1376 | |
| 793 | 3.21 | 3.57 | 167.7 | 0.1463 | |
| 793 | 3.21 | 8.08 | 340.2 | 0.1312 | |
| 801 | 2.93 | 0.296 | 18.95 | 0.2185 | 0.2185 ± 0.02[c] |
| 809 | 2.93 | 0.296 | 21.68 | 0.2500 | 0.2500 ± 0.02[c] |

[a] M = mol dm$^{-3}$

[b] $\bar{k}_{DA,T}$ = the mean value of $k_{DA}$ at the temperature $T$, $\sigma$ = standard deviation

[c] standard deviation estimated

The calculated rate coefficients are shown in Table III. Finally, the Arrhenius expression for $k_{DA}$ calculated from the exponential form of the Arrhenius equation is

$$\log(k_{DA}/dm^3\,\mathrm{mol}^{-1}\,s^{-1}) = (7.74\pm0.28)-(129.3\pm6.1)\,\mathrm{kJ\,mol}^{-1}/2{,}303\,RT$$

where the indicated uncertainties represent one standard deviation of the mean values of the parameters. (The weighting factor was $1/\sigma_i^2$).

A comparison of the parameters obtained with those determined for similar reactions (Table IV) shows reasonable agreement, although our data seem to be on the high side. We also conclude that these parameters are high enough to support our assumption concerning the negligible contribution of radical reactions.

*Table IV*

*Arrhenius parameters of some DA reactions of B*

| Diene | Dienophile | T/K | $\log(A/dm^3 mol^{-1} s^{-1})$ | $E$/kJ mol$^{-1}$ | Ref. |
|---|---|---|---|---|---|
| B | ethene | 760—921 | 7.48 | 115.1 | [23] |
| B | P | 900—1150 | 7.40 | 122.7 | a |
| | | 753—809 | $7.74 \pm 0.28$ | $129.3 \pm 6.1$ | this work |
| B | B | 464—557 | 6.95 | 102.6 | [6] |
| | | 446—660 | 6.95 | 99.2 | [24] |
| | | 691—923 | 8.14 | 112.2 | [23] |

[a] Calculated from equilibrium constant obtained from thermochemical calculations (data in Table V) using the rate constant of the retro—DA reaction [20].

*Table V*

*Thermochemical data used in the calculations [52, 26]*

| Compounds | $\Delta H^0_{f,298\,K}$/kJ mol$^{-1}$ | $S^0_{298}$/J mol$^{-1}$ K$^{-1}$ | $C_p$/J mol$^{-1}$ K$^{-1}$ | | | |
|---|---|---|---|---|---|---|
| | | | $a \cdot 10$ | $b \cdot 10^2$ | $c \cdot 10^5$ | $d \cdot 10^9$ |
| P | 20.42 | 266.94 | 50.895 | 22.560 | −99.873 | 13.283 |
| B | 110.16 | 278.74 | −163.03 | 41.339 | −342.38 | 114.92 |
| 4-methyl-cyclohexene | −33.372 | 355.11 | −627.24 | 77.921 | −521.73 | 136.82 |

The mechanism of the DA reaction and thus the retro-DA reaction is still under discussion. The thermal decompositions of many $C_3$ and $C_4$ rings are accepted as occurring by a biradical mechanism [19], and those of $C_6$ rings by a concerted mechanism. The decomposition of 4-vinylcyclohexene [20] the DA adduct of **B** (formed in our system, too), is considered to be a biradical process made possible by the formation of two relatively stable allylic radical centres [21]. Our experimentally determined activation energy for the DA reaction between **P** and **B** appears to confirm the concerted mechanism of this reaction, in disagreement with the results of SAKAI et al. [22]. A plausible biradical route would be:


(3)

$\Delta H^\circ_{f,793K}$/kJ mol$^{-1}$ −64.4 ~253 102.2 23.0

The heat of formation of the biradical was estimated following the argumentation used by BENSON [21]. The corrections used in the estimation were twice a half 1,5H-repulsions, one *cis*, and two alkene gauche corrections. The structure of this adduct was assumed to be similar to a $C_6$ ring, with $E_{-a}$ about 0—4 kJ mol$^{-1}$. Starting from the thermochemical data (see also Table V), $\Delta H^0_{a,793\,K}$ is 317.4 kJ mol$^{-1}$. For the activation energy of reaction *a*

$$E_{a,\text{calc.}} > \Delta H^0_{a,793} + E_{-a} \cong 317.4\ \text{kJ mol}^{-1}$$

obtained by the calculations above, and

$$E_a = 285.4 \text{ kJ mol}^{-1}$$

from the present work and the calculated equilibrium constants. The difference is about 32 kJ $mol^{-1}$, supporting the concerted mechanism.

*Acknowledgements*

The authors are indebted to Miss M. Markovits for her technical assistance.

**References**

[1] *Kallend, A. S., J. H. Purnell. B. C. Shurlock:* Proc. Roy. Soc. **A300**, 120 (1967).
[2] *Cundall, R. B., D. E. Fussey, A. J. Harrison, D. Lampard:* J. C. S. Faraday I. **75**, 1390 (1979).
[3] *Kunugi, T., T. Sakai, K. Soma, Y. Sasaki:* Ind. Eng. Chem. Fundamentals **9**, 314 (1970).
[4] *Kunugi, T., K. Soma, T. Sakai:* Ind. Eng. Chem. Fundamentals **9**, 319 (1970).
[5] *Seres, L., P. Ausloos:* Symp. on the Mechanism of Hydrocarbon Reactions, Siófok, Hungary p. 37. (1973).
[6] *Huybrechts, G., L. Luyckx, Th. Vandeaboom, B. van Mele:* Int. J. Chem. Kinet. **9**, 283 (1977).
[7] *Sevelkova, L. V., L. M. Vedenezva, R. A. Kalinyenko, K. P. Lavrovszkij:* Neftekhimia, **12**, 693 (1972).
[8] *Kopinke, F. D., B. Ondruschka, G. Zimmermann:* Tetrahedron Lett. **24**, 869 (1983).
[9] *Sakai, T., D. Nohara, T. Kunugi:* Symp. on Ind. and Lab. Pyrolysis, ACS Symp. Mexico City Meeting p. 129 (1976).
[10] *Sakai, T., K. Soma, Y. Sasaki, H. Tominaga, T. Kunugi:* Refining Petroleum for Chemicals, Adv. Chem. Ser. **97**, p. 68 (1970).
[11] *Schröder, H.:* J. High Res. Chrom. and Carom. Comm. **3**, 38, 95, 199, 361 (1980).
[12] *Martin, R. L.:* Anal. Chem. **34**, 896 (1962).
[13] *Simon, M., M. H. Back:* Can. J. Chem. **48**, 317 (1970).
[14] *Simon, M., M. H. Back:* Can. J. Chem. **48**, 3313 (1970).
[15] *Amano, A., M. Uchiyama:* J. Phys. Chem. **68**, 1133 (1964).
[16] *Burcat, A:* Fuel **54**, 87 (1975).
[17] *Sauer, J., R. Sustmann:* Angew. Chem. Int. Ed. **19**, 779 (1980).
[18] *Richard. C., M. H. Back:* Int. J. Chem. Kinet. **10**, 389 (1978).
[19] *O'Neal, H. E., S. W. Benson:* J. Phys. Chem. **72**, 1866 (1968).
[20] *Tsang, W.:* J. Chem Phys. **42**, 1805 (1965).
[21] *Benson, S. W.:* Thermochemical Kinetics, Wiley, New York, N. Y., 1976.
[22] *Sakai, T., T. Nakatani, N. Takahashi, T. Kunugi:* Ind. Eng. Chem. Fundam. **11**, 529 (1972).
[23] *Rowley, D., H. Steiner:* Disc. Faraday Soc. **10**, 198 (1951).
[24] *Kistiakowsky, G. B., W. W. Ransom:* J. Chem. Phys. **7**, 725 (1939).
[25] *Seres, L., L. Zalotai, F. Márta:* Acta Phys. et Chem. Szeged **23**, 433 (1977).
[26[ *Seres, L:* Acta Phys. et Chem. Szeged **27**, 31 (1981).

## ТЕРМИЧЕСКИЙ РАСПАД ПРОПЕНА В ПРИСУТСТВИИ 1,3 БУТАДИЕНА РОЛЬ РЕАКЦИИ ДИЛЬСА-АЛДЕРА

*Т. Кёртвелеши, М. Гергени Л. Шереш*

Изучтен термический распад пропена в присутствии 1,3 бутадиена в интервале температур 745—809 К. Идентифицировано 45 соединений и установлены начальные скорости их образования на основании данных газо-хроматографического анализа. Образование продуктов проходит как радикально-цепным, так и молекулярным механизмом. Полученные результаты подтверждают концертную природу реакции Дильса-Алдера.

# MILD OXIDATION OF *n*-BUTENES OVER MIXED TIN—VANADIUM OXIDES

By

K. HERNÁDI, J. HALÁSZ, K. VARGA, AND P. FEJES

Applied Chemistry Department, Attila József University, Szeged, Hungary

*(Received 9th December, 1983)*

The oxidation of *n*-butenes in the gaseous phase over mixed oxide catalysts $V_2O_5$—$SnO_2$ has been investigated in a pulse reactor at 523—673 K. The main products of the reaction are acetaldehyde and acetic acid; methyl ethyl ketone, butyraldehyde and other compounds are formed in smaller quantities. Maximum selectivity is found in the oxidation of 1-butene over catalysts in the composition interval $3:1 \cong V_2O_5:SnO_2 \cong 2:1$ at 523—573 K. Above 620 K the selectivity is independent of the nature of the initial butene. This can be explained in that a gas mixture of thermodynamic equilibrium is undergoing conversion, because of the rapid isomerization of the double bond-containing compounds. Formation of the main products can be interpreted by a mechanism including adsorption of 1-butene on a surface Brönsted acid site, oxidation of butylcarbonium ion by lattice oxygen, and oxidative cracking of the same surface ion; in the case of 2-butene, oxidation occurs only after isomerization to 1-butene.

## *Introduction*

Heterogeneous selective oxidation is a practicable possibility for the processing of the $C_4$ fraction formed as a by-product of cracking. *n*-Butenes can be converted into 1,3-butadiene over $Bi_2O_3$—$MoO_3$ or $SnO_2$—$Sb_2O_4$ catalysts [1,2], or they can be oxidized into maleic anhydride (MA) over $V_2O_5$—$P_2O_5$ [3]. Little attention has been paid to conversion into saturated carbonyl compounds, because of the low selectivity, though the results of POPOVA and MILMAN [4] demonstrated that methyl ethyl ketone is formed with high selectivity from *n*-butenes over copper oxide.

The oxidation of *n*-butenes into acetic acid has been investigated by BROCKHAUS [5] over various transition metal vanadates and it has been found that the selectivity for acetic acid was nearly 70% in the temperature range 513—543 K. The only side-reactions observed were total oxidation and the formation of small amounts of maleic anhydride, which contrasts with the results of other authors [6—8] who have described the formation of numerous by-products.

The gas-phase oxidation of 1-butene over unsupported $V_2O_5$ has been investigated by HAUFFE and ABD EL-SALAAM [9], who found that the yields of the main products (acetic acid and maleic anhydride) are correlated to the extent of reduction of the catalyst; this depends on the reaction temperature. The steady-state composition of the catalyst at 623 K, which has the highest selectivity, is $V_2O_{4,8}$; the catalyst is a solid solution containing $V^{5+}$ and $V^{4+}$.

Although $V_2O_5$-based mixed oxide catalysts promote the formation of maleic anhydride during the mild oxidation of *n*-butenes [10, 11], in the presence of certain additives saturated carbonyl compounds such as acetic acid, acetaldehyde, methyl ethyl ketone and possibly propionic acid can be formed. KANEKO et al. [12, 13] investigated the relationship between the structure and the activity of V—Sn—W oxide catalysts for butene oxidation, and found that the effective catalyst, which has 40—60% selectivity for acetic acid, contains $V_2O_5$ and $V_4O_9$ phases simultaneously, the optimum atomic ratio $V^{5+}/V_{total}$ being 0.65. As concerns the mechanism of acetic acid formation, it has been proposed [14] that AcOH is mainly formed from acetaldehyde, which in turn is produced through the direct reaction of the active O species with the carbonium ion formed from the olefin on the acidic sites of the catalyst. The authors suggest that both isomerization and oxidation reactions take place on the same Brönsted acidic sites, which result from lattice defects of the catalyst. In connection with the acid-base properties of $V_2O_5$-based binary catalysts, mention must be made of the work of AI [15, 16], who studied the relation between the acidity of the catalyst and the selectivity for maleic anhydride; in the $V_2O_5$—$SnO_2$ system the highest acidity was measured for the catalyst with atomic ratio V:Sn = 1:1, which proved to be the most effective catalyst in the production of maleic anhydride.

The rates of oxidation of $C_3H_6$, $C_2H_4$, $C_3H_8$ and CO have been investigated by ONO et al. [17] over V—Sn oxides of various compositions. The catalytic activity exhibits two maxima at very different compositions, and it has been proposed that different oxygen species are responsible for the oxidation. For the catalyst with atomic ratio V/Sn = 2/1 an amorphous material has been found from which lattice oxygen is easily released. The activity maximum for the oxide with V/Sn = 1/8 is associated with the presence of $V^{4+}$ ions dissolved in $SnO_2$. The presence of $V^{4+}$ ions appears to faciliate the formation of adsorbed oxygen species, which play a significant role in the oxidation reaction.

Although the basic features of the mild oxidation of olefins over $V_2O_5$—$SnO_2$ have been clarified in previous work, the overall picture is still somewhat inconsistent and incomplete. The present paper, connected with studies on mild oxidation over $SnO_2$-based mixed oxide catalysts [18 19], deals with the oxidation of *n*-butenes over $SnO_2$—$V_2O_5$. We set out to establish catalyst compositions suitable for the production of saturated carbonyl compounds, and the optimum reaction conditions.

## *Experimental*

The oxidation of *n*-butenes over pure $V_2O_5$, pure $SnO_2$, and their mixtures in various ratios, was investigated in a pulse reactor, while isomerization was studied in a recirculatory flow reactor. $V_2O_5$ was prepared from ammonium metavanadate by calcination at 623 K. For the preparation of $SnO_2$, metallic tin was dissolved in conc. HCl. Tin(IV) hydroxide was precipitated with $NH_4OH$, then washed and dried. The binary oxides were prepared by mixing the respective components in the correct proportions, followed by calcination at 873 K for 6 hours.

The thermal behaviour of the catalysts was investigated by derivatography (Q Derivatograph, MOM) and X-ray diffraction (DRON—3, USSR).

The microcatalytic reactor was made of stainless steel in a heated aluminium block

situated in a CHROM—4 gc unit. The reactor contained 0.5 g catalyst. The conditions selected (if not stated otherwise) were: pulse volume: 3 $cm^3$; composition: $C_4H_8:O_2:N_2 = 1:3:11.2$; flow rate of $N_2$ carrier gas: 0.4 $cm^3s^{-1}$; and pressure: $10^5$ Pa.

For gc analysis, a 2.5 m column was used containing Carbowax 20M and phosphoric acid as stationary phase on Chromosorb W.

*n*-Butene isomerization measurements were carried out in a recirculatory flow reactor 243 $cm^3$ in volume. Product compositions were determined by gc analysis on samples withdrawn through a 0.5 $cm^3$ sampling valve at regular intervals. For separation of the components, a 2.5 m column containing dinonyl phthalate on Chromosorb W was used.

## *Results*

### *Thermal analysis of the catalysts*

Figure 1 depicts DTA curves of the pure and mixed oxides. The DTA curve of pure $V_2O_5$ displays three endotherms. The first, at 203 K, is a result of the loss of adsorbed and structural water; this peak is observed only in the case of samples 2 and 3 indicating the absence of water from catalysts with higher tin contents. The peak at 963 K corresponds to the melting of $V_2O_5$. In the case of samples 3, 4, and 5 there are endothermic and exothermic peaks above the melting point of $V_2O_5$. Since no loss of weight was found in this range, these peaks relate to the formation of a new compound, probably tin vanadate.

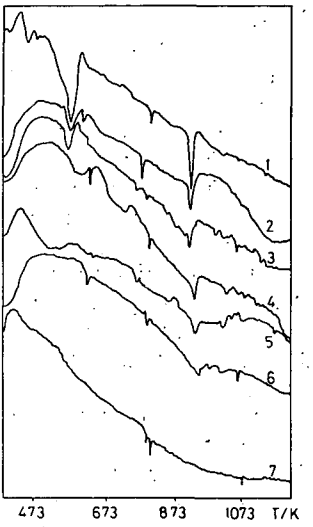


*Fig. 1.* DTA curves for catalysts of different compositions (heating rate 10 K/min)
Compositions: 1. $V_2O_5$; 2. $V_2O_5:SnO_2 = 3:1$; 3. $V_2O_5:SnO_2 = 2:1$; 4. $V_2O_5:SnO_2 = 1:1$; 5. $V_2O_5:SnO_2 = 1:2$; 6. $V_2O_5:SnO_2 = 1:3$; 7. $SnO_2$

The formation of a new compound (and possibly a new phase) is proved by X-ray diffraction measurements. New peaks can be found in the X-ray diffraction patterns of the catalysts calcined at various temperatures, but new compound formation is inextensive, for the original peaks of $V_2O_5$ and $SnO_2$ remain dominant. Calcination above 973 K does not cause any further change in the structure of the catalyst.

### *Oxidation of n-butenes*

In the oxidation of *n*-butenes in a pulse reactor, the applied catalysts were characterized by the conversion (**x**) (the ratio of the oxidized and initial amounts of butene) and by the selectivity (**y**) (the ratio of the amount of a given product to the amount of butene oxidized). Average conversion and selectivity values for different catalysts and reaction conditions were calculated by using data obtained from the 4th—5th pulse on, which practically correspond to a stationary state.

*Properties of the catalysts as a function of composition*

Since the properties of the mixed oxide catalysts used in the mild oxidation reactions are not the additive resultants of the properties of the pure components, we investigated how the properties change as a function of composition.

For the oxidation of both *n*-butenes, the conversion depends only slightly on the composition of the catalyst; maximum conversion is attained at a tin content of 75—30%.

During the oxidation, acetaldehyde and acetic acid are obtained as main products. Methyl ethyl ketone, butyraldehyde, propionaldehyde, propionic acid, crotonaldehyde, acrolein and some other products are also formed in small quantities.

The selectivity for acetaldehyde (one of the main products) formation as a function of the catalyst composition is shown at three different reaction temperatures in Fig. 2. Over the catalyst with $V_2O_5$:$SnO_2$ = 3:1, this selectivity is higher than 50%, but in the range $1:1 \geqq V_2O_5:SnO_2 \geqq 1:2$ and over pure $SnO_2$ an insignificant amount of acetaldehyde is found.

The selectivity for acetic acid (the other main product) can be seen in Fig. 3. Over pure $SnO_2$, acetic acid is not formed, and its quantity does not attain 1% in the catalyst composition range $1:1 \geqq V_2O_5:SnO_2 \geqq 1:2$. However, the selectivity reaches 30—35% at ratios $4:1 \geqq V_2O_5:SnO_2 \geqq 2:1$. During the oxidation, butyraldehyde is produced in relatively large amount. The appearance of this $C_4$ saturated aldehyde deserves particular attention, as its formation in this reaction has never been described before. Its selectivity as a function of composition is shown in Fig. 4. The course of the curve is similar to the previous ones, with the difference that butyraldehyde is formed in appreciable amount over pure $SnO_2$. The quantity of methyl ethyl ketone as a function of catalyst composition can be seen in Fig. 5. This is the second $C_4$ satura-

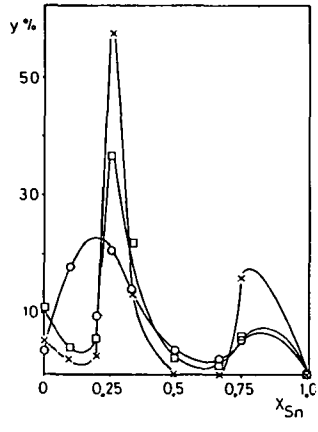


*Fig. 2.* Selectivity for acetaldehyde as a function of catalyst composition in the oxidation of 1-butene $T_{reaction} = x$: 523 *K*; □: 598 *K*; ○: 673 *K*

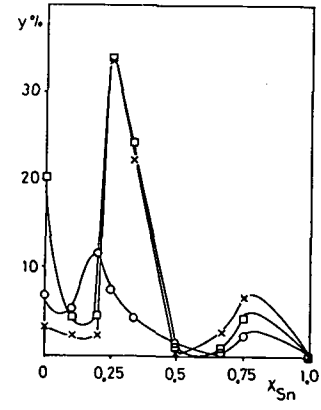


*Fig. 3.* Selectivity for acetic acid as a function of catalyst composition in the oxidation of 1-butene. ($T_{reaction}$ are the same as in Fig. 2)

ted carbonyl compound formed in large amount. The formation of butyraldehyde and methyl ethyl ketone can be explained by the participation of Brönsted-type acidic surface sites, in a carbonium ion mechanism [20].

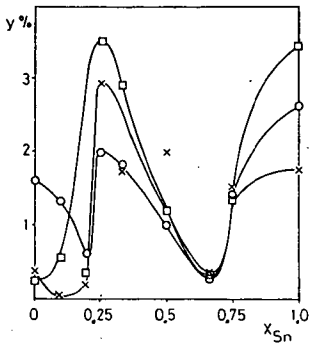


*Fig. 4.* Selectivity for butyraldehyde as a function of catalyst composition in the oxidation of 1-butene ($T_{reaction}$ are the same as in Fig.2)

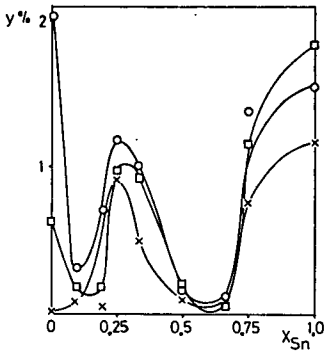


*Fig. 5.* Selectivity for methyl ethyl ketone as a function of catalyst composition in the oxidation of 1-butene ($T_{reaction}$ are the same as in Fig. 2)

*Conversion and selectivity as functions of reaction temperature*

At all reaction temperatures, the conversions in the oxidation of 1-butene over pure $V_2O_5$ and $SnO_2$ are much higher than the conversions of 2-butene, but the products are obtained in small amounts. Maximum selectivity in the oxidation of 1-butene has been found over the mixed oxide $V_2O_5$:$SnO_2$=3:1. In Fig. 7, the conversions and the selectivities for the main products (acetic acid and acetaldehyde) are shown as functions of the reaction temperature. At low temperatures the conversion increases sharply, attains a maximum at 623 K, and then decreases. In the range 523—573 K, the quantities of acetaldehyde and acetic acid are each about 50%. The selectivities for these products decrease as the reaction temperature increases, and total oxidation resulting in $CO_2$ becomes dominant.

The difference between the oxidation of 1- and 2-butenes is illustrated in Figs. 6, 8. The conversion over the mixed oxide $V_2O_5$:$SnO_2$=1:1 is shown as a function of temperature in Fig. 6. At low temperatures (below 623 K), 2-butene is oxidized less extensively than 1-butene, which undergoes 31—38% conversion in the temperature interval considered. The conversion of 2-butene depends strongly on the reaction temperature; at 523 K it is 18%, whereas at 673 K it is over 70%.

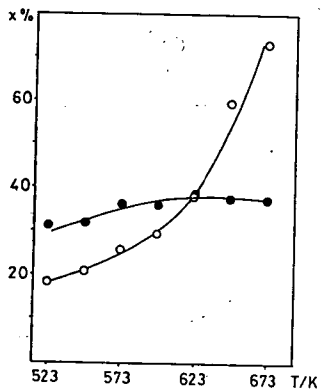


*Fig. 6.* Temperature-dependence of conversion in oxidation of 1-butene (●) and 2-butene (○) over $V_2O_5$:$SnO_2$=1:1

A comparison of the selectivities in the reactions of the two *n*-butenes revealed a great difference at low temperature (Fig. 8), but above 623 K the products and their selectivities are practically the same, independently of the initial compound. Below 623 K, the oxidation of 1-butene is more selective, with 2-butene the selctivity for each product being less than 20%.

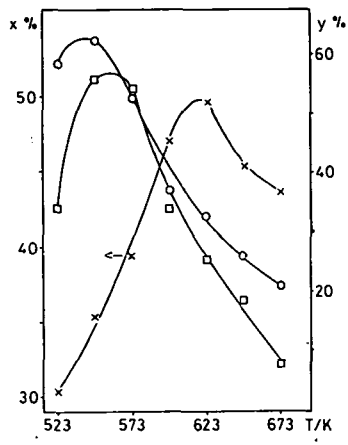


*Fig. 7.* Temperature-dependence of 1-butene oxidation over $V_2O_5$:$SnO_2$=3:1 (x: conversion, ○ selectivity for acetaldehyde, □: selectivity for acetic acid)

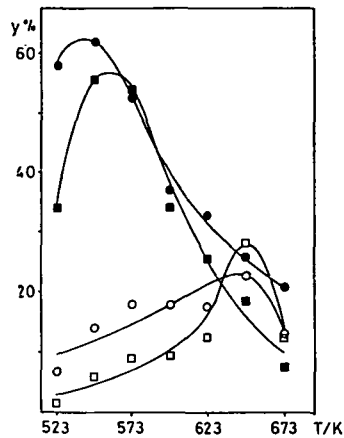


*Fig. 8.* Temperature-dependence of selectivity for acetaldehyde (○ ●) and acetic acid (□ ▨) in the oxidation of 1-butene (● ▨) and 2-butene (○ □) over $V_2O_5$:$SnO_2$=3:1

*Isomerization of n-butenes*

The identical selectivities point to the rapid occurrence of isomerization of the *n*-butenes, especially above 623 K. Accordingly, the isomerization of 1- and 2-butenes was studied over $V_2O_5$:$SnO_2$=3:1 at 473 K and 523 K in a recirculatory flow reactor, in the absence of dioxygen. The results are to be seen in Figs. 9—10. For both

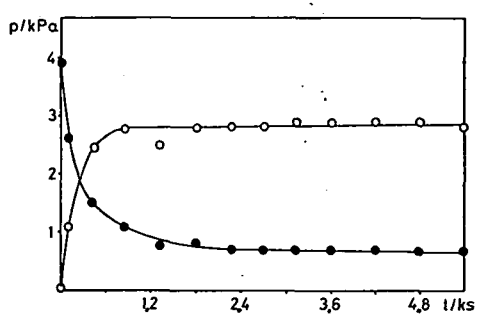


*Fig. 9.* Double bond isomerization of 1-butene over $V_2O_5$:$SnO_2$=3:1 at 523K; $p^0_{1\text{-butene}}$=4 kPa; ●: 1-butene; ○: 2-butene

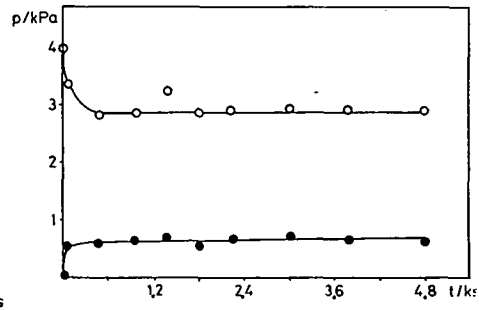


*Fig. 10.* Double bond isomerization of 2-butene over $V_2O_5$:$SnO_2$=3:1 at 523 K; $p^0_{2\text{-butene}}$=4 kPa; ●: 1-butene; ○: 2-butene

starting substances the reactants reach thermodynamic equilibrium in less than 10 minutes. At higher temperatures (above 623K), the rate of isomerization is probably larger than the rate of oxidation, so that a reaction mixture in thermodynamic equilibrium (ca. 25% 1-butene and 75% 2-butene) is involved in the oxidation. The isomerization was investigated above 523 K too, but the results were difficult to interpret, as the catalyst was reduced by the olefins.

## *Discussion*

The pulse reactor measurements show that 1-butene can be converted into acetaldehyde and acetic acid with high selectivity over the mixed oxide $V_2O_5$:$SnO_2$=3:1 in the temperature range 523—573 K. Comparison of the oxidations of the two *n*-butenes demonstrates that both the conversion and the selectivity for useful products are lower in the oxidation of 2-butene at low temperature than in that of 1-butene. However, above 623 K the selectivities yielded by the two *n*-butenes are practically the same. This can be explained in that the rate of double bond isomerization is much larger than the rate of oxidation at higher temperature, so that the oxidation involves a reaction mixture of *n*-butenes in thermodynamic equilibrium. Below 623 K (when the rate of isomerization is commensurable with or less than the rate of oxidation), 1- and 2-butenes behave differently. Under these circumstances the oxidation of 1-butene is more rapid and the selectivity is much higher too. It must be assumed that the two components are adsorbed in different ways and that two different species are formed on the catalyst surface, these species yielding products characteristic of the initial reagents. The formation of acetaldehyde and acetic acid from 2-butene can be explained by associative adsorption with cracking of the double bond [21]:

$$CH_3{-}CH{=}CH{-}CH_3\ (gas) \longrightarrow CH_3{-}\underset{|}{CH}{-}\overset{+}{CH}{-}CH_3$$
$$\qquad\qquad\qquad\qquad\qquad\qquad\quad \wwww$$

Interaction of the surface species and an $O^{2-}$ ion gives

$$CH_3{-}\underset{\wwww}{\overset{|}{CH}}{-}\overset{O^-}{\overset{|}{CH}}{-}CH_3$$

Further oxidation of this surface ion leads to acetaldehyde and acetic acid. However, our measurements indicate that oxidation of 1-butene into acetaldehyde or acetic acid cannot be explained either by associative adsorption or by $\pi$-type adsorption; in this latter case allyl-type unsaturated products such as 1,3-butadiene are formed. Associative adsorption resulting in cracking of the double bond would give propionaldehyde and propionic acid in the oxidation of 1-butene, but we found only small amounts of these products. Since the oxidation of 1-butene is more rapid than that of 2-butene, 2-butene formed by double bond isomerization is inconceivable as a transition product. The formation of acetic acid in the oxidation of 1-butene over transition metal oxides has been explained by two types of mechanism. KANEKO et al. [14] found that oxidation takes place over acidic sites resulting from lattice defects on the cata-

lyst surface. YAMASHITA et al. [22], however, concluded that hydration and oxidation steps play a significant role in this reaction and *sec*-butanol, methyl ethyl ketone and diacetyl were proposed as transition products. Both mechanisms assume the same transition products in the reaction of 1-butene and 2-butene, and similar rates of oxidation too.

In our opinion, both the formation of $C_2$ and $C_4$ carbonyl compounds in the oxidation of 1-butene can be described by a carbonium ion mechanism, the first step of which is the adsorption of the olefin on a surface site containing an —OH group. This reaction therefore takes place over a catalyst containing Brönsted acid sites capable of further oxidizing the surface carbonium ion. V—Sn mixed oxide catalysts contain Brönsted acid sites. AI [16] reported that the acidity depends considerably on the composition. Maximum acidity was found for the mixed oxide containing 50% vanadium, and this catalyst seemed to be the most active in the oxidation of 2-butene into maleic anhydride. However, in accordance with our results, this mixed oxide did not prove to be selective in the oxidation of 1-butene. As concerns the relation between the identification of the oxidation centres, the structure of the catalyst, and the properties displayed in mild oxidation reactions, it can be stated that the selectivities given by the pure oxides are much lower than those with certain mixed catalysts. The derivatographic and X-ray diffraction results revealed that a new compound, tin vanadate, is formed only above the temperature of calcination of the catalyst. Hence neither the pure oxides nor the new phase is responsible for the selectivity. On the other hand, it can be assumed that the presence of the phase $V_6O_{13}$ mentioned by ANDERSSON [23] results in the selectivity. The role of $SnO_2$ is to weaken the surface V=O bonds, thereby mobilizing the lattice oxygens and promoting the incorporation of oxygen into the products.

Thus, the oxidation of 1-butene over $V_2O_5$—$SnO_2$ can be explained by the following mechanism. The first step is the adsorption of 1-butene on a surface acidic site:

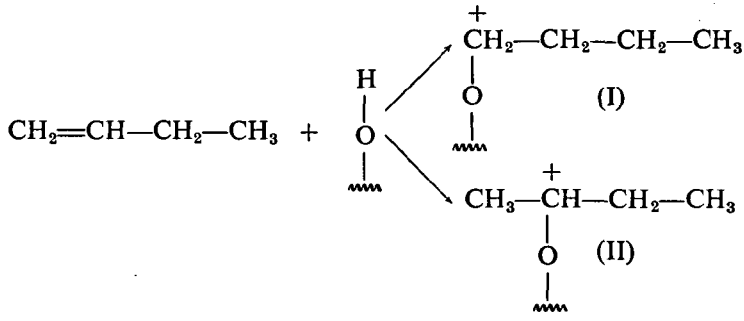

During the chemisorption, two kinds of carbonium ion can be formed on the surface; these are attached *via* the oxygen of the —OH group. Reaction between *via* 1-butylcarbonium ion (I) (the formation of which is much less probable than that of the 2-butylcarbonium ion (II)) and $O^{2-}$ of the lattice results in butyraldehyde:

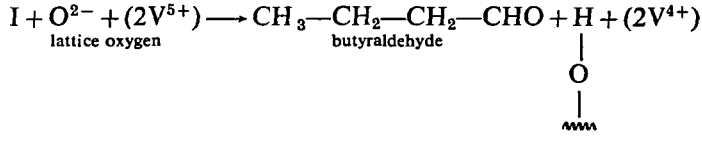

In the similar reaction of the 2-butylcarbonium ion, methyl ethyl ketone is formed:

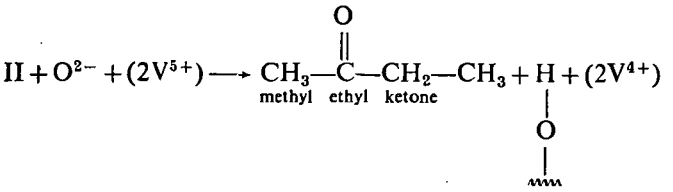


However, oxidative cracking is more probable in the reaction of the 2-butylcarbonium ion, with the formation of ethyloxonium ions:

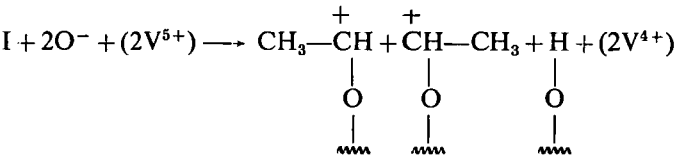


Desorption of the ethyloxonium ion results in the formation of acetaldehyde, and further oxidation leads to acetic acid:

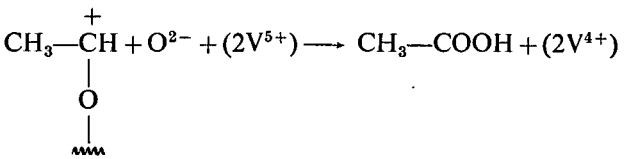


Gaseous dioxygen plays an important role in reoxidation of the catalyst:

$$0.5\,O_2 + 2V^{4+} \longrightarrow O^{2-} + 2V^{5+}$$

Adsorbed oxygen enters the lattice in this way and subsequently participates in the reaction as lattice oxygen.

Selective product formation in the reaction of 2-butene is due to double bond isomerization; 2-butene is first converted into 1-butene, which yields acetaldehyde and acetic acid *via* the mechanism desribed above. Saturated $C_2$ and $C_4$ carbonyl compounds can be formed only in the oxidation of 1-butene.

## References

[1] *Hucknall, D. J.:* Selective Oxidation of Hydrocarbons, Academic Press, New York, 1974.
[2] *McAteer, J. C.:* J. C. S. Faraday Trans. I. **75**, 2768 (1979).
[3] *Varma, R. L., D. N. Saraf:* Ind. Eng. Chem. Prod. Res. Dev. **18**, 7 (1979).
[4] *Popova, N. I., F. A. Milman:* Kinet. Katal. **6**, 944 (1965).
[5] *Brockhaus, R.:* Chem. Ing. Tech. **38**, 1039 (1966).
[6] *Tan, S., Y. Moro-Oka, A. Ozaki:* J. Catal. **17**, 132 (1970).
[7] *Vanhove, D., S. R. Op, A. Fernandez, M. Blanchard:* J. Catal. **57**, 573 (1979).
[8] *Morselli, L., F. Trifiro, L. Urban:* J. Catal . **75**, 112 (1982).
[9] *Hauffe, K., K. M. Abd El-Salaam:* Ber. Bunsenges. Phys. Chem. **82**, 1321 (1978).

[10] *Ai, M.:* Bull. Chem. Soc. Jpn. **44**, 761 (1971).
[11] *Ostrushko, V. I., J. D. Kernos, I. I. Ioffe:* Neftekhim. **12**, 362 (1972).
[12] *Kaneko, K., T. Koyama, S. Wada:* Bull. Jpn. Petrol. Inst. **16**, 17 (1974).
[13] *Kaneko, K., T. Hoshino, S. Wada:* Bull. Jpn. Petrol. Inst. **16**, 24 (1974).
[14] *Kaneko, K., T. Koyama, H. Furukawa, S. Wada:* Nippon Kagaku Kaishi 1264 (1974),
[15] *Ai, M., S. Suzuki:* Bull. Chem. Soc. Jpn. **47**, 3074 (1974).
[16] *Ai, M.:* J. Catal. **40**, 318 (1975).
[17] *Ono, T., Y. Nakagawa, Y. Kubokawa:* Bull. Chem. Soc. Jpn. **54**, 343 (1981).
[18] *Halász, J., M. Rávai, K. Varga, P. Fejes:* React. Kinet. Catal. Lett. **15**, 41 (1980).
[19] *Halász, J., K. Varga, P. Fejes:* React. Kinet. Catal. Lett. **18**, 261 (1981).
[20] *Moro-Oka, Y., S. Tan, A. Ozaki:* J. Catal. **17**, 125 (1970).
[21] *Seiyama, T., K. Nita, T. Maehara, N. Yamazoe, Y. Takita:* J. Catal. **49**, 164 (1977).
[22] *Yamashita, T., S. Ninagawa, T. Kato:* Bull. Jpn. Petrol. Inst. **18**, 167 (1976).
[23] *Andersson, A.:* J. Catal. **69**, 465 (1981).

## ЧАСТОЧНОЕ ОКИСЛЕНИЕ Н-БУТЕНОВ НАД СМЕШАННЫМИ ОЛОВО-ВАНИДИЕВЫМИ ОКСИДАМИ

*К. Гернади, Я. Галас, К. Варга, П. Фееш*

Изучено окисление н-бутенов в газовой фазе над смешанными оксидными катализаторами $V_2O_5$—$SnO_2$ в импульсном реакторе при температурах 523—673 К. Основными продуктами являются ацетальдегид, уксусная кислота, метилэтилкетон, бутиральдегид, а другие продукты образуются в меньших количествах. Наибольшая селективность в окислении 1-бутена найдена над катализаторами с сотавом $3:1 \cong V_2O_5:SnO_2 \cong 2:1$ в интервале температур 523—573 К. Выше температуры 620 К селективность реакции не зависит от строения исходного бутена.

# DEALUMINATION OF ZEOLITES WITH VOLATILE REAGENTS. MODIFICATION OF THE ADSORPTION PROPERTIES OF HUNGARIAN NATURAL ZEOLITES WITH PHOSGENE*

I. HANNUS, I. KIRICSI, I. DÉKÁNY** AND P. FEJES
Applied Chemistry Department, and Colloid Chemistry Dept.**,
Attila József University, Szeged, Hungary

*(Received 29th November, 1983)*

A novel dealuminating procedure was applied to natural mordenites and clinoptilolites originating from the Tokaj Mountain deposits in Hungary, and the ensuing changes in composition, structure and adsorption properties were assessed. The highest adsorption capacity was attained at a dealumination temperature of 873 K; this was a result of the removal of impurities and bulky cations while near perfect crystallinity was maintained. Crystallinity was retained up to 1073 K in the case of mordenite, whereas clinoptilolite underwent loss of crystallinity above 873 K. The immersion wetting enthalpies decreased monotonously due to the increasing hydrophobicity. The procedure seems to be promising for the production of zeolites with varying surface energies.

## *Introduction*

Among the mineral resources of Hungary, the natural zeolites occurring in and near the Tokaj Mountains are playing an ever increasing role. Besides the efforts to synthesize "tailor-made" zeolites for the petrochemical and organic industries, extensive research is being carried out to widen the field of application of the natural zeolites, too [1]. In this respect promising results have been achieved in their use for the adsorptive purification of gaseous exhausts (*e.g.* environmental protection [2]), air separation [3] and agricultural application (upgrading of soils [4], animal breeding, etc.).

NEMECZ and VARJÚ first reported on the clinoptilolite deposits in the Tokaj Mountains in the early 1960's [5]. Since that time a great number of papers have dealt with the structures, compositions and potential uses of mordenite- and clinoptilolite-bearing sediments [6—11]. Recently, a conference was organized on these topics [12].

It is well known that natural zeolites crystallized in a saline environment from volcanic sediments and, depending on the circumstances, contain various amounts of impurities in the form of crystalline minerals and amorphous constituents (volcanic glass, etc.). For practical applications, some sort of pretreatment (grinding, ion-exchange, etc.) is indispensable. Among the possible modifications influencing adsorption, ion-exchange, etc., the different dealuminating procedures are of paramount importance [13].

---

* This paper is being published in Hungarian in Hung. J. Chem.

If a proportion of the framework aluminium is dissolved or removed the thermal and hydrothermal stability of zeolites is influenced beneficially. In the process the electronegativity of the framework increases, rendering the Brönsted centres more acidic. Simultaneously, the dealuminating agents remove most of the impurities blocking the interconnecting windows between the large cavities and/or pore entrances.

A dealuminating procedure developed at the Applied Chemistry Department of József Attila University [14—15] has been used to investigate natural mordenites and clinoptilolites from the aspects of their compositions, structures and adsorption properties.

## *Experimental*

The specimens under study were sediments from the Tokaj Mountains, containing mordenite and clinoptilolite in various amounts.* The zeolite-bearing rocks were crushed and sieved. The sieve fraction of 1.0—1.6 mm was used subsequently. Its composition was determined by measuring the $NH_3$ content of the $NH_4^+$ forms obtained after multiple ion-exchange with $NH_4Cl$ solution [10]. For the mordenite and clinoptilolite sediments, a mordenite content of 31% and a clinoptilolite content of 48% resulted. Quartz, clay minerals and volcanic glass constituted the non-zeolitic impurities.

The dealumination was carried out in a tube reactor made of quartz, with phosgene ($COCl_2$) and a 1:1 mixture of CO and $Cl_2$. No significant difference could be observed in the effectiveness of the agents, because phosgene decomposition reached 50% at 773 K and completeness at 1073 K [16].

Prior to dealumination, the samples were heat-treated at 773 K in a stream of $N_2$ for 2 h. Thereafter, the dealumination followed at the preselected temperature (between 773 K and 1073 K) in a stream of $COCl_2$ (rate of flow: 20 $cm^3$/min) for 2 h. The gas stream was next changed again: the flow of $N_2$ was maintained for a further 2 h in order to desorb the products. The cool sample was washed free of $Cl^-$ ions and dried at 390 K.

The volatile metal halides (from the impurities and metal ions in ion-exchange and framework positions, respectively) produced a fall-out after the reactor tube. This was dissolved and analysed for $Al^{3+}$ (by complexometry) and $Fe^{3+}$ (spectrophotometry). The same ions were determined in a caustic melt of the non-treated samples.

Structural changes in the treated samples were assessed by X-ray diffraction and i.r. spectroscopy. X-ray diffractions were registered in the interval $3° < 2\theta < 34°$ using a Dron—3 diffractometer. The i.r. spectra were recorded on KBr pressed pellets containing 0.5% zeolite, on a Specord IR—75 instrument.

Water contents were determined by thermogravimetry with a MOM—Q Derivatograph. Adsorption of $N_2$ was measured volumetrically at 77 K on samples heat-treated at 507 K under continuous pumping. The immersion wetting enthalpies were measured in an LKB—2107 sorption microcalorimeter at 298 K after appropriate pretreatment.

* The authors express their sincere thanks to Ernő Mátyás, Hungarian National Ore and Mineral Mines Hegyaljai Plant, for supplying the samples.

*Results and discussion*

The amounts of Al and Fe removed by dealumination are plotted in Figs. 1 and 2 as functions of the temperature. Table I contains the same data as percentages of the original contents.

In contrast to synthetic mordenites [14], phosgene removes only less than 40% of the Al, even at 1073 K, whereas the loss reaches 90% for Fe. The differences might be accounted for by the fact that in the case of natural zeolites the zeolite crystals are embedded in a glass-like matrix which is difficult for the gaseous reactant(s) to penetrate, while ion constitutes a separate haematite phase [7, 17], only a minor amount residing in the zeolite, and even this part being found in exchange positions.

For checks on the crystallinity retained after dealumination, X-ray diffractograms were taken as well. Figure 3 shows the respective intensities relative to the most

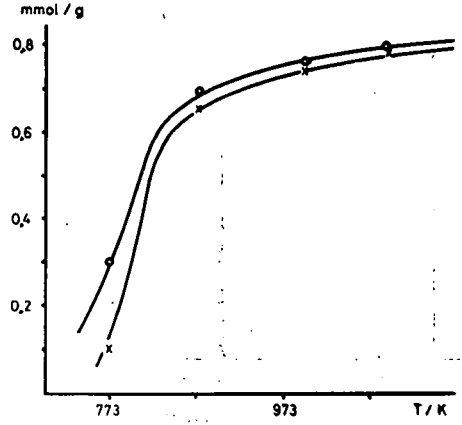


*Fig. 1.* Amount of Al removed from zeolites as a function of the temperature of dealumination (x mordenite, o clinoptilolite)

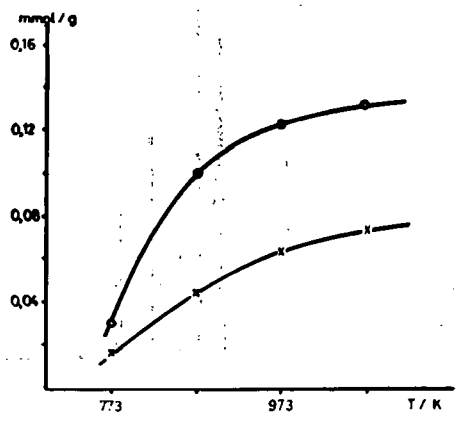


*Fig. 2.* Amount of Fe removed from zeolites as a function of the temperature of dealumination (x mordenite, o clinoptilolite)

*Table I*

*Amounts of* $Al^{3+}$ *and* $Fe^{3+}$ *removed as percentages of* $Al^{3+}$ *and* $Fe^{3+}$ *originally present*

| | | base sample mmol/g | temperature of dealumination/K | | | |
|---|---|---|---|---|---|---|
| | | | 773 | 873 | 973 | 1073 |
| | | | % | | | |
| mordenite | Al | 2.2 | 4.55 | 30.7 | 34.6 | 36.8 |
| | Fe | 0.093 | 18.3 | 47.3 | 78.5 | 86.1 |
| clinoptilolite | Al | 2.04 | 14.7 | 34.3 | 37.8 | 39.2 |
| | Fe | 0.146 | 19.8 | 68.5 | 84.2 | 91.7 |

intense reflexion of the original samples. (In fact, the most intense reflexion appears at 0.33 nm, due to quartz [6]; this was omitted from the drawing). The Figure reveals that crystallinity is well retained even after treatment of the samples with phosgene at 1073 K, though a systematic change in the intensities is clearly discernible: the intensities of the low-index planes decrease, while simultaneously a few of the higher-index planes become more intense. Similar results have been obtained for the dealumination of synthetic mordenite [18, 19]. A precise explanation is not yet available.

Clinoptilolite behaves differently, due to its lower thermal stability. A diffractogram is presented for this sample in Fig. 4. In agreement with literature data, an appreciable loss of crystallinity accompanies dealumination at 973 K, followed by complete structural collapse at 1073.

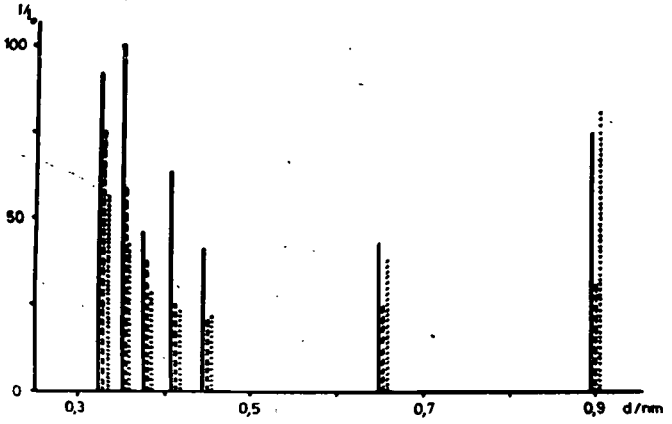


*Fig. 3.* Simplified X-ray patterns of mordenites: — base sample, -- sample dealuminated at 873 K, ... sample dealuminated at 1073 K

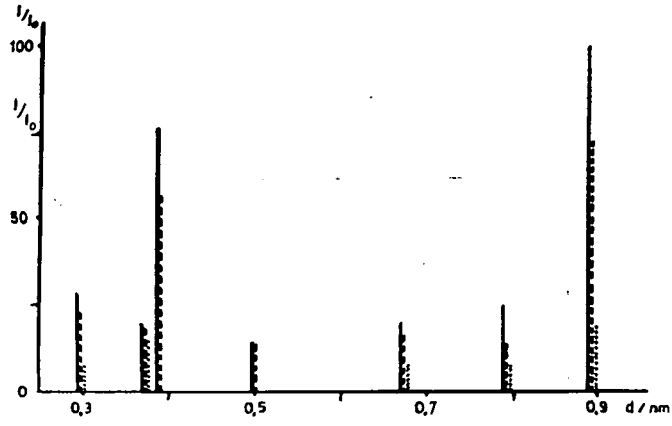


*Fig. 4.* Simplified *X*-ray patterns of clinoptilolites: — base sample, --- sample dealuminated at 773 K, ... sample dealuminated at 973 K

Similar conclusions can be drawn from the i.r. spectra: it follows from Fig. 5 that elevation of the temperature of treatment leads to removal of the impurities, the specimens becoming increasingly "clean", and the spectrum taken after dealumination at 973 K is nearly indistinguishable from that of synthetic mordenite. These effects are observable in the clinoptilolite spectra too, but from 873 K on the i.r. bands reflect the first signs of lattice destruction (Fig. 6).

These results are in excellent agreement with Beyer's observations on acid- and heat-treated mordenites and clinoptilolites [20].

The adsorption isotherms of the original and the treated samples are shown in Figs. 7 and 8. The specific surface areas (listed in Table II) attain a maximum at 873 K, due to two opposite effects: increase of the temperature of dealumination "cleans up" the structure; and impurities and bulky cations blocking the channels are

*Table II*

*BET surface areas of samples dealuminated at different temperatures* ($m^2/g$)

| | base sample | 773 K | 873 K | 973 K | 1073 K |
|---|---|---|---|---|---|
| natural mordenite | 47.0 | 53.0 | 127.8 | 117.2 | 91.6 |
| natural clinoptilolite | 32.8 | 52.25 | 82.9 | 48.6 | — |

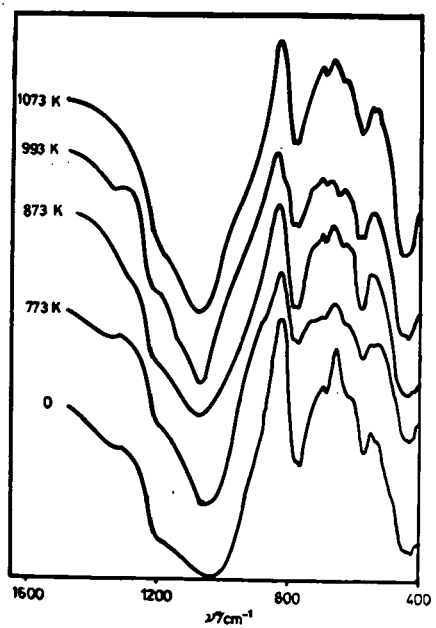


*Fig. 5.* I.r. spectra of dealuminated mordenites at different temperatures

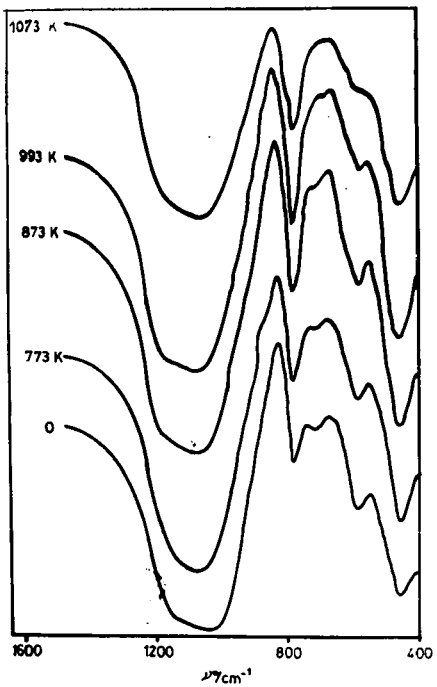


*Fig. 6.* I.r. spectra of dealuminated clinoptilolites at different temperatures

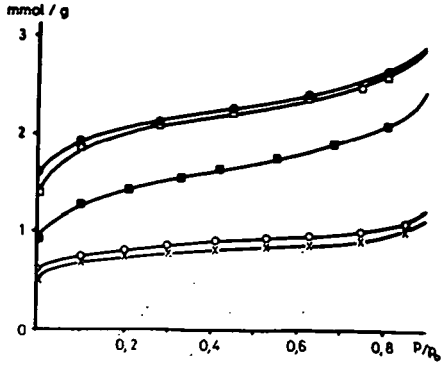


*Fig. 7.* Adsorption isotherms of nitrogen on dealuminated mordenites: x base sample, o sample dealuminated at 773 K, ● sample dealuminated at 873 K, □ sample dealuminated at 973 K, ■ sample dealuminated at 1073 K

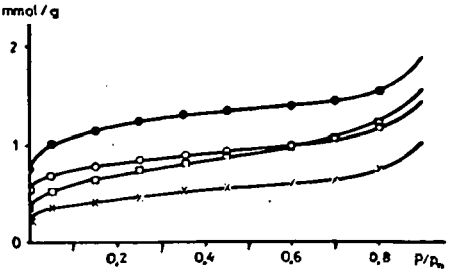


*Fig. 8.* Adsorption isotherms of nitrogen on dealuminated clinoptilolites: x base sample, o sample dealuminated at 773 K, ● sample dealuminated at 873 K, □ sample dealuminated at 973 K

removed or replaced by $H^+$ ions in the subsequent washing. Above 873 K, a partial lattice collapse results in enlargement of the channels, causing a reduction in the microporosity (mordenite) or a loss of crystallinity (clinoptilolite).

The immersion wetting enthalpies ($\Delta_w h$, in J $g^{-1}$) for the different samples are given in Table III. With regard to the 31% pure mordenite phase in the natural sample,

*Table III*

*Immersion wetting enthalpies of dealuminated zeolites*

| | Temperature of dealumination/K | $\Delta_w h$ J/g zeol. | $a$ mmol $H_2O$ / g zeol. | $\Delta_w H$ J/mmol $H_2O$ |
|---|---|---|---|---|
| Na-mordenite | — | 190.4 | 7.22 | 26.4 |
| natural mordenite | base sample | 47.4 | 3.33 | 14.2 |
| | 773 | 33.6 | 3.61 | 9.31 |
| | 873 | 12.7 | 2.78 | 4.57 |
| | 973 | 11.5 | 1.94 | 5.93 |
| | 1073 | 6.3 | 1.94 | 3.25 |
| natural clinoptilolite | base sample | 68.3 | 4.72 | 14.47 |
| | 773 | 58.5 | 5.56 | 10.52 |
| | 873 | 33.8 | 4.72 | 7.16 |
| | 973 | 16.7 | 3.33 | 5.02 |
| | 1073 | 2.1 | 1.39 | 1.5 |

the value agrees well with that for synthetic mordenite. For clinoptilolite a larger value was obtained.

Dealumination results in a monotonous decrease of the immersion wetting enthalpies. This can be accounted for by two effects: a reduction in the amount of water penetrating the pore structure (as a consequence of the greater hydrophobicity), and/or a decreasing interaction of the water with the framework and exchange cations. If the amount of *adsorbed* water is measured at 2.66 kPa partial pressure (corresponding to a saturated solution of $NH_4Cl$ in water) by thermogravimetry (column 4), and if complete pore filling is assumed in this process, the immersion wetting enthalpy values may be recalculated and expressed in J/mmol water (column 5). Up to 873 K the amount of water adsorbed at 2.66 kPa equilibrium pressure does not change considerably, and therefore it can be conjectured that the decrease of the immersion wetting enthalpy is due to the increasing hydrophobicity caused by the removal of cations, the heat of hydration of this comprising the main contribution to the wetting enthalpies. A great number of similar observations have accumulated in the past decade [21]. This dealumination procedure might allow the production of zeolites with varying surface energies, but without maintenance of the number of cations per u.c.

## References


[1] Natural Zeolites, Occurrence, Properties,Use, L. B. Sand, F. A. Mumpton, Eds, Pergamon Press Oxford, etc. 1978.
[2] *Klopp, G., I. Markovics, Á. Kovács:* Magyar Kémikusok Lapja, **37**, 255 (1982).
[3] *Kotsis, L., J. Árgyelán, P. Szolcsányi, K. Pataki:* React. Kinet. Catal. Lett., **18**, 149 (1981).
[4] *Valente, S., N. Burriesci, S. Cavallaro, S. Galvagno, C. Zipelli:* Zeolites, **2**, 271 (1982).
[5] *Nemecz, E., Gy., Varjú:* Földtani Közlemények, **93**, 77 (1963).
[6] *Papp, J., J. Valyon, Lné Czárán:* Magyar Kémiai Folyóirat, **81**, 442 (1975).
[7] *Jánossy, A., Lné Czárán, J. Papp:* Magyar Kémiai Folyóirat, **83**, 289 (1977).
[8] *Kalló, D., J., Papp, J. Valyon:* Zeolites, **2**, 13 (1982).
[9] *Valyon, J., J. Papp, D. Kalló:* Magyar Kémiai Folyóirat, **85**, 55 (1979).
[10] *Valyon, J., J. Papp:* Magyar Kémiai Folyóirat, **85**, 195 (1979).
[11] *Klopp, G., J. Sütő, I. Szebényi:* Proc. 5th Int. Conf. Zeolites, Napoli, 1980. p. 841.
[12] "Proc. of Invest. and Use of Hungarian Natural Zeolites Conf." MTA VEAB, Veszprém, 1982.
[13] *Fejes, P., I. Kiricsi, I. Hannus, Gy. Schöbel:* Magyar Kémiai Folyóirat **89**, 264 (1983).
[14] *Fejes, P., I. Kiricsi, I. Hannus, Á. Kiss, Gy. Schöbel:* React. Kinet. Catal. Lett. **4**, 481 (1980).
[15] *Fejes, P., I. Kiricsi, I. Hannus, Á. Kiss, Gy. Schöbel:* Hungarian patent application no. JO—276.
[16] *Náray—Szabó, I.:* Szervetlen Kémia, Akadémiai Kiadó, Budapest, 1956. Vol. I., p. 533.
[17] *Olaszi, V., Csné Csikós, A. Jánossy:* Proc. of Invest. and Use of Hungarian Natural Zeolites Conf., MTA VEAB, Veszprém, 1982, p. 155.
[18] *Fejes, P., I. Kiricsi, I. Hannus:* Acta Phys. et Chem. Szeged **28**, 173 (1982).
[19] *Kranich, W. L., Y. H. Ma, L. B. Sand. A. H. Weiss, I. Zwiebel:* Adv. Chem. Ser., **101**, 502 (1971).
[20] *Beyer, H., I. Belenkaja:* Proc. of Invest. and Use of Hungarian Natural Zeolites Conf., MTA VEAB, Veszprém, 1982, p. 43.
[21] *Chen, N. Y.:* J. Phys. Chem. **80**, 60 (1976).

## ДЕАЛЮМИНАЦИЯ. ЦЕОЛИТОВ ЛЕТУЧИМИ РЕАГЕНТАМИ. МОДИФИКАЦИЯ ВЕНГЕРСКИХ ЕСТЕСТВЕННЫХ ЦЕОЛИТОВ ФОСГЕНОМ

*И. Ганнуш, И. Киричи, И. Декань, П. Фееш*

Применен новый метод деалюминирования естественных морденитов и клиноптилолитов Токайского месторождения (Венгрия), были оценины изменения, происходящие в результате этого в их составе, структуре и адсорбционных свойствах. Наибольшая адсорбционная емкость получена при удалении загрязнений и катионов больших размеров, когда сохраняется почти полная кристалличность. Метод может быть рекомендован для изготовления цеолитов с различной поверхностной энергией.

# Information for Contributors

1. Manuscripts should be submitted to Prof. Pál Fejes, Institute of Applied Chemistry, József Attila University, Szeged, Rerrich tér 1, Hungary, H-6720.
2. The manuscripts must not exceed in any case 32 pages (Figures, legends, Tables and Summary included). Manuscripts should be submitted in duplicate.
3. The format of the text: A/4, double spaced, 25 lines per page and 50 characters per line. Title: all capital characters; underlined twice. Subtitle(s) should be written in new line(s) in normal writing, underlined also twice, first characters: capital. (See the following example).

STEREOCHEMICAL STUDIES

Studies on Cyclic-2-Hydroxycarboxylic Acids

By

PÁL KISS

Research Institute for Industrial Chemistry, Budapest
(Received.....)

4. After these comes the summary, which is followed by the text proper. If the parts of the paper are separated by secondary titles like: Introduction. Experimental etc., the following rule holds: secondary titles of equal rank are to be written in new lines, the first word with capital letter, otherwise running text underlined once.
   Example:
   Introduction
   Experimental part
5. The names of the authors in the running text are written in capital letters. Exceptions are the names in connection with scientific instruments, etc. where only the first letter should be capital.
6. Citations in the text with reference to selected literature at the end of the paper are to be made with squared brackets, like: [5], [4, 9], [4—9].
7. To make printing easier, mathematical formulas are to be simplified as much as possible. Reference to mathematical equations is made by numbers in parenthesis, like: (16).
8. Tables should be typen on separate pages. Please supply numbers and titles for all tables (Numbering occurs with Roman numerals: Table I).
   Throughout the whole text the IUPAC nomenclature should be used.
   Insert of Tables in the text will be indicated at the appropriate place of the margin, like this: Table I.
9. Figures must be drawn clearly with Chinese ink on oily drawing paper, the thickness of lines as well as size of letters and symbols should be selected with care, the minimum size is nearly 0.3 cm.
   The maximum width of Figures is 24 cm, however, Figures of width equal or less than 12 cm are preferred.
   Please, use upwright on the Figures.
   In the case of real numbers points are used instead of commas.
   The place of Figures in the text is indicated on the margin like this: Figure 13.
   Please supply legends for all figures and compile these on separate sheets. Indicate only the number of the Figures in the original drawing, for this purpose use blue pencil.
10. Literature will be given under the heading References, like this: (on a separate sheet at the end of the manuscript)
    [1] Allinger, N. L., M. T. Tribble: J. Phys. Chem. 33, 1565 (1976).
    [2] Abraham, J. K., H. S. Hoover: Principles of Competitive Oxidation. Mc Graw-Hill, New York, 1977, p. 133.

## INDEX